

Hard-body models of bulk liquid crystals

This content has been downloaded from IOPscience. Please scroll down to see the full text.

2014 J. Phys.: Condens. Matter 26 463101

(<http://iopscience.iop.org/0953-8984/26/46/463101>)

View [the table of contents for this issue](#), or go to the [journal homepage](#) for more

Download details:

IP Address: 163.117.132.163

This content was downloaded on 22/10/2014 at 14:57

Please note that [terms and conditions apply](#).

Topical Review

Hard-body models of bulk liquid crystals

Luis Mederos¹, Enrique Velasco² and Yuri Martínez-Ratón³

¹ Instituto de Ciencia de Materiales de Madrid, CSIC, Sor Juana Inés de la Cruz, 3, E-28049 Madrid, Spain

² Departamento de Física Teórica de la Materia Condensada and Instituto de Ciencia de Materiales Nicolás Cabrera, Universidad Autónoma de Madrid, E-28049 Madrid, Spain

³ Grupo Interdisciplinar de Sistemas Complejos (GISC), Departamento de Matemáticas, Escuela Politécnica Superior, Universidad Carlos III de Madrid, Avenida de la Universidad 30, E-28911, Leganés, Madrid, Spain

E-mail: lmederos@icmm.csic.es, enrique.velasco@uam.es and yuri@math.uc3m.es

Received 24 April 2014, revised 30 July 2014

Accepted for publication 5 August 2014

Published 21 October 2014

Abstract

Hard models for particle interactions have played a crucial role in the understanding of the structure of condensed matter. In particular, they help to explain the formation of oriented phases in liquids made of anisotropic molecules or colloidal particles and continue to be of great interest in the formulation of theories for liquids in bulk, near interfaces and in biophysical environments. Hard models of anisotropic particles give rise to complex phase diagrams, including uniaxial and biaxial nematic phases, discotic phases and spatially ordered phases such as smectic, columnar or crystal. Also, their mixtures exhibit additional interesting behaviours where demixing competes with orientational order. Here we review the different models of hard particles used in the theory of bulk anisotropic liquids, leaving aside interfacial properties and discuss the associated theoretical approaches and computer simulations, focusing on applications in equilibrium situations. The latter include one-component bulk fluids, mixtures and polydisperse fluids, both in two and three dimensions, and emphasis is put on liquid-crystal phase transitions and complex phase behaviour in general.

Keywords: liquid crystals, phase transitions, hard-body models

(Some figures may appear in colour only in the online journal)

1. Introduction

1.1. Liquid-crystalline phases

Common states of matter are gas, liquid and crystal. Therefore, the term ‘liquid crystal’ seems, in principle, a contradiction in itself. However, liquid crystals have been known since their discovery by Reinitzer [1] 125 years ago. The name suggests an intermediate behaviour between liquid and crystal and, in fact, this is the case: liquid crystals are states of matter that exhibit liquid and crystal properties simultaneously. They can flow and form droplets (liquid-like properties) but, at the same time, they present some kind of long-range molecular order (orientational and sometimes also partial positional order) which translates into anisotropic macroscopic optical, electric and magnetic properties and also elasticity (crystal-like properties). Liquid crystals are then *mesophases*, i.e. phases or

states of matter intermediate between liquid and crystal phases and their properties have been used with advantage in many technological applications (for an introduction to the subject see e.g. [2–7]; for a review on applications see the excellent series of books edited by Bahadur [8]).

The common feature of all liquid-crystalline phases is that they exhibit orientational order. Liquid crystals are formed by anisotropic molecules. Orientational long-ranged order means that molecules align, on average, along a particular direction, called the *director*, specified by a unit vector \hat{n} referred to the laboratory-fixed reference frame. Distinction between different liquid-crystal phases comes from the occurrence of partial positional order. A nematic (N) liquid crystal is a mesophase characterized by the presence of orientational order but the lack of positional order; therefore, molecular centres of mass are completely disordered, see figure 1(a). In a smectic

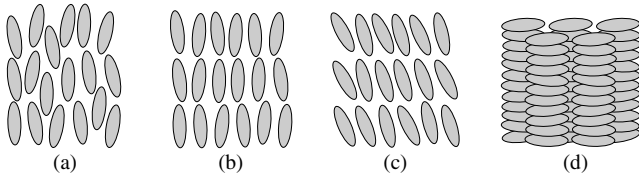


Figure 1. Schematic of four liquid-crystal phases. (a) Nematic. (b) Smectic A. (c) Smectic C. (d) Columnar.

(S) phase, the centres of mass of the molecules are arranged in liquid-like layers, so that the system shows 1D positional order⁴. In the case that the layers are perpendicular to the director, figure 1(b), the smectic is called smectic A (S_A). In a smectic C phase (S_C), the liquid layers are tilted with respect to the director, see figure 1(c). Disc-like particles usually form N phases and, at higher densities, they tend to form the so-called columnar (C) phase, which consists of a regular 2D array of liquid-like columns, figure 1(d). A complete description of the different mesophases can be found, e.g. in [2–4].

1.2. The role of hard interactions in systems of isotropic particles

In simple atomic or effectively spherical molecular systems interacting through physical interactions (no chemical bonds), for example argon or methane at sufficiently high temperatures, the repulsive part of the two-body interaction at short distances plays a crucial role in determining the local liquid structure. In particular, the radial distribution function $g(r)$, which gives the probability of finding a particle at a distance r from a given particle at the origin, can be reasonably approximated by that of a system of hard spheres (HS), a system of spheres interacting via overlap interactions (no configurations involving overlap of spheres are allowed in the partition function). Moreover, computer simulations first [9–11] and theory later [12] showed that a HS system undergoes a first-order freezing transition when the packing fraction (fraction of volume occupied by spheres) of the liquid is equal to $\eta_l = 0.494$. This liquid coexists with a face-centred cubic (f.c.c.) solid of packing fraction $\eta_s = 0.545$. This result is a bit surprising because, on a first look, it is not easy to accept that a system with no attractions can freeze. The explanation, of course, relies on entropy: when the packing fraction is high enough, spheres as a whole have more free volume available (hence entropy) in the ordered than in the liquid phase.

In summary, hard-core interactions in simple systems can qualitatively explain most of their equilibrium properties; the phenomenon of condensation from a vapour (liquid-vapour transition) and the dependence of freezing with temperature are due to the attraction between particles and can be treated perturbatively. It is therefore not surprising that perturbation theories for simple systems have given excellent results, even with quantitative agreement, in the theory of condensed matter, not only for the liquid [13], but also for the solid phase [14].

⁴ From the translational point of view, a smectic-A phase consists of a stacking of liquid-like planes perpendicular to the director.

1.3. Hard interactions in systems of anisotropic particles

One of the first questions one can ask about the equilibrium properties of liquid crystals concerns the role of anisotropic hard repulsions between particles in determining the structure of the system. Is that role similar to that of HS in the case of simple liquids? The answer to this question is more complicated than in the case of simple liquids, mainly because of the coupling between orientational and positional order. See [15] for an early review about the role of hard particle models in liquid-crystalline phases.

It soon became clear, thanks to the seminal paper of Onsager [16], that a system made solely of anisotropic bodies interacting through hard interactions, e.g. hard spherocylinders (HSC), undergoes an entropy-driven first-order isotropic-nematic transition when its packing fraction is high enough. There is an intuitive argument to understand this transition. Imagine that you want to accommodate needles or matches into a box. If there are only a few matches, you can arrange them as you want and you will have a completely disordered system of needles, i.e. an isotropic phase. But when many needles have to go into the box they will have to be oriented in an ordered arrangement in order to fit into the box. Therefore, packing considerations require the equilibrium phase at high packing fraction to be a nematic phase.

An equivalent argument to explain the nematic-smectic transition at yet higher packing fraction is more subtle. If we consider the nematic-smectic transition as due to the generation of a 1D positional-order wave in an already perfectly aligned nematic, then we have to address additional questions such as the role of the specific particle shape. It is not enough, as in the case of the isotropic-nematic transition, to demand a sufficiently anisotropic particle shape since, for example, a fluid of parallel hard ellipsoids (HE) does not exhibit a smectic phase, while one made of parallel HSC does when the length-to-breadth ratio is high enough.

In fact, does the fact that a given model system possesses some particular stable liquid-crystal phase mean that a hard interaction is responsible for the stability of such a phase? Even though many features of phase behaviour can be explained by hard models, the general answer to this question is no. But the possibility to fabricate tailor-made colloidal particles that behave close to size-monodisperse hard bodies with virtually any shape has revitalized hard-particle models and their research and applications. Also, because virus particles are completely monodisperse and their interactions are known with a high accuracy, they are ideally suited for testing theoretical ideas and results. Granular matter made of macroscopic grains that interact through overlap interactions can also be modelled by hard models where particles interact elastically. Systems of vibrated grains can in some regimes behave like hard particles that explore phase space with a Boltzmann probability and some ordered patterns obtained in these systems resemble liquid-crystal phases.

In summary, hard-body models in the theory of liquid crystals may play a role similar to that of the HS model in the theory of simple fluids. Moreover, carefully prepared and stabilized colloidal particles may behave essentially as hard bodies and, therefore, hard-body models for liquid crystals can

be directly tested experimentally using anisotropic colloidal particles. Vibrated granular matter made of anisotropically-shaped grains is another field of exploration for hard models. The applications of the statistical mechanics of mesophases for hard models are very numerous in many fields.

1.4. Scope of this review

In this paper we review hard-body models as applied to the study of the equilibrium properties of liquid-crystal phases. The scope of the review is on fluids made of convex hard bodies, with emphasis on liquid-crystalline phases and phase transitions. Only bulk properties are covered; interfacial properties and inhomogeneous systems are reviewed in separate work [17]. Theories and results for the bulk isotropic phase will not be reviewed (excellent reviews exist; see e.g. Nezbeda [18]). Nor will dynamical properties and lattice models be mentioned. Also, the topic of flexibility, so important for real liquid-crystal-forming molecules, filamentous viruses and other colloidal particles, is left aside. An enormous volume of literature is devoted to the theory and computer simulation of the liquid-crystal phases of hard-model fluids; as a consequence and in order to present a manageable exposition of the subject, we have referenced only our personal choice of representative literature. Experimental results are mentioned insofar as they help to illustrate, motivate or support studies on hard-body fluids. Some reviews partially cover this subject [19–22]. For more specific resources on liquid crystals we refer the reader to the works cited in the introduction.

2. Hard-body models

Let us consider a collection of N particles in a volume V . Let $\mathbf{r}^{(n)}$ be the centre of mass position of the n -th particle with respect to the laboratory frame and $\{\hat{\Omega}_i^{(n)}\}$, with $i = 1, 2, 3$, a set of three unit vectors describing its orientation with respect to the same frame. If the particles are hard bodies, the potential energy of an arbitrary configuration of the particles can be strictly written as a sum of two-body potentials,

$$U(\mathbf{r}^{(n)}, \{\hat{\Omega}_i^{(n)}\}) = \sum_{n \neq m} \phi(\mathbf{r}_{nm}, \{\hat{\Omega}_j^{(n)}\}, \{\hat{\Omega}_k^{(m)}\}),$$

$$\mathbf{r}_{nm} \equiv \mathbf{r}^{(n)} - \mathbf{r}^{(m)} \equiv r_{nm} \hat{\mathbf{r}}_{nm}. \quad (1)$$

The two-body potential ϕ has a simple structure:

$$\phi(\mathbf{r}_{nm}, \{\hat{\Omega}_j^{(n)}\}, \{\hat{\Omega}_k^{(m)}\}) = \begin{cases} \infty, & r_{nm} < \sigma(\hat{\mathbf{r}}_{nm}, \{\hat{\Omega}_j^{(n)}\}, \{\hat{\Omega}_k^{(m)}\}) \\ & (n \text{ and } m \text{ overlap}) \\ 0, & r_{nm} > \sigma(\hat{\mathbf{r}}_{nm}, \{\hat{\Omega}_j^{(n)}\}, \{\hat{\Omega}_k^{(m)}\}) \\ & (n \text{ and } m \text{ do not overlap}) \end{cases} \quad (2)$$

The function $\sigma(\hat{\mathbf{r}}_{nm}, \{\hat{\Omega}_j^{(n)}\}, \{\hat{\Omega}_k^{(m)}\})$ is the so-called *contact distance*, which gives the minimum distance between two non-overlapping particles at fixed orientations and fixed relative interparticle vector. This function in fact is sufficient to define the particle model.

Since the probability of a given configuration is proportional to the Boltzmann weighting factor $\exp(-\beta U)$,

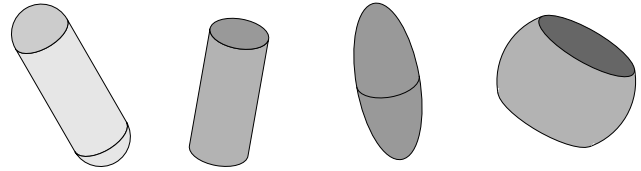


Figure 2. Some popular models of hard body. From left to right: spherocylinder, cylinder, ellipsoid and cut sphere.

where $\beta = 1/kT$, with k Boltzmann's constant and T temperature, all permissible configurations of the N -particle system will have zero potential energy and the Boltzmann factor is independent of T . The average internal energy E at temperature T only contains the kinetic contribution, $E = 3NkT/2$ and the equilibrium state of the system, given by $\delta F = 0$, $\delta^2 F > 0$ (where δ indicates variations with respect to particle configurations at fixed density ρ_0 and T), is independent of the thermal energy kT , which appears as an irrelevant scaling factor in the free energy $F/kT = 3N/2 - S/k$, where the entropy S only depends on the density $\rho_0 = N/V$. The physical behaviour is solely controlled by the entropy, which is related to the volume of the configurational space (hence actual volume) accessible to particles. One of the fascinating properties of hard-body systems is that all ordered stable arrangements of particles have an entropic origin. The only relevant parameter in the canonical ensemble is the density ρ_0 or, equivalently, the packing fraction η , defined as the fraction of volume occupied by particles; in a monodisperse system, $\eta = \rho_0 v$, where v is the volume of the particles.

2.1. Particles in 2D and 3D

A virtually infinite number of hard-particle models can be defined. Here we focus on convex hard particles characterized by a shape and two aspect ratios. For bodies of revolution only one aspect ratio, $\kappa = l/d$, measuring the length (l) over width (d) ratio, is necessary. Prolate bodies ('rods') have $\kappa > 1$, while oblate bodies ('platelets') have $\kappa < 1$. In the limit $\kappa \rightarrow \infty$ all particles are equivalent and the virial coefficients tend to the same values. The limit $\kappa \rightarrow 0$ corresponds to infinitely thin platelets; here not all particles are equivalent and the cross section of the particles is crucial in characterizing the virial coefficients and statistical mechanics of the fluid.

A popular model for prolate uniaxial particles is the *hard spherocylinder* (HSC), figure 2: a cylindrical rod of length L and diameter D capped by a hemisphere of the same diameter at each end. The aspect ratio in this case is $\kappa = (L + D)/D$. This was the particle model used by Onsager [16] in his seminal paper on ordering of hard rods. Onsager considered the limit $\kappa \rightarrow \infty$ (hard needles), where the exact shape of the rod is not important. This limit is still used very often but is not realistic. In the case of a finite and more realistic value of κ (comparable to that of liquid-crystal molecules or colloidal particles), the particle shape plays a role. The limit $L = 0$ corresponds to the hard sphere (HS).

A second popular model is the *hard ellipsoid* (HE), with axes lengths a, b, c , figure 2. If all three axes are different, $a \neq b \neq c$, the model represents a biaxial particle. If the particle has symmetry of revolution, two lengths are identical, say

$b = c$, only a single aspect ratio $\kappa = a/b$ is relevant and we have a model for a uniaxial particle. A numerically convenient approximation for the HE model is the hard Gaussian overlap model (HGO) [23]. In the limit $\kappa \rightarrow \infty$ the physical properties of all of these fluids coincide but for even moderate aspect ratios virial coefficients are very close [24–26]. Other models for prolate particles include *hard cylinders* (HC, figure 2), *chain spheres*, *fused spheres*, *rectangular prisms* (boards) and combinations of all these. For example, banana-shaped particles meant to reproduce biaxial nematic phases can be constructed by attaching two rods by their ends with a fixed angle between them [27]. When considering rigid models for simple phases, however, the most obvious choices are HSC, HE, HGO and HC.

In the case of oblate particles, meant to reproduce molecular or colloidal discotic-forming liquid crystals, there is also a great variety of models. In his paper, Onsager [16] used infinitely thin discs (i.e. infinitely flattened cylinders) to compute the ordering properties of model discotic particles. In real systems the particle thickness may be small compared to the width, but in any case finite. An advantage of the HE and HGO models is that they can also be used for oblate particles when one of the lengths is very small compared to the others ($a \ll b \simeq c$). Apart from flattened HE or HGO models, workers have used other models such as *hard cut spheres*, HCS, i.e. spheres cut by two planes at the same distance from the equator, figure 2), HC with $L \leq D$ and *hard square platelets* (rectangular prisms of side lengths l_1, l_2, l_3 with $l_1 \ll l_2 \simeq l_3$).

In 2D corresponding models can be defined: *hard ellipses*, *hard rectangles* and *hard discorectangles*, which are projections of respectively ellipsoids, cylinders and spherocylinders on a plane parallel to their uniaxial axes. Fused discs can also be used. Zigzag or cross particles have been examined by attaching a number of rods at fixed angles [28, 29].

As we have seen, a huge number of models have been used to represent real molecular or colloidal systems. The only requirement when defining a model is the possibility to be able to explicitly or implicitly compute, in an efficient way, the contact distance $\sigma(\hat{r}, \{\hat{\Omega}\}, \{\hat{\Omega}'\})$ between two particles. If particles are not identical (mixtures or size polydisperse systems), contact distances between all pairs of species must be known. Particles made of attached units are easily handled since the total contact distance can be obtained from the partial contact distances between the units.

2.2. Contact with real materials

Hard models are approximate models for systems made of anisotropic molecules, since they can provide the essential correlation characteristics originating from the closed-shell electronic distributions of simple, non-covalent systems and explain ordering as an entropy effect. However, hard models are athermal and therefore cannot account for the temperature dependence of material properties. Even density-dependent properties are not, in general, quantitatively described by hard models. For example, calculations of the I–N phase transition using hard-rod models predict too low a value for the density gap at the transition as compared to real materials. Properties related to cohesion cannot be quantitatively described by

overlap interactions and anisotropic attractive interactions need to be included in the theoretical treatments (either theory or simulation) of liquid crystals. The effect of these interactions are usually treated theoretically using perturbation theory, which requires the correlation structure of the corresponding hard model. Nevertheless, hard models are useful tools to qualitatively analyze the properties of molecular matter.

Hard models also find application in stabilized colloidal suspensions of Coulomb-screened anisotropic particles in a solvent. In this case the agreement with real materials is more quantitative. An important field of application is in suspensions of filamentous viruses. Early investigations on the first virus to be isolated, the Tobacco Mosaic Virus (TMV), indicated that it formed a N phase. Onsager [16] explained the formation of this phase in terms of a solution of charged hard rods of an effective diameter D_{eff} that depends on the ionic strength of the solution; the transition was explained solely as a competition between orientational and correlation entropies. More recent experiments on virus suspensions are analyzed with hard models of the same type [30, 31].

Another type of experimental colloidal system, which can be closely modelled by hard models, is a suspension of mineral or polymeric particles. Several groups have been working on these systems for a long time and a huge list of interesting results concerning phases with orientational and spatial ordering has been obtained. For example, suspensions of goethite nanorods have been shown to exhibit liquid-crystalline ordering [32, 33]. The particle interactions can be made to be approximately hard by suitable chemical treatments. Anisotropic particles made from sheets of the layered gibbsite mineral have been stabilized by layers of grafted polymer, a method that, in a good solvent such as toluene, produces size polydisperse platelets which interact approximately through hard interactions [34]. Various liquid-crystalline phases have been observed in this system, as predicted by theoretical models of hard platelets. Other particles made from layered mineral materials, e.g. ZrP, have also been shown to exhibit liquid-crystal phases [35]. Also, prolate particles made from polymeric materials have been synthesized [36] and their interactions can be closely approximated by hard interactions.

In summary, hard models are very useful to qualitatively understand phase behaviour in real liquid-crystal-forming molecular systems. But they can also be used to analyze colloidal suspensions of anisotropic particles made of viruses, mineral or polymeric particles, in many cases with quantitative agreement.

3. Theories and simulations

In this section we make a short revision of the theories for the liquid-crystal bulk state of anisotropic hard-particle models in the language of Density Functional Theory (DFT). This language is essential to understand inhomogeneities and phase transitions in condensed systems made of hard particles since the structure and correlations in the fluid are core ingredients of DFT. For a general, recent review on DFT see [37]. The physical properties of hard bodies are governed by entropy, which is related to the volume accessible to particles. Therefore

DFT theories, which are based on geometry and excluded volume between two particles, have played an essential role in the development of the field.

The revision is not extensive but stresses the main ideas and concepts used to construct theories and the success, or otherwise, of the resulting theories. The application of the theories to explain the formation of the different LC phases is then mentioned, first for the nematic, then for the phases with spatial order. In accord with the spirit of this review, we do not mention theories that incorporate soft attractive interactions (of Maier–Saupe type or perturbation theories). A more complete review on the fundamentals and applications of theoretical approaches to a larger variety of models for liquid crystals can be found in [38].

3.1. Density functional theory for anisotropic hard bodies

3.1.1. Uniaxial particles. The key ingredient of DFT is the ensemble average local density of particles, $\rho(\mathbf{r}, \hat{\Omega})$, giving the local density of particles at position \mathbf{r} and with orientation given by the unit vector $\hat{\Omega}$; this is the orientation of the symmetry axis of the particle, assuming it only has one (uniaxial particle); in the case of less symmetric particles, more vectors are needed. One can define a local orientational distribution function $h(\mathbf{r}, \hat{\Omega})$ by extracting the density dependence, $\rho(\mathbf{r}, \hat{\Omega}) = \rho(\mathbf{r})h(\mathbf{r}, \hat{\Omega})$. The local orientational distribution function is normalized, $\int d\hat{\Omega}h(\mathbf{r}, \hat{\Omega}) = 1$. In the uniform I and N phases there is no spatial dependence, $\rho(\mathbf{r}) = \rho_0$ and one can write $\rho(\mathbf{r}, \hat{\Omega}) = \rho_0h(\hat{\Omega})$.

In DFT the Helmholtz free energy F is written as a functional of the local density, $F[\rho]$. In the grand canonical ensemble, where μ, V, T are fixed (μ is the chemical potential), one defines the grand canonical functional,

$$\Omega[\rho] = F[\rho] - \mu \int_V d\mathbf{r} \int d\hat{\Omega} \rho(\mathbf{r}, \hat{\Omega}). \quad (3)$$

The equilibrium state of the fluid follows by functionally minimising the functional,

$$\left. \frac{\delta \Omega[\rho]}{\delta \rho(\mathbf{r}, \hat{\Omega})} \right|_{\text{eq}} = 0 \quad \text{at constant } \mu, V \text{ and } T. \quad (4)$$

Once the equilibrium local density $\rho(\mathbf{r}, \hat{\Omega})$ is obtained, the equilibrium free energies follow by evaluating the corresponding functional.

To microscopically characterize orientational ordering in a uniaxial liquid crystal a set of order parameters $\{f_{nm}(\mathbf{r})\}$ is defined in terms of a spherical harmonic expansion of the orientational distribution function:

$$\rho(\mathbf{r}, \hat{\Omega}) = \rho(\mathbf{r}) \sum_{l=0}^{\infty} \sum_{m=-l}^l f_{lm}(\mathbf{r}) Y_{lm}(\hat{\Omega}),$$

$$f_{lm}(\mathbf{r}) = \int d\hat{\Omega} h(\mathbf{r}, \hat{\Omega}) Y_{lm}^*(\hat{\Omega}), \quad (5)$$

where $Y_{lm}(\hat{\Omega})$ are spherical harmonics. Since $\int d\hat{\Omega} \rho(\mathbf{r}, \hat{\Omega}) = \rho(\mathbf{r})$, the local number density, one obtains $f_{00}(\mathbf{r}) = 1$. It is common to limit the expansion to the $l = 2$ level and

define order parameters f_{1m} , with $m = -1, 0, +1$ and f_{2m} , with $m = -2, \dots, 2$, to quantify the orientational order. For non-polar particles, if one chooses the z axis of the reference frame along the director \hat{n} , the order parameters reduce to

$$Q(\mathbf{r}) = \int d\hat{\Omega} h(\mathbf{r}, \hat{\Omega}) P_2(\hat{n} \cdot \hat{\Omega}), \quad (6)$$

where $P_2(x)$ is the second-order Legendre polynomial and $\hat{n} \cdot \hat{\Omega} = \cos \theta$, where θ is the angle between the molecular axis and the director.

The standard practise is to split the functional in ideal, $F_{\text{id}}[\rho]$, and excess (or interaction), $F_{\text{ex}}[\rho]$, contributions, so that

$$F[\rho] = F_{\text{id}}[\rho] + F_{\text{ex}}[\rho]. \quad (7)$$

$F_{\text{id}}[\rho]$ would be the free energy of a fluid of non-interacting particles with local density $\rho(\mathbf{r}, \hat{\Omega})$. It has an exact expression and it was first derived by Onsager [16] by mapping the possible particle orientations onto a mixture of different ‘chemical’ species, each species corresponding to a different orientation $\hat{\Omega}_i$. With this idea $h(\hat{\Omega}_i)$ is akin to x_i , the composition of the i -th species in a multicomponent mixture, and the ideal free energy can be built from the mixing entropy of a multicomponent mixture. Generalizing to systems with positional order:

$$\begin{aligned} \beta F_{\text{id}}[\rho] &= \int_V d\mathbf{r} \int d\hat{\Omega} \rho(\mathbf{r}, \hat{\Omega}) \left\{ \log \left[\rho(\mathbf{r}, \hat{\Omega}) \Lambda^3 \right] - 1 \right\} \\ &= \int_V d\mathbf{r} \rho(\mathbf{r}) \left\{ \log \left[\frac{\rho(\mathbf{r}) \Lambda^3}{4\pi} \right] - 1 \right\} \\ &\quad + \int_V d\mathbf{r} \rho(\mathbf{r}) \left\langle \log \left[4\pi h(\mathbf{r}, \hat{\Omega}) \right] \right\rangle_h, \end{aligned} \quad (8)$$

where $\langle \dots \rangle_h$ is an angular average weighted by the distribution function $h(\mathbf{r}, \hat{\Omega})$. In the expression above Λ is the thermal wavelength. The first term corresponds to the positional entropy, whereas the second is the orientational entropy (the factor 4π is introduced so that the latter vanishes in an orientationally disordered fluid). The local orientational entropy per particle (‘mixing entropy’) in units of the Boltzmann constant k is defined as

$$\begin{aligned} s_{\text{or}}(\mathbf{r}) &\equiv - \left\langle \log \left[4\pi h(\mathbf{r}, \hat{\Omega}) \right] \right\rangle_h \\ &= - \int d\hat{\Omega} h(\mathbf{r}, \hat{\Omega}) \log \left[4\pi h(\mathbf{r}, \hat{\Omega}) \right]. \end{aligned} \quad (9)$$

For uniform phases, i.e. I or N phases, we have

$$\frac{\beta F_{\text{id}}[h]}{N} = \log \left(\frac{\rho_0 \Lambda^3}{4\pi} \right) - 1 - s_{\text{or}}[h]. \quad (10)$$

The orientational entropy s_{or} is one of the key actors in the theory of liquid-crystal phase transitions. s_{or} has a maximum value when particles are disordered, i.e. the I phase, with $h(\hat{\Omega}) = (4\pi)^{-1}$.

The other actor is the excess free energy (excess entropy) functional $F_{\text{ex}}[\rho]$, which does not have an exact expression. Essentially two routes have been followed to construct $F_{\text{ex}}[\rho]$: the Onsager theory, based on the concept of excluded volume, and theories based on weighted densities.

3.1.2. Excluded volume: Onsager theory. In Onsager theory the excess free energy is written in terms of a central quantity in hard-body systems, the *excluded volume* between two particles. The excluded volume is directly related to the second virial coefficient. Onsager's derivation of the excess functional considers the cluster or virial expansion of the equivalent multicomponent mixture. One obtains:

$$\frac{\beta F_{\text{ex}}[h]}{N} = B_2[h]\rho_0 + \frac{1}{2}B_3[h]\rho_0^2 + \dots \quad (11)$$

where $B_n[h]$ are the virial coefficients (functionals of the orientational distribution function), the first of which is

$$B_2[h] = -\frac{1}{2} \left\langle \left\langle \int_V d\mathbf{r} f(\mathbf{r}, \hat{\Omega}, \hat{\Omega}') \right\rangle \right\rangle_h, \quad (12)$$

where $f(\mathbf{r}, \hat{\Omega}, \hat{\Omega}') = \exp[-\beta\phi(\mathbf{r}, \hat{\Omega}, \hat{\Omega}')] - 1$ is the Mayer function and \mathbf{r} the relative position vector joining the centres of mass of two particles (or the position vector of one particle, with orientation $\hat{\Omega}'$, assuming the other, oriented along $\hat{\Omega}$, lies at the origin). $\langle \langle \dots \rangle \rangle$ denotes double angular average over the function $h(\hat{\Omega})$. For two bodies that interact via a hard potential, the Mayer function is particularly simple:

$$f(\mathbf{r}, \hat{\Omega}, \hat{\Omega}') = \begin{cases} -1, & \text{particles overlap} \\ 0, & \text{particles do not overlap} \end{cases} \quad (13)$$

As a consequence, the second virial coefficient is directly related with the so-called 'excluded volume':

$$\begin{aligned} B_2[h] &= \frac{1}{2} \left\langle \left\langle v_{\text{excl}}(\hat{\Omega}, \hat{\Omega}') \right\rangle \right\rangle_h \\ &= \frac{1}{2} \int d\hat{\Omega} \int d\hat{\Omega}' v_{\text{excl}}(\hat{\Omega}, \hat{\Omega}') h(\hat{\Omega}) h(\hat{\Omega}'). \end{aligned} \quad (14)$$

$v_{\text{excl}}(\hat{\Omega}, \hat{\Omega}') = - \int_V d\mathbf{r} f(\mathbf{r}, \hat{\Omega}, \hat{\Omega}')$ is the volume excluded to one particle because of the presence of the other. We could approximately obtain the entropy of the system by noting that, if the two particles were isolated (low-density limit), the total volume accessible to a particle would be $V - \frac{N-1}{2} \langle \langle v_{\text{excl}} \rangle \rangle_h \simeq V - NB_2[h]$ (the factor 1/2 accounts for the fact that two particles are involved and the excluded volume has to be shared by the two). The partition function would then be

$$Q = \frac{\Lambda^{3N}}{N!} (V - NB_2[h])^N = Q_{\text{id}} (1 - \rho_0 B_2[h])^N, \quad (15)$$

and the excess free energy per thermal energy unit $\beta F_{\text{exc}} = -\log(Q/Q_{\text{id}})$ would read

$$\frac{\beta F_{\text{exc}}}{N} = -\log(1 - \rho_0 B_2[h]) = B_2[h]\rho_0 + \dots \quad (16)$$

The first term of this expansion coincides with that of equation (11). Onsager qualitatively demonstrated that, for hard rods in the isotropic phase, the ratio $B_3/B_2^2 \rightarrow (D/L) \log(L/D)$ so that, in the limit $L/D \rightarrow \infty$, the third virial coefficient is indeed negligible for very long rods (hard-needle limit). It is then plausible that higher-order virial coefficients also vanish in the same limit.

Now the excluded volume has to be specified. For HSC particles, the excluded volume is given by

$$v_{\text{excl}}(\hat{\Omega}, \hat{\Omega}') = 8v_0 + 2L^2D \left| \sin(\hat{\Omega}, \hat{\Omega}') \right|, \quad (17)$$

where $v_0 = \frac{\pi}{4}LD^2 + \frac{\pi}{6}D^3$ is the volume of a HSC. To simplify the calculations, Onsager considered the excluded volume in the limit of infinite aspect ratio, $\kappa \gg 1$ (hard needles), i.e. $L \gg D$: $v_{\text{excl}}(\hat{\Omega}, \hat{\Omega}') = 2L^2D \left| \sin(\hat{\Omega}, \hat{\Omega}') \right|$. Applying the equilibrium condition

$$\left. \frac{\delta F[h]}{\delta h(\hat{\Omega})} \right|_{\text{eq}} = \lambda, \quad (18)$$

where λ is a Lagrange multiplier ensuring the normalization condition on $h(\hat{\Omega})$, one obtains an integral, Euler-Lagrange, equation for $h(\hat{\Omega})$,

$$h(\hat{\Omega}) = \frac{e^{-\rho_0 \int d\hat{\Omega}_1 h(\hat{\Omega}_1) v_{\text{excl}}(\hat{\Omega}, \hat{\Omega}_1)}}{\int d\hat{\Omega}_3 e^{-\rho_0 \int d\hat{\Omega}_2 h(\hat{\Omega}_2) v_{\text{excl}}(\hat{\Omega}_3, \hat{\Omega}_2)}}. \quad (19)$$

This is an integral equation, which has to be solved numerically. In addition, Onsager used a trial function in terms of a variational parameter, α :

$$h(\hat{\Omega}) = \frac{e^{\alpha \cos(\hat{\Omega} \cdot \hat{n})}}{\int d\hat{\Omega}' e^{\alpha \cos(\hat{\Omega}' \cdot \hat{n})}}. \quad (20)$$

In the I phase, $\alpha = 0$, whilst in the N phase $\alpha > 0$. Note that, in the hard-needle limit, the solution only depends on the scaled density $\rho^* = \rho_0 L^2 D$. The theory predicts a first-order phase transition between the I and N phases for the following values of packing fraction $\eta = (\pi D/4L)\rho^*$:

$$\eta_I = 3.340 \frac{D}{L}, \quad \eta_N = 4.486 \frac{D}{L}. \quad (21)$$

The density gap becomes smaller as the particles go to the hard-needle limit. As the ratio L/D is reduced, end-particle effects in the excluded volume (first term in equation (17)) become important, there is no universal scaled density and the coexistence values depart from the values (21). The relative density gap is $\Delta\eta/\eta_N = (\eta_N - \eta_I)/\eta_N \simeq 26\%$, too high compared with typical experimental values. The value of the uniaxial order parameter at the transition is $Q_{\text{IN}} = 0.84$, also too high with respect to experiment. Lasher [39] numerically solved the problem without resorting to the variational function (20), but by using an expansion in Legendre polynomials. The study included the $8v_0$ factor of the excluded volume in the calculation of the coexistence densities, thus incorporating the dependence on aspect ratio.

Onsager theory has been more closely examined, from a numerical point of view, by Kayser and Raveche [40] and Herzfeld *et al* [41], focusing on an iterative algorithm to obtain the solution. This algorithm has been shown to be convergent.

Also, Stroobants *et al* [42], examined the convergence properties of an exponentiated truncated Legendre expansion,

$$h(\hat{\Omega}) = \frac{\exp \left\{ \sum_{n=0}^{\infty} \alpha_{2n} P_{2n}(\hat{\Omega} \cdot \hat{n}) \right\}}{\int d\hat{\Omega}' \exp \left\{ \sum_{n=0}^{\infty} \alpha_{2n} P_{2n}(\hat{\Omega}' \cdot \hat{n}) \right\}}. \quad (22)$$

The convergence of the results was studied as a function of the number of terms included in the expansion. As a main conclusion, it was found that the coexistence results depend very much on the form of distribution function used.

The Onsager theory was modified by Zwanzig [43] by considering an idealized model where rods can only point along a discrete set of orientations. Despite this drastic simplification, but as a bonus, Zwanzig could extend the theory to the seventh-order virial coefficient and study the robustness of Onsager's orientational transition. Zwanzig was able to confirm the transition. However, the convergence of the expansion is probably poor since coefficients are oscillatory. A later analysis by Runnels and Colvin [44] used a Padé expansion to limit this problem and they confirmed in turn Zwanzig's result.

Calculation of virial coefficients for various models have been done for the isotropic phase, with a view to constructing accurate resummations of the equation of state [18, 45–53]. All of these studies are focused on short particles and therefore say nothing about the validity of Onsager theory. Frenkel [54] has calculated the scaled third, fourth and fifth virial coefficients of hard spherocylinders in the isotropic phase (i.e. B_n/B_2^{n-1} for $n = 3, 4, 5$) for aspect ratios $\kappa = L/D$ in the range $1-10^6$, using Monte Carlo integration. He concluded that all coefficients vanish in the hard-needle limit. However, the vanishing limit value is obtained rather slowly with κ , which means that Onsager theory is not quantitatively valid for realistic values of aspect ratio. This does not imply that excluded volume effects are not responsible for nematic formation in hard-body fluids, but rather that it is necessary to improve Onsager's theory in order to obtain quantitative predictions. To this effect, some proposals have been considered and are reviewed later.

Calculation of virial coefficients are normally done for a constant orientational distribution $h(\hat{\Omega}) = 1/4\pi$ or zero-order parameter $Q = 0$. In contrast, Velasco and Padilla [26] used Monte Carlo integration to calculate $B_3[h]-B_5[h]$ for the HGO model, in the range $\kappa = 1-10^5$, by parameterizing $h(\hat{\Omega})$ in terms of Q , thus obtaining the virial coefficients in the nematic phase as $B_n(Q)$ in the range $Q = 0-1$. The vanishing of the virial coefficients in the hard-needle limit was confirmed and convergence was seen to be rather insensitive with respect to the order parameter, indicating that Onsager theory is valid in the limit $\kappa \rightarrow \infty$.

Onsager theory has played a very important role in our qualitative understanding of orientational ordering, bringing the concept of particle excluded volume to the forefront. It is indeed remarkable that a simple second-order virial theory, based solely on two-particle interactions, can explain a phase transition; this is a singular case in the theory of phase

transitions. The virial expansion is useful to connect the ideal gas to denser gases, i.e. fluids where interactions begin to be relevant, but in standard fluids of isotropic particles there is still a long way between the low-order virial expansion and the real equation of state of a liquid. However, the nematic phase is a peculiar example where a phase transition to an ordered state can be understood in terms of the first term in the virial expansion, i.e. the second virial coefficient.

By the time Onsager presented his theory, computer simulations of phase transitions for condensed matter were not feasible. With the advent of powerful computers in the 70s, it was possible to obtain accurate predictions and put Onsager's theory to the test. Up to now many simulations on hard bodies have been performed, using MC or MD techniques. A good starting point to review the subject is [19]. Several works have specifically focused on devising algorithms for efficiently obtaining contact distances of hard bodies, particularly ellipsoids [55]. The first simulations of a liquid crystal were performed by Vieillard-Baron [56] (1972), who used Monte Carlo simulation to study a fluid of 2D hard ellipses. He observed the formation of an orientationally ordered phase, although the system studied was later revealed to be too small to obtain any quantitative conclusion. Much later, Frenkel *et al* [24] (1984) studied a fluid of hard ellipsoids. The entire phase diagram, including I, N and crystal phases, was mapped out as a function of density and aspect ratio, including prolate and oblate particles. For low aspect ratios a plastic phase was also detected. The smectic phase was not stabilized in this fluid.

In a more extensive simulation work involving free energy calculations, Frenkel and Mulder [57] studied the density stability interval of the N phase of hard ellipsoids and concluded that, for aspect ratio 3, it was very narrow. But the stability of this fluid was called into question by Zarragoicoechea *et al* [58], who concluded from their own MC simulations that the stability of the nematic phase was due to the small system size of the samples. In an effort to solve the issue, Allen and Mason [313] performed MC and MD simulations to examine the stability of the N phase of hard ellipsoids with aspect ratio 3, using system sizes larger than previously. Although they recognized the existence of system size effects, the N phase was observed to be stable. The first simulations of a liquid crystal exploring the effect of fluctuations was performed in 1987 [60], where dynamical precursors of the I–N transition in hard ellipsoids were observed. All analyses and simulation works have concluded that the Onsager theory is qualitatively valid, but the truncated virial expansion after the second coefficient is only valid for aspect ratios $L/D \gtrsim 100$ and predictions for particles with realistic aspect ratios are unreliable [61].

3.1.3. Extended Onsager theories. There have been a number of attempts to improve Onsager theory, in an effort to make it applicable to realistic particle lengths. Three approaches have been proposed. The first incorporates the contribution of third- and higher-order virial coefficients to the Onsager functional. In the second, angular correlations are treated at the Onsager level (second virial coefficient), but spatial correlations are improved using the decoupling approximation. Mixed theories have been proposed in an attempt to treat the

coupling of both, spatial and angular correlations, in a more quantitative fashion. Finally, an approach based on the developments of Fundamental Measure Theory for HS, extended to anisotropic bodies, has been proposed. In principle, this approach improves the spatial-orientational coupling. Except for the special case of a mixture of freely rotating needles and discs, it has been applied in the restricted-orientation approximation, although there have been recent developments to extend the theory to freely rotating particles, as reviewed later.

Straley [62] calculated B_3 numerically for hard rods of aspect ratios 10–100 and proposed a corresponding model which approximated its angular dependence. He estimated the correction of B_3 to the results of Onsager's theory and concluded that the theory is not accurate for $\kappa < 100$. Tjijto-Margo and Evans [63] considered the incorporation of the third virial coefficient B_3 , using hard ellipsoids as a particle model. For aspect ratios larger than 5, the extended theory predicts the correct variation of the order parameter with density as compared with simulations. The results are poorer in the case of shorter particles. A way to incorporate the third virial coefficient in the y -expansion of Barbooy and Gelbart [64] was presented and the corresponding results for the transition densities were seen to agree with the MC simulations of Frenkel and Mulder [65]. Padilla and Velasco [25] obtained the virial coefficients B_3 and B_4 of HGO particles from Monte Carlo integration, both as functions of the uniaxial nematic order parameter and used them to study the convergence of the virial series in terms of the results for the I–N transition. The series was seen to converge quite fast in the case of $\kappa = 5$, but not for aspect ratio equal to 3. Although theoretically interesting, all of these approaches are not practical since the calculation of high-order virial coefficients is intractable for most hard-particle models.

More recently, You *et al* [53] calculated virial coefficients up to seventh-order for the isotropic phases of hard ellipsoids, spherocylinders and truncated hard spheres for different aspect ratios, with a view to studying the convergence properties of the virial series. The radius of convergence was seen to be close to the close-packing limit for low aspect ratio and to be considerably less than the close-packed density for higher aspect ratios.

In the 70s, Cotter and co-workers [66, 67] derived equations of state for a fluid of perfectly aligned rods, applying a generalization of the scaled-particle theory (SPT) of Reiss *et al* for HS [68] to parallel anisotropic particles. The theory was then generalized to a set of restricted orientations and results for the equation of state and the I–N transition were obtained [69]. Lasher [39] modified SPT theory and obtained an extended Onsager expression that corrected Onsager theory. The results of the generalized SPT theory, in the low-density limit, were compared to the then existing theories, including that of Flory [70] and Alben [71] (formulated on a lattice), by Straley [61] (a review of these early theories can be found in this reference). A problem with these theories is that angular correlations are still considered at the level of two particles but, for short particles, it is clear that higher-order angular correlations, represented by virial coefficients beyond the second, are important. Despite recent efforts in this direction, this question is as yet unsolved.

SPT and similar theories can be regarded as resummations of the virial expansion. Barbooy and Gelbart [64] introduced the y -expansion for general hard bodies, a type of truncated Padé approximant resummation based on the variable $y = \eta/(1 - \eta)$, where η is the packing fraction. This expansion is closely related with the SPT theory, exhibits better convergence properties than the usual virial expansion based on the density and incorporates higher-order virial coefficients in a systematic way (providing these are known for the model at hand). The method was applied, in particular, to dumbbells and spherocylinders in the isotropic phase [64], but oriented fluids (hard parallelepipeds) were studied later, using the restricted-orientation (Zwanzig) approximation, in [72]. Comparison with previous virial expansions and Padé approximants was made, but no clear superiority of the theory, both quantitatively and in the practical implementation, was inferred.

In the 80s some further proposals in the theory of nematic ordering were made, using a seemingly different perspective which at the end was interpreted as yet another resummation theory providing qualitatively, if not quantitatively, similar results as previous theories. Therefore, in all of these approaches angular correlations are kept at the level of the second-order virial coefficient. Already in 1979 Parsons [73] made an interesting proposal, considering potentials of the form $\phi(r/\sigma(\hat{r}, \hat{\Omega}, \hat{\Omega}'))$, where $\sigma(\hat{r}, \hat{\Omega}, \hat{\Omega}')$ is the contact distance function. He showed that, if the radial distribution function $g(r, \hat{\Omega}, \hat{\Omega}')$ can be scaled as

$$g(r, \hat{\Omega}, \hat{\Omega}') = g_0\left(\frac{r}{\sigma(\hat{r}, \hat{\Omega}, \hat{\Omega}')}\right), \quad (23)$$

where g_0 is the corresponding function for a reference isotropic fluid, then the orientational and translational degrees of freedom decouple to all orders in the density expansion of the free energy. This approximation was proposed for the first time by Pynn [74, 75] and later used by Wulf [76] for the direct correlation function in the context of the solution of the Ornstein–Zernike equation for the I–N transition. Interestingly, as $\rho_0 \rightarrow 0$, the resulting free energy reduces to that of Onsager. By using a HS reference system and the corresponding equation of state, Parsons predicted a I–N phase transition at a packing fraction which decreased with rod aspect ratio. Also, using a perturbation theory in the softness m of the potential $\phi(r) = \epsilon/r^m$, predictions for soft potentials were made and seen to agree with experimental results for $m = 12$. Finally, Parsons concluded that most of the features of the I–N transition are due to the repulsive part of the interactions.

Later, Lee [77] rederived Parson's theory from a different but equivalent point of view, giving rise to the now known as *Parsons-Lee* (PL) theory. In Lee's approach the emphasis is on the equation of state. The approach starts from the Carnahan–Starling equation of state for HS and generalizes it to the nematic case using a simple (but a priori purely heuristic) functional scaling for the excess free energy, as

$$\frac{\beta F_{\text{ex}}[h]}{N} = \psi_{\text{HS}}(\eta) \frac{B_2[h]}{B_2^{(\text{HS})}}, \quad (24)$$

where $B_2[h]$ is the angle-averaged second virial coefficient, which was defined in (14), and $B_2^{(\text{HS})} = 4v_0$ is the second-order

virial coefficient of HS, equal to half the excluded volume of two HS ($v_{\text{exc}}^{(\text{HS})} = 8v_0$, $v_0 = \frac{\pi}{6}\sigma^3$ being the HS volume). η is the packing fraction of the actual fluid *and* of the reference HS fluid; therefore, the fluid is mapped onto a HS fluid of equal packing fraction and density consisting of hard spheres of a volume equal to that of the actual anisotropic particles and any density-dependent function is scaled with the ratio of excluded volumes between the actual fluid and the reference HS fluid. $\Psi_{\text{HS}}(\eta)$ is the excess free energy per unit thermal energy kT and per particle of the HS fluid, obtained from the Carnahan–Starling theory, $\Psi_{\text{HS}}(\eta) = (4 - 3\eta)\eta/(1 - \eta)^2$, or from any other theory for the equation of state of the HS fluid. This approximation can be seen to be completely equivalent to the decoupling approximation of Parsons [73]. The theory was applied to HSC and good agreement with simulation as concerns the I–N transition was reported, even for fairly short particles. Lee also applied the theory to hard ellipsoids of revolution [78] and compared it with computer simulation. Again, as the aspect ratio of the particles becomes higher, the agreement is seen to improve. The theory again reduces to that of Onsager in the limit of low density.

The PL scaling, equation (24), can be obtained by approximating the virial coefficients of the fluid $B_n[h]$, which are functionals of the orientational distribution function $h(\hat{\Omega})$, in terms of those of the HS fluid, $B_n^{(\text{HS})}$, as

$$B_n[h] = B_n^{(\text{HS})} \frac{B_2[h]}{B_2^{(\text{HS})}}. \quad (25)$$

The virial expansion of the excess free energy functional $F_{\text{ex}}[h]$ can then be written as

$$\begin{aligned} \frac{\beta F_{\text{ex}}[h]}{N} &= \rho_0 B_2[h] + \frac{1}{2} \rho_0^2 B_3[h] + \dots \\ &\simeq \left(\rho_0 + \frac{1}{2} \rho_0^2 \frac{B_3^{(\text{HS})}}{B_2^{(\text{HS})}} + \dots \right) B_2[h] \\ &= \Psi_{\text{HS}}(\eta) \frac{B_2[h]}{B_2^{(\text{HS})}}. \end{aligned} \quad (26)$$

which coincides with equation (24). Since $\Psi_{\text{HS}}(\eta) \rightarrow 4\eta$ as $\eta = \rho_0 v_0 \rightarrow 0$ and $B_2^{(\text{HS})} = 4v_0$, we see that $\beta F_{\text{ex}}[h]/N \rightarrow \rho_0 B_2[h]$ and therefore the PL theory recovers the Onsager theory (16) in the low-density limit.

By about the same time as Lee but independently, a close version of the PL theory was proposed by Baus and co-workers [79, 80], using yet another perspective. These authors started from the exact excess free energy functional for a general nonuniform fluid in terms of the direct correlation functional,

$$c^{(2)}(\mathbf{r}, \mathbf{r}', \hat{\Omega}, \hat{\Omega}') = - \frac{\delta^2 \beta F_{\text{ex}}[\rho]}{\delta \rho(\mathbf{r}, \hat{\Omega}) \delta \rho(\mathbf{r}', \hat{\Omega}')}. \quad (27)$$

Double functional integration of this equation along a path joining a reference uniform fluid of density ρ_0 and the actual nonuniform fluid, $\rho_\lambda(\mathbf{r}, \hat{\Omega}) = \rho_0 + \lambda[\rho(\mathbf{r}, \hat{\Omega}) - \rho_0]$, where λ is a coupling parameter, leads to

$$\begin{aligned} F_{\text{ex}}[\rho] &= F_{\text{ex}}^{(0)}(\rho_0) - \int_V d\mathbf{r} \int_V d\mathbf{r}' \int d\hat{\Omega} \int d\hat{\Omega}' \int_0^1 d\lambda (1 - \lambda) \\ &\quad \times [\rho(\mathbf{r}, \hat{\Omega}) - \rho_0][\rho(\mathbf{r}', \hat{\Omega}') - \rho_0] \\ &\quad \times c^{(2)}(\mathbf{r}, \mathbf{r}', \hat{\Omega}, \hat{\Omega}'; [\rho_\lambda]). \end{aligned} \quad (28)$$

Baus *et al* consider the uniform phases $\rho(\mathbf{r}, \hat{\Omega}) = \rho_0 h(\hat{\Omega})$, of a fluid of HE particles of lengths σ_{\parallel} (along the symmetry axis) and σ_{\perp} (in the directions perpendicular to the symmetry axis), aspect ratio $\kappa = \sigma_{\parallel}/\sigma_{\perp}$ and volume $v_0 = \pi \sigma_{\parallel} \sigma_{\perp}^2/6$. Now one approximates the direct correlation function by introducing a decoupling approximation:

$$c^{(2)}(\mathbf{r}, \mathbf{r}', \hat{\Omega}, \hat{\Omega}') \simeq c_0^{(2)} \left(\frac{|\mathbf{r} - \mathbf{r}'|}{\sigma_0}; \bar{\eta} \right) \frac{v_{\text{excl}}(\hat{\Omega}, \hat{\Omega}')}{v_0}, \quad (29)$$

where the reference system is a fluid of HS of diameter σ_0 and the same volume, $v_0 = \frac{\pi}{6}\sigma_0^3$. This expression has a structure reminiscent of that in PL theory, see equations (23)–(25). The angular factor $v_{\text{excl}}(\hat{\Omega}, \hat{\Omega}')$ is the excluded volume of two HE particles, which is further approximated by that of two hard Gaussian overlap particles, i.e.

$$v_{\text{excl}}(\hat{\Omega}, \hat{\Omega}') = \left\{ \frac{1 - \chi^2(\hat{\Omega} \cdot \hat{\Omega}')^2}{1 - \chi^2} \right\}^{1/2}, \quad (30)$$

with $\chi = (\kappa^2 - 1)/(\kappa^2 + 1)$. The direct correlation function of the reference HS fluid is taken from the Percus–Yevick approximation. All that remains to specify is the criterion to calculate the effective packing fraction $\bar{\eta}$ where the correlation function is to be evaluated. In the I phase they take $\bar{\eta} = \eta = \rho_0 v_0$. However, in the N phase orientational order leads to an effective reduction of interactions. This is similar to the situation in the HS crystal: the highly oscillating spatial structure of the distribution function comes from the highly peaked periodic local density and the proper correlation is a smooth function of the particle positions similar to that of a low-density fluid. In the N phase, the high anisotropy of the orientational correlations comes mainly from the distribution function $h(\hat{\Omega})$ and proper orientational correlations are very accurately given by the two-particle low-density limit. Consequently, in the N phase we expect $\bar{\eta} < \eta$. To establish the precise relationship between η and $\bar{\eta}$, Baus *et al* proposed a criterion based on a structural scaling condition between the HE and the reference HS which takes into account the geometric constraints of the nematic phase. To do that, they assumed that, at contact, the direct correlation functions of the HS system, evaluated at the real and at the effective density, are related by,

$$c_{\text{PY}} \left(\frac{|\mathbf{r}|}{\sigma_0} = 1; \eta \right) = c_{\text{PY}} \left(\frac{|\mathbf{r}|}{\sigma_0} = x(\kappa); \bar{\eta} \right). \quad (31)$$

σ_0 , the reference HS diameter, is the average contact distance of the HE in the isotropic phase, whereas $\sigma_0 x$ (with $x < 1$) is the average contact distance of the HE in the nematic phase. Since κ is the natural length scale of the problem, they put $x = \kappa$ when $\kappa < 1$ and $x = 1/\kappa$ when $\kappa > 1$. The Percus–Yevick result for the direct correlation function of HS was used in the practical implementation of the criterion. It is then easy to realize that the theory of Baus *et al* reduces to the PL theory: it is a decoupling approximation with the same orientational factor, a different density prefactor, the same reference fluid but evaluated at a different effective density in the N phase. The theory was applied to the study of the I and N equations of state and the I–N transition in systems of HE of different aspect

ratios. Results in fair agreement with the computer simulation studies were obtained (see original papers for details).

The PL theory and other resummations incorporating higher-order virial coefficients have been contrasted with computer simulations by Padilla and Velasco [25] for moderately long particles in the case of the hard Gaussian overlap fluid. They used DFT to obtain the pressure, order parameter and I–N transition point and compared this with computer simulation results for aspect ratios 3–5. Different theories were used. First, a decoupling approximation with an isotropic hard Gaussian overlap fluid instead of a hard-sphere fluid as a reference fluid was used. The former was seen to give a closer agreement with the simulation, but both overestimate the transition density since angular correlations are represented at the same level in both theories. Second, extended decoupling approximations incorporating B_3 and B_4 , obtained using a technique similar to that in [63], were seen to give improved results over the standard decoupling approximation since they incorporate higher-order angular correlations.

Williamson [81] made a comparison of the results from PL scaling and related theories with simulation, using an annealing technique to minimize the functional that does not assume any particular form for the orientational distribution function. The original PL scaling was found to give the best results. Further comparison between Parsons–Lee and MC simulation was made in [82], where excellent agreement for the isotropic and nematic branches and reasonably accurate coexistence densities and pressures were found. Again, the corresponding orientational distribution function at the phase transition was not accurately reproduced.

Some of the previous works on calamitic (rod-like) nematics have been paralleled by corresponding studies on discotic systems. These systems are made of disc-like particles, which can also form nematic phases. In fact, many of the studies have been motivated by, or have motivated, experimental studies on colloidal suspensions of plate-like particles. Many of these particles can be synthesized and prepared such that the particles interact in solution like (or close to) hard particles, which made it possible to test the predictions of theories for oblate hard bodies. However, except for the early observation of nematic ordering in solutions of platelets by Langmuir [83], the nematic phase of these colloids has been elusive until relatively recently [34, 84], due to the large tendency of these systems to form gel phases.

In fact, Onsager already made predictions for a model of oblate particle consisting of infinitely thin circular platelets. The first simulation of nematic ordering was made precisely on a system of infinitely thin platelets [85]. Comparing with Onsager’s theory, this study evidenced the poorer predictions made by the Onsager theory in the case of platelets. This is no surprise: Onsager theory neglects virial coefficients beyond the second, which are very important in the case of platelets. Discotic liquid crystals will be discussed in more detail in section 3.2.

3.1.4. Nonuniform phases: extended Onsager and others. Since entropy alone can explain freezing of the HS fluid into a stable periodic face-centred cubic structure, it is legitimate

to wonder if anisotropic hard interactions can stabilize the S phase, the more symmetric liquid-crystalline phase beyond the N phase. The first attempts to formulate statistical-mechanical theories to deal with nonuniform liquid-crystalline phases date back to the 70s [86, 87] and 80s [88]. Hosino *et al* [86] and Wen *et al* [88] investigated a fluid of aligned rods using a second-order virial approximation and a bifurcation analysis. The first group also studied the effect of orientational fluctuations [87] using a discrete-orientation approximation. These works were the first evidence that hard rods and, consequently, excluded volume interactions, could induce the formation of liquid-crystalline phases with spatial order. The origin lies in the more efficient packing of rods in a layered configuration. Specifically, the entropy reduction associated with ordering along one dimension is more than compensated, at sufficiently high density, by the increased entropy due to an optimized free volume due to the arrangement of particles into layers.

Some time after the work of Hosino *et al*, Stroobants *et al* [89, 90] studied a fluid of perfectly parallel HSC by MC simulations and observed a N–S continuous transition, followed by a first-order S-crystal transition. The formation of a layered phase in a fluid of parallel HSC is a nontrivial result, considering that the parallel HE model cannot stabilize into a layered structure (since its free energy can be exactly mapped onto that of a HS fluid, which does not possess order intermediate between the fluid and the crystal). Evidence that S ordering was robust when free particle orientations were included came a few years later [91]. Confirmation of the stability of the smectic phase in colloidal fluids of approximately hard rods came from the work of Wen *et al* [92], who observed layered phases in colloidal suspensions of the tobacco mosaic virus and in-layer undulational fluctuations.

A few years before, Mulder [93] proposed a virial expansion for the excess free energy of a fluid of parallel hard rods, including an Onsager-like, second-order term, and also the third- and fourth-order virial coefficients, assuming smectic symmetry. Since particle orientations are assumed to be frozen along the director, taken along the \hat{z} unit vector, the full local particle density can be simplified, $\rho(\mathbf{r}, \hat{\Omega}) = \rho(z)\delta(\hat{\Omega} - \hat{z})$. As usual, the Helmholtz free energy functional is split in ideal and excess terms, $F[\rho] = F_{id}[\rho] + F_{ex}[\rho]$. The ideal part is

$$\begin{aligned} \beta F_{id}[\rho] &= \int_V d\mathbf{r} \int d\hat{\Omega} \rho(\mathbf{r}, \hat{\Omega}) \left[\log(\rho(\mathbf{r}, \hat{\Omega})\Lambda^3) - 1 \right] \\ &= A \int_L dz \rho(z) \left[\log(\rho(z)\Lambda^3) - 1 \right], \end{aligned} \quad (32)$$

where L is the linear dimension of the system along the z direction and A the system area in the other two perpendicular directions. The excess part can be written as a virial expansion:

$$\begin{aligned} \beta F_{ex}[\rho] &= -\frac{1}{2} \int_V d\mathbf{r} \int_V d\mathbf{r}' \int d\hat{\Omega} \int d\hat{\Omega}' \\ &\quad \times \rho(\mathbf{r}, \hat{\Omega}) \rho(\mathbf{r}', \hat{\Omega}') f(\mathbf{r} - \mathbf{r}', \hat{\Omega}, \hat{\Omega}') \\ &\quad - \frac{1}{6} \int_V d\mathbf{r} \int_V d\mathbf{r}' \int_V d\mathbf{r}'' \int d\hat{\Omega} \int d\hat{\Omega}' \\ &\quad \times \int d\hat{\Omega}'' \rho(\mathbf{r}, \hat{\Omega}) \rho(\mathbf{r}', \hat{\Omega}') \rho(\mathbf{r}'', \hat{\Omega}'') \end{aligned}$$

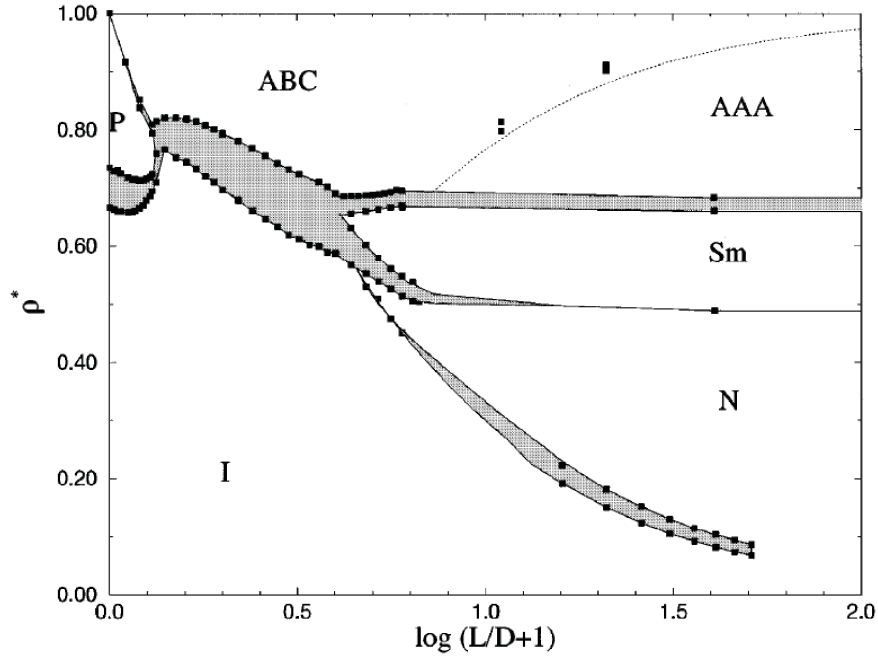


Figure 3. Phase diagram of a system of freely rotating HSC, as calculated from computer simulation [96], in the density-aspect ratio plane (density is $\rho^* = \rho/\rho_{CP}$, where ρ_{CP} is the close-packing density). Symbols indicate regions of stability of the phases: *I*, isotropic; *N*, nematic; *Sm*, smectic; *P*, plastic solid; *AAA* and *ABC*, different stackings of crystal phases. Shaded regions correspond to two-phase regions. Reprinted with permission from [96]. Copyright (1997), AIP Publishing LLC.

$$\begin{aligned} & \times f(\mathbf{r} - \mathbf{r}', \hat{\Omega}, \hat{\Omega}') f(\mathbf{r}' - \mathbf{r}'', \hat{\Omega}', \hat{\Omega}'') \\ & \times f(\mathbf{r} - \mathbf{r}'', \hat{\Omega}, \hat{\Omega}'') + \dots \end{aligned} \quad (33)$$

Invoking the translational symmetry of the fluid in the *xy* plane, the functional can be written as

$$\begin{aligned} \frac{\beta F[\rho]}{A} &= \int_L dz \rho(z) [\log(\rho(z) \Lambda^3) - 1] \\ &+ \int_L dz \int_L dz' \rho(z) \rho(z') B_2^{\parallel}(z, z') \\ &+ \frac{1}{2} \int_L dz \int_L dz' \int_L dz'' \rho(z) \rho(z') \rho(z'') \\ &\times B_3^{\parallel}(z, z', z'') + \dots \end{aligned} \quad (34)$$

where B_n^{\parallel} are projected virial coefficients, the first two of which are given by

$$\begin{aligned} B_2^{\parallel}(z, z') &= -\frac{1}{2} \int_A d\mathbf{r}'_{\perp} f_{\parallel}(\mathbf{r}'_{\perp}, z - z'), \\ B_3^{\parallel}(z, z', z'') &= -\frac{1}{3} \int_A d\mathbf{r}'_{\perp} \int_A d\mathbf{r}''_{\perp} f_{\parallel}(\mathbf{r}'_{\perp}, z - z') \\ &\times f_{\parallel}(\mathbf{r}'_{\perp} - \mathbf{r}''_{\perp}, z' - z'') f_{\parallel}(\mathbf{r}''_{\perp}, z - z''), \end{aligned} \quad (35)$$

and f_{\parallel} is the Mayer function of parallel particles. Expressions for higher-order virial coefficients can be written from the standard virial expansion (see, e.g. [94, 95]). The frozen-orientation approximation facilitates enormously the calculation of the first virial coefficient and Mulder [93] managed to calculate virial coefficients for parallel HC up to the fourth. The occurrence of S order was analyzed using a bifurcation analysis of the free energy functional truncated

at second-order and the effect of the higher-order terms in the bifurcation point was discussed. A continuous transition from the nematic to the smectic phase was found, at a density and smectic period in quite good agreement with computer simulations of the same model.

The complete phase diagram of hard spherocylinders, in the density versus aspect ratio $\kappa = L/D$ plane, has now been mapped out in detail by simulation [96, 82] for the whole range of aspect ratios $\kappa = 0 - \infty$ and for the freely rotating model (see figure 3). There exists a terminal aspect ratio, below which the N phase ceases to be stable and there is direct coexistence between I and S_A phases. For low values of κ a plastic phase is formed. The crystal phase has AAA or ABC stacking depending on the aspect ratio.

Esposito and Evans [97] presented an Onsager-like density functional theory for the nematic-smectic bifurcation point which was in fair agreement with the simulation data. The theory incorporated third- and higher-order correlations in an ad hoc manner and included orientational freedom, which allowed these workers to present a density-aspect ratio phase diagram including isotropic, nematic and smectic A phases. The triple point location coincided with that from the then existing theories, but the nematic-to-smectic transition was always found to be of first-order, regardless of the value of aspect ratio. This is in contrast with predictions from more sophisticated theories, which found either a continuous transition or a tricritical point at which the character of the transition changed from first-order to continuous. Therefore, this theory indicated that the N-S transition is of first-order and becomes continuous only in the strict limit of parallel particles.

The reason why a fluid of hard parallel spherocylinders induces a layered phase is a subtle one, since a corresponding

system of ellipsoid does not. This point has been investigated by Evans [98], who considered a PL theory on particles of different shapes: ellipsoids, spherocylinders and ellipo-cylinders (a particle that interpolates between the latter two). Nematic fluids of particles with both frozen and free orientations were considered. All particles formed a S phase, except ellipsoids, which were revealed as pathological in that respect.

This conclusion was further supported by Martínez-Ratón and Velasco [99] in 2008, who considered systems of parallel hard superellipsoids of revolution, which can be viewed as an interpolation between ellipsoids of revolution and cylinders. The shape of the particles is given by the equation:

$$\left(\frac{R}{a}\right)^{2\alpha} + \left(\frac{z}{b}\right)^{2\alpha} = 1, \quad R = \sqrt{x^2 + y^2}. \quad (36)$$

Particles are characterized by a shape parameter α (with $\alpha = 1$ corresponding to ellipsoids of revolution, while $\alpha = \infty$ is the limit of cylinders). Using computer simulation, it was shown that above a critical value $\alpha > 1.2$, the smectic phase is stabilized. This value is surprisingly close to that of ellipsoids. Also, Martínez-Ratón and Velasco used a PL approach combined with free-volume theory for the solid phases to obtain a complete phase diagram exhibiting regions of smectic, columnar and crystalline ordering (see figure 4). Comparison with simulation results of Veerman and Frenkel [100] for cylinders and superellipsoids of different shapes [99] was reasonable.

In 1989, Taylor *et al* [102] presented a theory for a fluid of parallel HSC that combined ideas from scaled particle theory and cell theory. The idea was to decouple the spatial directions associated with order from those where the system is disordered and apply a cell theory to the first and scaled particle theory to the second. Correspondingly the total free energy was written as a sum of two contributions. The theory was the first to give a complete phase diagram of the model and good qualitative agreement with existing simulations [90] was shown. The layer spacing at the N–S transition, in particular, was quantitatively correct. However, the theory was limited in that all phase transitions were required to be discontinuous by construction, which is incorrect in most instances, in particular in the case of the N–S transition. Also, density gaps are overestimated for first-order phase transitions.

In 1992, Baus and co-workers [103] studied the N–S transition of the same model using their version of the scaled Onsager theory, together with ideas from the density functional theory for HS freezing. They start from the exact expression for the excess free energy functional in terms of the direct correlation function, given by equation (28). The direct correlation function is then approximated as that of a spatially uniform fluid evaluated at an effective density $\bar{\rho}$,

$$c^{(2)}(\mathbf{r}, \mathbf{r}', \hat{\Omega}, \hat{\Omega}'; [\rho]) = c_0^{(2)}(\mathbf{r} - \mathbf{r}', \hat{\Omega}, \hat{\Omega}'; \bar{\rho}[\rho]). \quad (37)$$

Since the determination of the function $c_0^{(2)}(\mathbf{r}, \hat{\Omega}, \hat{\Omega}'; \bar{\rho})$ in the case of nonspherical particles is a rather complicated problem by itself, Baus *et al* proposed a further simplification by approximating $c_0^{(2)}(\mathbf{r}, \hat{\Omega}, \hat{\Omega}'; \bar{\rho})$ in the case of parallel HSC in terms of the Percus–Yevick direct correlation function of hard spheres of diameter σ equal to the contact distance between

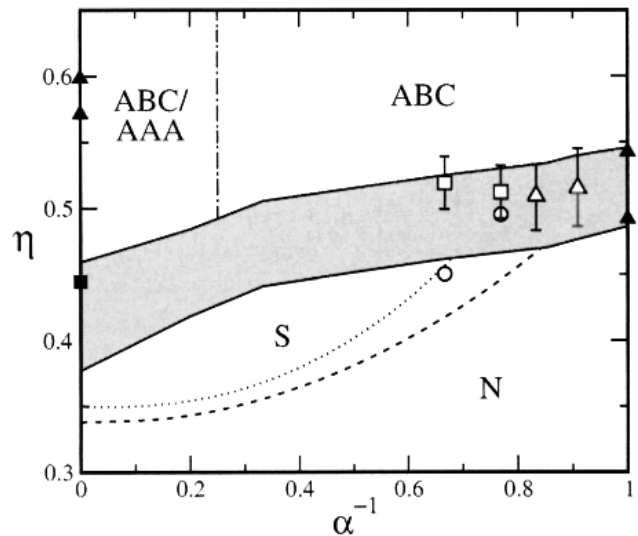


Figure 4. Phase diagram packing fraction-inverse shape parameter α^{-1} of parallel hard superellipsoids as obtained in [99]. Continuous lines: coexistence boundaries for the smectic-solid transition using PL theory for the smectic and free-volume theory for the solid. Dashed line: nematic-smectic spinodal line from PL theory; dotted line: nematic-smectic spinodal line from the theory of Mulder [93]. Filled triangles: simulation results for the smectic-solid transition of parallel cylinders [100] and for liquid-solid coexistence in hard spheres [101]. Filled square: nematic-smectic spinodal from computer simulation of Veerman and Frenkel [100]. Open symbols: simulation estimates for nematic-smectic spinodal (circles), first-order smectic-solid transition (squares) and for first-order nematic-solid transition (triangles) [99]. Labels indicate stable phases: *N*, nematic; *S*, smectic; *ABC* and *AAA*, crystalline solids with corresponding symmetries. Vertical dot-dashed line: approximate limit of degeneracy of *ABC* and *AAA* structures within free-volume theory. Reprinted with permission from [99]. Copyright (2008), AIP Publishing LLC.

two (parallel) HSC. To complete the approximation, a recipe to determine $\bar{\rho}$ in terms of the density profile $\rho(\mathbf{r})$ in the different phases is needed. In the *N* phase the density profile is constant, $\rho(\mathbf{r}) = \rho$ and, therefore, $\bar{\rho}$ is also constant and equal to ρ . In the *S* phase, however, the density profile has to reproduce the layered structure. Taking the layers to be perpendicular to the *z* direction, the density profile in the *S* phase only depends on *z* and it was parameterized as $\rho(z) = \rho [1 + \epsilon \cos(2\pi z/z_0)]$, ρ being now the mean smectic density, z_0 the layer spacing and ϵ , with $0 \leq \epsilon \leq 1$, the amplitude of the smectic-like oscillation. In the work of Baus *et al* only a bifurcation analysis was carried out, studying the stability of the *N* phase against smectic-like fluctuations with $\epsilon \ll 1$. In that case the density profile $\rho(z)$ only departs slightly from the mean smectic density ρ and, therefore, the same approximation $\bar{\rho}(z) = \rho$ was used for the *S* phase. The N–S transition of parallel HSC of aspect ratios up to $\kappa = 5$ was studied and good agreement with computer simulations was obtained.

3.1.5. Weighted density theories. More sophisticated and accurate theories, incorporating the orientational degrees of freedom, have been proposed to explain the transition to the smectic phase and other nonuniform phases such as the columnar. One of the problems with all existing theories was that they

assumed the parallel particle approximation, which is qualitatively valid in the N and S regimes but limits the possibility of quantitative analysis. Also, density correlations, crucial in understanding phases with spatial order, are poorly accounted for in all theories deriving from virial expansions. Some of the theories have been formulated for general nonuniform fluids and have also been applied to interfacial phenomena. The new theories grew out from developments made for HS in an effort to improve the local density approximation (which is useless to describe crystallization in the HS model) and used ideas from the corresponding density functional approximations for HS. The central quantity in these theories is the *average density*, a local density that takes into account the density distribution in the neighbourhood of a point. The average density is a convolution of the real density and a weighting function which describes the properties of the environment and whose details are optimized to give the correct bulk properties of the HS fluid. A review of these *weighted density approximation* (WDA) functionals can be found, among other sources, in [104].

In WDA theory for the HS system, the excess free energy is written as

$$\beta F_{\text{ex}}[\rho] = \int_V d\mathbf{r} \rho(\mathbf{r}) \Psi(\bar{\rho}(\mathbf{r})), \quad (38)$$

where $\Psi(\bar{\rho})$ is the excess free energy per particle of a uniform isotropic fluid evaluated at the local weighted density $\bar{\rho}(\mathbf{r})$, which averages the fluid structure within a neighbourhood of the point \mathbf{r} . The weighted density is calculated as a convolution $\bar{\rho}(\mathbf{r}) = \int_V d\mathbf{r}' \omega(\mathbf{r} - \mathbf{r}') \rho(\mathbf{r}')$ and the weight function $\omega(\mathbf{r})$ is obtained by imposing the functional to recover a particular approximation for the equation of state and direct correlation function of the uniform phase. This function, which has a range of the order of the sphere diameter σ_0 , can be made to depend on the averaged density, which gives a powerful self-consistency to the theory. Two extensions of the WDA for HS to hard-rod fluids have been proposed to account for the effects of particle anisotropy and free orientations.

Poniewierski and Hołyst [105] proposed a weighted density functional (called the *smoothed density approximation*, SDA) for general convex anisotropic bodies, focusing on a fluid of HSC. This theory used ideas from the corresponding density functional approximations for hard spheres. Let $\rho(\mathbf{r})$ be the angle-averaged one-particle distribution function $\rho(\mathbf{r}, \hat{\Omega})$, i.e. $\rho(\mathbf{r}) = \int d\hat{\Omega} \rho(\mathbf{r}, \hat{\Omega})$. The orientational dependence in the model is taken care of by assuming the following form for the average density:

$$\begin{aligned} \bar{\rho}(\mathbf{r}) &= \frac{1}{\rho(\mathbf{r})} \int_V d\mathbf{r}' \int d\hat{\Omega} \int d\hat{\Omega}' \omega(\mathbf{r} - \mathbf{r}', \hat{\Omega}, \hat{\Omega}') \\ &\quad \times \rho(\mathbf{r}, \hat{\Omega}) \rho(\mathbf{r}', \hat{\Omega}'), \end{aligned} \quad (39)$$

The model is specified by giving $\Psi(\rho)$ and $\omega(\mathbf{r}, \hat{\Omega}, \hat{\Omega}')$. The latter was taken as

$$\omega(\mathbf{r}, \hat{\Omega}, \hat{\Omega}') = -\frac{1}{2B_2^{(\text{iso})}} f(\mathbf{r}, \hat{\Omega}, \hat{\Omega}'), \quad (40)$$

where f is the Mayer function of two spherocylinders and $B_2^{(\text{iso})}$ is the second virial coefficient for the isotropic fluid. The

excess free energy density is chosen as

$$\beta \Psi(\rho) = \rho_0 B_2^{(\text{iso})} + [\beta \Psi^{(\text{cs})}(\eta) - 4\eta]. \quad (41)$$

Here $\Psi^{(\text{cs})}(\eta)$ is the Carnahan–Starling excess free energy per particle of a fluid of HS and the packing fraction is $\eta = \rho_0 v_0$, with v_0 the volume of a spherocylinder. This choice for $\Psi(\rho)$ guarantees that the correct first term of the virial expansion is recovered when $\rho_0 \rightarrow 0$ (and hence the Onsager limit when $L/D \rightarrow \infty$). Interestingly, in the opposite limit $L/D \rightarrow 0$ (HS limit), $\Psi(\rho) \rightarrow \Psi^{(\text{cs})}(\eta)$ and Tarazona’s first version of WDA for HS [106] is recovered. The theory was applied to a fluid of hard spherocylinders with full orientational freedom. The isotropic-nematic transition was obtained, using the parameterized form (19). As usual, the order parameter at the transition is overestimated and the pressure underestimated. A lower bound $L/D = 2.46$ for the existence of a nematic phase was found (to be compared with 3.7 from the simulations [96]). Also, the nematic-smectic transition was located using a bifurcation analysis, assuming the transition was continuous. Lifting this assumption, the nature of the transition was found to change from first-order to continuous at $L/D = 6$, which is then a tricritical point. For $L/D = 5$ the results were compared with simulations and very good agreement was found for the spinodal density and the smectic spacing at the transition (although the latter exhibits an unphysical maximum near the transition). More details on the theory and of its implementation were given later [107]. Hołyst and Poniewierski [108] also applied their theory to study a simpler system where orientations are frozen, i.e. a system of hard parallel cylinders. At the level of a bifurcation analysis, they obtained the spinodal line for the nematic-smectic A transition and argued that, at even higher densities, the system exhibits smectic B, columnar and solid phases.

At about the same time as Hołyst and Poniewierski but independently, Somoza and Tarazona (ST) [109–111] proposed an extension of Onsager theory in the line of the PL approach but valid for inhomogeneous fluids. The basic idea is that the mapping onto a HS fluid is inaccurate in a fluid with orientational order since the correlation structure along the director is very different from that in perpendicular directions. To correct this, Somoza and Tarazona proposed a reference fluid consisting of parallel HE of lengths σ_{\parallel} and σ_{\perp} , whose thermodynamics in turn can be mapped onto an equivalent fluid of HS of diameter σ_0 . The expression for the excess free energy is

$$\begin{aligned} \beta F_{\text{ex}}[\rho] &= \int_V d\mathbf{r} \int d\hat{\Omega} \rho(\mathbf{r}, \hat{\Omega}) \Psi(\bar{\rho}(\mathbf{r})) \\ &\quad \times \left\{ \frac{\int_V d\mathbf{r}' \int d\hat{\Omega}' \rho(\mathbf{r}', \hat{\Omega}') f(\mathbf{r} - \mathbf{r}', \hat{\Omega}, \hat{\Omega}')}{\int_V d\mathbf{r}' \rho(\mathbf{r}') f_{\text{PHE}}(\mathbf{r} - \mathbf{r}')} \right\}, \end{aligned} \quad (42)$$

where the weighted density $\bar{\rho}(\mathbf{r})$ is calculated from $\rho(\mathbf{r}) = \int d\hat{\Omega} \rho(\mathbf{r}, \hat{\Omega})$ as in the WDA theory for HS, but with a weight function $\omega(\mathbf{r})$ scaled by the factors $\sigma_{\parallel}/\sigma_0$ and σ_{\perp}/σ_0 in the directions parallel and perpendicular to the ellipsoids,

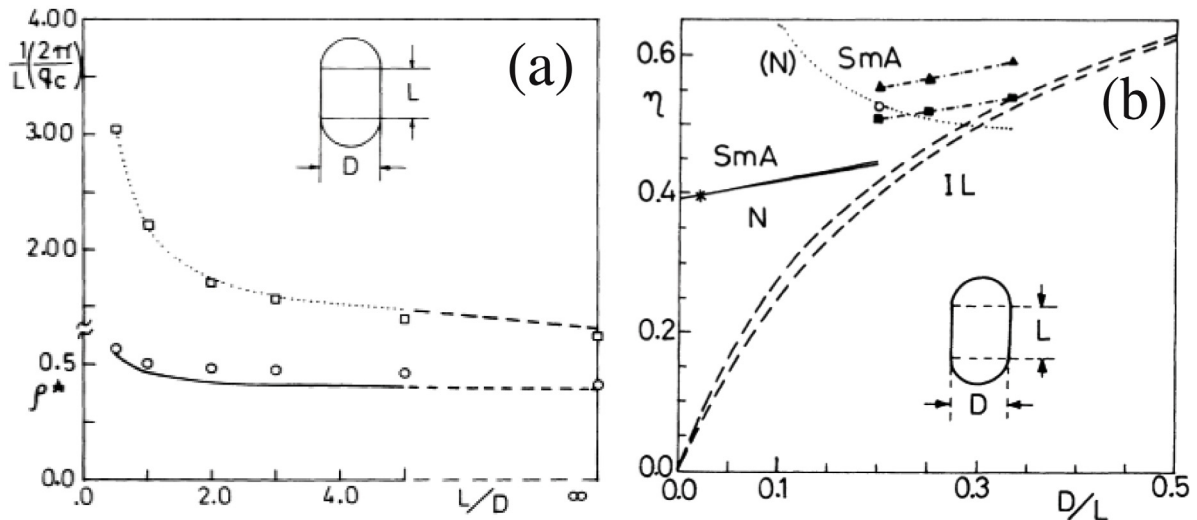


Figure 5. Results for the phase diagram of hard spherocylinders from the Somoza–Tarazona theory. (a) Parallel particles [109]. (b) Freely oriented particles [111]. Reprinted with permission from [109, 111]. Copyright (1988, 1990) by the American Physical Society.

respectively. In the N phase, $\rho(r, \hat{\Omega}) = \rho_0 h(\hat{\Omega})$ and $\bar{\rho}(r) = \rho_0$. Then equation (42) coincides with that from the Parsons–Lee theory (27), since the thermodynamics of a fluid of parallel HE is identical to that of HS. Therefore:

$$\beta F_{\text{ex}}[\rho] = \frac{\rho_0 \Psi(\rho_0)}{\int dr' f_{\text{PHE}}(r - r')} \int dr \int d\hat{\Omega} \times \int d\hat{\Omega}' h(\hat{\Omega}) h(\hat{\Omega}') v_{\text{excl}}(\hat{\Omega}, \hat{\Omega}'). \quad (43)$$

Note that the factor between curly brackets in (42) is the ratio between excluded volumes of the actual fluid and that of a reference fluid of parallel hard ellipsoids with the same spatial structure $\rho(r)$. The choice of reference ellipsoid can be made with different recipes (e.g. by demanding equal packing fraction and equal length-to-breadth ratio of the actual and ellipsoidal particles). A limited analysis of the theory was made in the first two papers [109, 110], assuming parallel particles. The phase diagram for parallel hard spherocylinders was calculated and remarkable agreement with computer simulations [90] was obtained, see figure 5(a). The ST theory was also applied to a fluid of parallel oblique cylinders and a full phase diagram with respect to the obliqueness parameter was obtained, containing nematic, smectic A, smectic C and biaxial (see figure 20 in section 3.3) phases. This work was the first to show that a transition between smectic A and smectic C phases was possible in a system of hard particles. A full implementation of the ST theory was made in [111], where the complete phase diagram of the hard-spherocylinder model was presented, figure 5(b). The theory included the isotropic-nematic transition, which gives the same results as the PL theory. An important feature of the theory is that it predicts a first-order nematic-smectic transition for $L/D < 50$ that changes over to continuous for $L/D > 50$, with $L/D = 50$ a tricritical point. In contrast, the SDA theory of Hołyst and Poniewierski predicted a tricritical point at $L/D = 6$. Although the results for the two transitions at $L/D = 5$ were

a bit worse than those of Hołyst and Poniewierski, the ST theory corrected the unphysical feature of the former in the predicted smectic spacing and also the slope of the nematic-smectic boundary with respect to the aspect ratio L/D and the limit $L/D \rightarrow \infty$. Overall the ST seems to work better for large aspect ratios, whereas the SDA theory is slightly more accurate for shorter particles. A discussion of the comparison between the SDA and ST theories was made by Poniewierski [112], who obtained a density functional based on the virial expansion, including the third-order term, valid in the asymptotic limit $L/D \rightarrow \infty$ but including corrections for finite L/D . However, the question on the existence and location of the tricritical point was not settled, since this point is very sensitive to higher-order particle correlations.

A more accurate implementation of the ST theory was done in [113], where the MC results of [96] were contrasted with the theory. Very good agreement with the simulations was found for both I–N and N–S transitions and for all the aspect ratios considered ($L/D = 3.5$ –10).

Graf and Lowën [114] made another proposal for a weighted density functional, adopting an extension of the modified weighted density approximation (MWDA) for the HS system. They write $F_{\text{ex}}[\rho]$ as

$$\beta F_{\text{ex}}[\rho] = N \Psi(\hat{\rho}), \quad (44)$$

where $\hat{\rho}$ is a global density obtained by averaging the average density

$$\bar{\rho}(r, \hat{\Omega}) = \int dr' \int d\hat{\Omega}' \omega(r - r', \hat{\Omega}, \hat{\Omega}') \rho(r', \hat{\Omega}') \quad (45)$$

in the whole volume:

$$\hat{\rho} = \frac{1}{N} \int dr \int d\hat{\Omega} \bar{\rho}(r, \hat{\Omega}) \rho(r, \hat{\Omega}). \quad (46)$$

The excess free energy $\Psi(\rho)$ and weighting function $w(r, \hat{\Omega}, \hat{\Omega}')$ are chosen as in the Poniewierski and Hołyst theory, i.e. using (41) and (40). The results of the ST theory are superior to those obtained by Graf and Lowën [114], since

the latter theory again predicts a wrong positive slope of the nematic-smectic phase boundary in the density– L/D phase diagram. The theory was later modified [115] to incorporate scaled particle and cell theory concepts, which results in correct slope and better predictions.

3.1.6. Fundamental measure theories. The Fundamental Measure Theory (FMT) is a WDA approximation, in that the free energy is built in terms of weighted densities, but has a deeper root based on geometrical grounds. The theory makes use of the concept of weighted densities, but here weighting functions are measures of one particle (and possibly more particles), whereas WDA approximations are built on measures of two particles.

The FMT was first developed by Rosenfeld [116, 117] for hard spheres. It is naturally formulated for a general mixture of hard particles. Rosenfeld proposed an excess free energy functional $F_{\text{ex}}[\{\rho_\nu\}]$ (where species are labelled with the index ν) that depends on a finite set of weighted densities $n_\alpha(\mathbf{r})$, the latter being a sum of convolutions of the local densities $\rho_\nu(\mathbf{r})$ and some weighting functions $\omega_\nu^{(\alpha)}(\mathbf{r})$, i.e.

$$n_\alpha(\mathbf{r}) = \sum_\nu \int d\mathbf{r}' \rho_\nu(\mathbf{r}') \omega_\nu^{(\alpha)}(\mathbf{r} - \mathbf{r}'). \quad (47)$$

The weights, which can be vectors or scalars, depend on the geometry of a single particle and their integrals result in the fundamental geometric measures of the sphere: the mean Gaussian curvature, the surface area and its volume. Let $\Phi(\mathbf{r})$ be the local excess free energy density in thermal energy units, so that

$$\beta F_{\text{ex}}[\{\rho_\nu\}] = \int_V d\mathbf{r} \Phi(\mathbf{r}). \quad (48)$$

To determine the dependence of the function $\Phi(\mathbf{r})$ on the weighted densities $\{n_\alpha\}$, two requirements were imposed. The first is related to the uniform limit, which was chosen to be obtained from the SPT theory [68]. The second requirement was related to the virial expansion of the direct correlation function, $c_{\mu\nu}^{(2)}(\mathbf{r}, \mathbf{r}') = -\delta^2 \beta F_{\text{ex}}[\{\rho_\nu\}] / \delta \rho_\mu(\mathbf{r}) \delta \rho_\nu(\mathbf{r}')$, which was demanded to recover the exact first (Mayer function) and second terms of the uniform limit.

A modified version of FMT for HS was subsequently proposed [118, 119] to correct a serious drawback of the first version, namely, the divergence of $F_{\text{ex}}[\{\rho_\nu\}]$ as the density profiles $\rho_\nu(\mathbf{r})$ become more and more localized. This problem caused the theory not to be able to predict crystallization in the one-component fluid of HS. In the new version the singularity was removed by redefining the dependence of $\Phi(\mathbf{r})$ on the weighted densities while maintaining the bulk equation of state and the correct low-density expansion of the direct correlation function. For a recent review of FMT for HS mixtures, see [120].

Finally, the modern versions of the FMT for HS were constructed from first principles using cavity theory [121]. The idea is to impose the fulfillment of an important requirement, namely the dimensional crossover property: when the density profile of a D -dimensional system is extremely constrained along one spatial dimension by freezing the degrees of

freedom of particles in that dimension (for example by making $\rho_D(x_1, \dots, x_D) = \rho_{D-1}(x_1, \dots, x_{D-1})\delta(x_D)$, where (x_1, \dots, x_D) are the components of a D -dimensional position vector), the D -dimensional density functional should reduce to the $D - 1$ functional. Also, the same principle holds for a collection of overlapping cavities with sizes such that only one particle fits in each cavity. Using this important property, density functionals for one-component HS [122] and HS mixtures [123] were obtained and it was realized that, apart from scalar and vectorial weighted densities, tensorial densities are also needed [124]. The resulting functional gives very accurate predictions for the HS crystal and, in particular, it was shown that the correct cell theory in the high density limit is recovered [122].

Recently it has been shown that the Rosenfeld functional, which was originally derived semi-heuristically, can be systematically calculated from the virial diagrammatic expansion including the clusters that represent particle overlap in one centre [125]. Further, this formulation has been extended to any particle geometry in any dimension and for any number of intersections [126]. Finally, the relation between the structures of the density functionals obtained from the dimensional crossover to 0D and from a resummation of a diagrammatic expansion that only considers certain classes of diagrams, was analyzed [127]. As a result, the zero-dimensional limit was reconciled, in an elegant way, with the virial approach.

In principle, the original ideas of Rosenfeld for HS mixtures could be applied to formulate a FMT functional for general hard anisotropic convex bodies. The procedure would involve first to exactly deconvolute the Mayer function in terms of one-particle weights and then use dimensional analysis to obtain a free energy as a sum of products of weighted densities up to third-order in density, ensuring that the expansion captures the exact first- and second-order terms of the direct correlation function. Since the free energy can be made to satisfy the same differential equation as in SPT, the packing fraction-dependent coefficients of this sum can be extracted, except for some numerical constants. These constants could be fixed by demanding the free energy to give the correct zeroth-dimensional (cavity) limit. In practice, this programme cannot be followed exactly for general convex bodies. Therefore, a version of FMT was proposed in the restricted-orientation or Zwanzig approximation (used before in some extended Onsager theories, see section 3.1.3) to treat fluids made of hard parallelepipeds (HP) [128–130]. An alternative procedure to obtain the density functional was proposed by Cuesta and Martínez-Ratón [129]. They realized that the free energy density of a mixture of HP can be obtained, in any dimensionality, starting solely from the exact zeroth-dimensional functional by applying a differential operator to it. For dimensionality $D = 3$ the result is

$$\Phi^{(3D)} = -n_0 \ln(1 - n_3) + \frac{n_1 \cdot n_2}{1 - n_3} + \frac{n_{2x} n_{2y} n_{2z}}{(1 - n_3)^2}, \quad (49)$$

with the usual definitions of weighted densities (47). The weights $\omega_\nu^{(\alpha)}(\mathbf{r})$ are given by

$$\omega_\nu^{(0)}(\mathbf{r}) = \frac{1}{8} \prod_\tau \delta \left(\frac{\sigma_\nu^{(\tau)}}{2} - |x_\tau| \right),$$

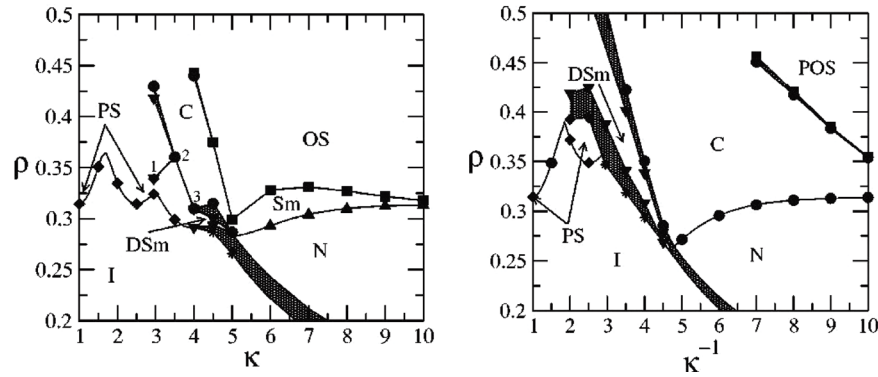


Figure 6. Phase diagrams in the density-aspect ratio plane for prolate (left) and oblate (right) hard parallelepipeds as obtained from a FMT using the restricted-orientation approximation, from [131]. Labels correspond to isotropic (I), nematic (N), columnar (C), smectic (Sm), discotic smectic (DSm), oriented solid (OS), plastic solid (PS) and perfectly oriented solid (POS) phases. Shaded areas correspond to two-phase coexistence regions. Reprinted with permission from [131]. Copyright (2004) by the American Physical Society.

$$\begin{aligned}\omega_v^{(1\alpha)}(\mathbf{r}) &= \frac{1}{4} \Theta\left(\frac{\sigma_v^{(\alpha)}}{2} - |x_\alpha|\right) \prod_{\tau \neq \alpha} \delta\left(\frac{\sigma_v^{(\tau)}}{2} - |x_\tau|\right), \\ \omega_v^{(2\alpha)}(\mathbf{r}) &= \frac{1}{2} \delta\left(\frac{\sigma_v^{(\alpha)}}{2} - |x_\alpha|\right) \prod_{\tau \neq \alpha} \Theta\left(\frac{\sigma_v^{(\tau)}}{2} - |x_\tau|\right), \\ \omega_v^{(3)}(\mathbf{r}) &= \prod_{\tau} \Theta\left(\frac{\sigma_v^{(\tau)}}{2} - |x_\tau|\right),\end{aligned}\quad (50)$$

where $\sigma_v^{(\alpha)} = \sigma + (L - \sigma)\delta_{\alpha v}$, with L the length of the parallelepipeds and σ^2 their cross-sectional area. $\Theta(x)$ and $\delta(x)$ are the Heaviside and Dirac delta functions, respectively. A particle of species v is defined as having its longest axis along the Cartesian axis v (with $v = x, y$ or z). $\sigma_v^{(\alpha)}$ is the length of species v in the direction of the axis α . Integrals of the weights give the fundamental measures, $M_v^{(\alpha)} \equiv \int d\mathbf{r} \omega_v^{(\alpha)}(\mathbf{r})$, of species v : $M_v^{(0)} = 1$, $M_v^{(3)} = v$ (with $v = L\sigma^2$ the particle volume), $M_v^{(1\tau)} = \sigma_v^{(\tau)}$ (the edge-length of species v parallel to τ) and $M_v^{(2\tau)} = L\sigma^2/\sigma_v^{(\tau)}$ (the surface area of the sides of species v perpendicular to τ). Note that within the same free energy density (49), it is possible to describe prolate (rod-like with $L > \sigma$) and oblate (plate-like with $L < \sigma$) particles.

The above theory was used in 2004 by Martínez-Ratón [131] to investigate the phase diagram of prolate and oblate HP. Transitions to different nonuniform phases (smectic, columnar, oriented or plastic solid) were considered. Results are shown in figure 6. On the left side, the phase diagram of prolate parallelepipeds is shown, while in the right side the results for oblate ones are presented. As can be inferred from the figure, for $\kappa = L/\sigma > 5$ (prolate) and $\kappa^{-1} > 4.5$ (oblate) the sequence of phase transitions from low to high densities is $I \rightarrow N \rightarrow S \rightarrow OS$ (prolate) and $I \rightarrow N \rightarrow C \rightarrow OS$ (oblate), similar to what is found for freely rotating particles of other geometries like HSC, HC and platelets. However, for low values of κ (prolate) or κ^{-1} (oblate), the phase diagram topology is quite different from that of freely rotating particles, reflecting the effect of the restriction of orientations on the stability of nonuniform phases. For example, the model predicts the stability of a so-called *discotic smectic* phase (labelled DSm in the figure). This peculiar phase is a layered structure, like the smectic phase but with the long (prolate) or short (oblate) axis of the particles lying in the

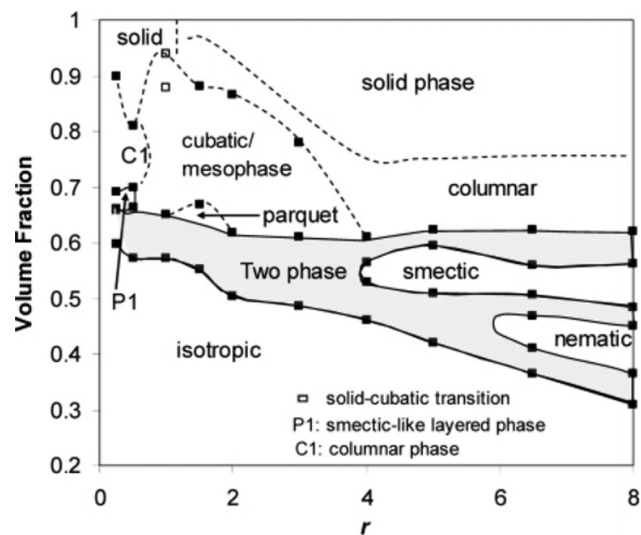


Figure 7. Phase diagram of freely rotating cuboids with aspect ratio r in the range 0.25–8, from [133]. Dashed lines indicate approximate phase boundaries. P1 is a smectic-like phase. C1 is a columnar. Open squares correspond to approximate boundaries of the solid-cubatic coexistence region. Reprinted with permission from [133]. Copyright (2005) American Chemical Society.

layers. Because there is no orientational order of this axis in the layers, the nematic order parameter takes negative values at the positions of the density maxima (which correspond to the position of the layers). FMT predicts a first-order phase transition from the I phase to the discotic smectic phase. This is in qualitative agreement with computer simulations of the Zwanzig model with $\kappa = 5$ on a lattice [132], which showed an I–DSm transition at a density between 0.47 and 0.55. However, it should be taken into account that the parallelepipedic geometry, especially for cuboids with $1 < \kappa \lesssim 4$, might stabilize the cubatic and the so-called *parquet* (a smectic with in-layer tetratic order) phases, as found by John and Escobedo [133] in recent MC simulations on freely rotating cuboids. The phase diagram predicted by the simulations is rather complex (see figure 7).

Martínez-Ratón *et al* [134] devised a differential procedure to generate functionals in higher dimensionalities from

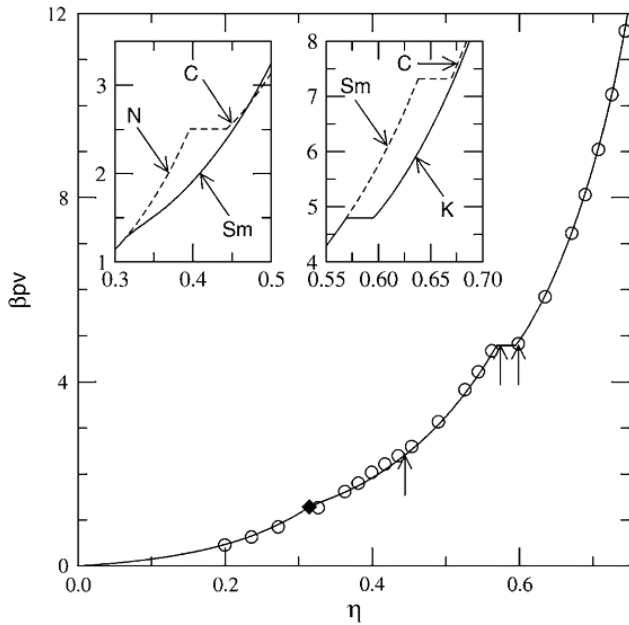


Figure 8. Equation of state (pressure in reduced units versus packing fraction) for all the stable phases obtained from the FMT for parallel HC [135]. These phases are nematic N (for η up to the point indicated by full rhombus), smectic Sm (from that point up to the discontinuity) and crystal K (from the discontinuity up to close packing). The open circles are MC simulation results from [100]. The arrows represent the N–Sm and Sm–K phase transitions as obtained from simulations. The two insets show the EOS for the metastable C phase in the neighbourhood of the N–C (left inset) and Sm–C (right inset) phase transitions. Reprinted with permission from [135]. Copyright (2008), AIP Publishing LLC.

low-dimensional functionals for parallel particles with constant cross sections. Using the dimensional crossover property mentioned above, these authors obtained a functional for a mixture of parallel cylinders from the corresponding functional for a mixture of hard discs. The theory was used by Capitán *et al* [135] to study the phase behaviour of a fluid of parallel HC and all the possible liquid-crystalline phases, as well as the crystalline phase, were considered (see figure 8). The functional was numerically minimized using a Gaussian parameterization for the density profiles and very good agreement with Monte Carlo simulations [90, 100] was obtained for the equation of state, particularly for the nonuniform phases. The main result was that the C phase was found to be metastable with respect to the S or K (crystal) phases, which explains the observation in the simulations of a region of stability of the C phase which disappears with system size. Since the present functional reduces to the SPT in the uniform phase limit, the description of the N phase was not as accurate as that of the nonuniform phases and a deviation between theory and simulations was evident in the location of the N–S transition.

An early attempt to use ideas from FMT for freely rotating anisotropic bodies was due to Cinacchi and Schmid [136], who proposed a density functional that interpolates between the FMT for HS and the Onsager theory for hard needles. They applied their approximation to hard ellipsoids and hard spherocylinders. The location of the isotropic-nematic transition was calculated and compared with simulation and

much better agreement was found than in the case of the Onsager theory. In fact, the theory was found to be almost as accurate as the PL theory.

Later, Schmidt extended the FMT formalism to a mixture of freely rotating particles, proposing a numerically tractable functional for a mixture of spheres and rods of vanishing thickness (needles) [137]. He showed that the Mayer function of spheres and needles can be exactly expressed as a sum of convolution products,

$$f_{sn}(\mathbf{r}, \hat{\Omega}) = [\omega_s^{(3)} * \omega_n^{(0)}](\mathbf{r}, \hat{\Omega}) + [\omega_{sn}^{(2)} * \omega_n^{(1)}](\mathbf{r}, \hat{\Omega}), \quad (51)$$

where s and n stand for spheres and needles, respectively and $*$ is a convolution product, $[a * b](\mathbf{r}) = \int d\mathbf{r}' a(\mathbf{r}') b(\mathbf{r} - \mathbf{r}')$. The HS scalar and vectorial weights are those of the original FMT [137],

$$\omega_s^{(3)}(\mathbf{r}) = \Theta(R - r), \quad \omega_s^{(2)}(\mathbf{r}) = \delta(R - r) \frac{\mathbf{r}}{R}, \quad (52)$$

with R the HS radius. For hard needles the weights are

$$\omega_n^{(1)}(\mathbf{r}, \hat{\Omega}) = \frac{1}{4} \int_{-L/2}^{L/2} dl \delta(\mathbf{r} + \hat{\Omega}l),$$

$$\omega_n^{(0)}(\mathbf{r}, \hat{\Omega}) = \frac{1}{2} \left[\delta\left(\mathbf{r} + \frac{\hat{\Omega}L}{2}\right) + \delta\left(\mathbf{r} - \frac{\hat{\Omega}L}{2}\right) \right], \quad (53)$$

with L the length of the needles. Note that both weights depend on the spatial and orientational coordinates of a single needle. However, recovering the exact Mayer function requires a new weight:

$$\omega_{sn}^{(2)}(\mathbf{r}, \hat{\Omega}) = 2|\omega_s^{(2)}(\mathbf{r}) \cdot \hat{\Omega}|, \quad (54)$$

which depends on the position \mathbf{r} of the HS and the needle orientation $\hat{\Omega}$. Therefore, strictly speaking it is not a one-body weight. Within this approximation, the free energy density is obtained as $\Phi = \Phi_s + \Phi_{sn}$ (i.e. the sum of the one-component HS free energy density and the contribution coming from the interaction between spheres and needles [137]). The excess part of the free energy functional is then obtained by integration, $\beta\mathcal{F}[\{\rho_\mu\}] = \int d\mathbf{r} \int d\hat{\Omega} \Phi(\{n_\mu^{(\alpha)}\})$.

To improve the theory, Schmidt *et al* took a step forward by including rod-rod interactions [138]. In order to do that, the residual surface of the rods was taken into account, in the asymptotic limit of high aspect ratios, by approximating the Mayer function between two rods. A new weight function is required which depends on the orientations of both needles, a fact that turns practical applications of this approach into a demanding numerical task.

In the case of HSC, the correction of order D/L to the Mayer function deconvolution was taken into account by introducing four new geometric weights which, in turn, define a new set of weighted densities [139]. The same formalism was also applied to a ternary mixture of HS, hard rods and hard platelets, with both anisotropic particles having vanishing thickness [140]. In particular, the I–N transition of a one-component hard-platelet fluid was calculated with this functional and the results compared with MC simulations and

Table 1. Isotropic-nematic coexistence data for hard platelets of radius R , as obtained from FMT [140], simulation [85] and Onsager theory [140].

	FMT	Simulation	Onsager
$\rho^{(\text{iso})} R^3$	0.418	0.473	0.667
$\rho^{(\text{nem})} R^3$	0.460	0.509	0.845
$\Delta\rho R^3$	0.041	0.036	0.178
S_{nem}	0.492	0.370	0.781

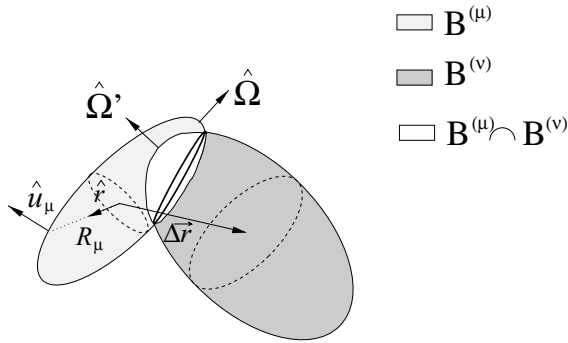


Figure 9. Sketch of two overlapping bodies $\mathcal{B}^{(\mu)}$ and $\mathcal{B}^{(\nu)}$ with fixed orientations given by the unit vectors $\hat{\Omega}$ and $\hat{\Omega}'$, respectively. Their common intersection volume $\mathcal{B}^{(\mu)} \cap \mathcal{B}^{(\nu)}$ is shown. Also, \hat{r} is a generic unit vector at the centre of the particle and $R_\mu(\hat{r})$ gives the distance from the centre to its surface $\partial\mathcal{B}^{(\mu)}$. \hat{u}_μ is the corresponding normal unit vector. The thick solid line represents the curve $\partial\mathcal{B}^{(\mu)} \cap \partial\mathcal{B}^{(\nu)}$.

the Onsager theory. The results compared well with simulations, as shown in table 1.

A new development, along the lines originally proposed by Rosenfeld [141], has recently been carried out in an attempt to formulate a general FMT approximation for freely rotating convex bodies. Again the theory is formulated for a mixture of hard particles with arbitrary number of species, labelled by index $\mu = 1, 2, \dots$. The main idea is based on the observation made by Rosenfeld that, in general, the deconvolution of the Mayer function as a product of single particle weights is intimately related to the Gauss–Bonnet theorem of differential geometry [141]. This idea has been followed by Hansen-Goos and Mecke [142, 143], who applied the Gauss–Bonnet theorem to approximately deconvolute the Mayer function of two convex particles. Figure 9 is a sketch of two overlapping convex bodies $\mathcal{B}^{(\mu)}$ and $\mathcal{B}^{(\nu)}$ which, in general, will be of different species μ and ν . Let the orientations of the bodies be given by the unit vectors $\hat{\Omega}$ and $\hat{\Omega}'$ and let their centre of mass relative position vector with respect to a fixed reference frame be Δr . Also, let $\partial\mathcal{B}^{(\mu)}$ be the surface of body $\mathcal{B}^{(\mu)}$ and $\partial\mathcal{B}^{(\mu)} \cap \mathcal{B}^{(\nu)}$ the surface of this body which is inside the body $\mathcal{B}^{(\nu)}$. Finally, $\partial\mathcal{B}^{(\mu)} \cap \partial\mathcal{B}^{(\nu)}$ denotes the curve generated by the intersection between the surfaces $\partial\mathcal{B}^{(\mu)}$ and $\partial\mathcal{B}^{(\nu)}$. Further, let \hat{r} be a generic unit vector from the centre of particle μ and $R_\mu(\hat{r})$ the distance from this centre to a point on the surface of the same particle. The Gaussian and mean curvatures at a point on the surface $\partial\mathcal{B}^{(\mu)}$ are $K_\mu(\hat{r}) = k_\mu^{(1)}(\hat{r})k_\mu^{(2)}(\hat{r})$ and $H_\mu(\hat{r}) = \frac{1}{2} [k_\mu^{(1)}(\hat{r}) + k_\mu^{(2)}(\hat{r})]$, with $k_\mu^{(\alpha)}(\hat{r})$ ($\alpha = 1, 2$) the principal curvatures of the surface $\partial\mathcal{B}^{(\mu)}$. These curvatures characterize the intrinsic geometry of

the surface $\partial\mathcal{B}^{(\mu)}$. The curve $\partial\mathcal{B}^{(\mu)} \cap \partial\mathcal{B}^{(\nu)}$ at a point on the surface $\partial\mathcal{B}^{(\mu)}$ is characterized by its geodesic curvature $k_{g\mu}(\hat{r})$.

In the present geometrical construction, the Gauss–Bonnet theorem can be expressed as

$$\int_{\partial\mathcal{B}_\mu \cap \mathcal{B}_\nu} \frac{K_\mu(\hat{r})}{4\pi} dA + \int_{\partial\mathcal{B}_\nu \cap \mathcal{B}_\mu} \frac{K_\nu(\hat{r})}{4\pi} dA + \int_{\partial\mathcal{B}_\mu \cap \partial\mathcal{B}_\nu} \left(\frac{k_{g\mu}(\hat{r}) + k_{g\nu}(\hat{r})}{4\pi} \right) dl = -f_{\mu\nu}(\Delta r, \hat{\Omega}, \hat{\Omega}'), \quad (55)$$

where $f_{\mu\nu}(\Delta r, \hat{\Omega}, \hat{\Omega}')$ is the Mayer function of the two particles. The first two surface integrals can be expressed as the spatial convolutions $\omega_\mu^{(0)} * \omega_\nu^{(3)}$ and $\omega_\mu^{(3)} * \omega_\nu^{(0)}$, respectively, with the one-particle weights defined as

$$\omega_\mu^{(0)}(\mathbf{r}) = \frac{K_\mu(\hat{r})}{4\pi} \delta(R_\mu(\hat{r}) - r),$$

$$\omega_\mu^{(3)}(\mathbf{r}) = \Theta(R_\mu(\hat{r}) - r). \quad (56)$$

However, the third integral can only be exactly deconvoluted in the case of two particle geometries: spheres (or parallel ellipsoids) and parallel or mutually perpendicular parallelepipeds. The last integral is a contour integral. The integral of the first term, $k_{g\mu}(\hat{r})/4\pi$, can be split into two contributions. The first is the integral of a term proportional to $H_\mu(\hat{r})$. The second is the integral of a term proportional to $\frac{k_\mu^{(1)}(\hat{r}) - k_\mu^{(2)}(\hat{r})}{2(1 + \mathbf{u}_\mu \cdot \mathbf{u}_\nu)}$. The presence of the denominator $1 + \mathbf{u}_\mu \cdot \mathbf{u}_\nu$ is the reason why the last integral in (55) cannot be exactly deconvoluted. Approximating this denominator by unity (the lowest order in the Taylor expansion with respect to $\mathbf{u}_\mu \cdot \mathbf{u}_\nu$) allows for the deconvolution of this contribution in terms of one-particle weights. The result is:

$$-f_{\mu\nu} = \omega_\mu^{(0)} * \omega_\nu^{(3)} + \omega_\mu^{(1)} * \omega_\nu^{(2)} - \omega_\mu^{(1)} * \omega_\nu^{(2)} - \zeta \overset{\leftrightarrow}{\omega}_\mu^{(1)} * \overset{\leftrightarrow}{\omega}_\nu^{(2)} + (\mu \leftrightarrow \nu), \quad (57)$$

with $\omega_\mu^{(1,2)}$, $\omega_\mu^{(1,2)}$ and $\overset{\leftrightarrow}{\omega}_\mu^{(1,2)}$, the scalar, vectorial and tensorial weighted densities (expressions for them can be found in [142, 143]). ζ is an adjustable parameter that allows for the improvement of the theory (in particular, it has been used to improve the results for the I–N transition as compared to simulations). A free energy density, which leads to this deconvolution of the Mayer function and, also, which recovers Tarazona’s FMT version for HS [122] (and, therefore, fulfills the dimensional crossover to 0D) is

$$\Phi = -n_0 \ln(1 - n_3) + \frac{n_1 n_2 - n_1 n_2 - \zeta \text{Tr} \left[\overset{\leftrightarrow}{n}_1 \overset{\leftrightarrow}{n}_2 \right]}{1 - n_3} + \frac{3}{16\pi} \frac{n_2^T \overset{\leftrightarrow}{n}_2 n_2 - n_2 n_2 n_2 - \text{Tr} \left[\overset{\leftrightarrow}{n}_2^3 \right] + n_2 \text{Tr} \left[\overset{\leftrightarrow}{n}_2^2 \right]}{(1 - n_3)^2}. \quad (58)$$

The weighted densities are calculated as

$$n_\alpha(\mathbf{r}) = \sum_\mu \int d\mathbf{r}' \int d\hat{\Omega} \rho_\mu(\mathbf{r}', \hat{\Omega}) \omega_\mu^{(\alpha)}(\mathbf{r} - \mathbf{r}', \hat{\Omega}). \quad (59)$$

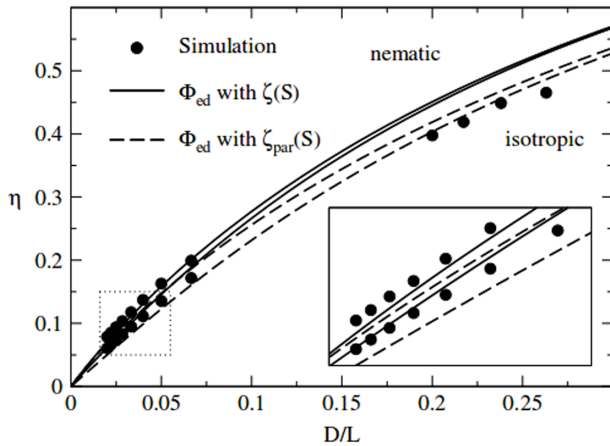


Figure 10. Results for the I–N transition of the HSC fluid as obtained from the FMT of Hansen and Mecke [143]. Symbols indicate simulation results from [96]. Solid and dashed lines were calculated using different choices of the parameter ζ (see [143] for details).

The free energy density (58) has the merit of being a function of one-particle densities and consequently its implementation is numerically cheaper than those based on the Mayer function. Also, the functional can be improved by adding more tensorial weighted densities in the second term of (58) as obtained from the expansion of $(1 + \mathbf{u}_\mu \cdot \mathbf{u}_\nu)^{-1}$. Note that the term proportional to ζ is necessary to generate an orientational phase transition; its absence destabilizes the N phase. The value of the parameter ζ can be chosen so as to improve the results of the model compared with computer simulations, as shown by Hansen-Goos and Mecke [142, 143]. These authors applied the present functional to study the I–N transition of HSC for general aspect ratio (see figure 10). The coexisting densities resulting from a particular value of ζ compare well with the simulation results. Härtel and Löwen [144] applied the same theory to study the static and dynamical response of a fluid of HSC subject to the presence of aligning fields.

3.2. Further studies on spatially nonuniform phases

Hard models have been used to analyze other nonuniform liquid-crystalline phases different from the smectic and also some effects and phenomena present in general liquid-crystal phases, especially concerning peculiar structural and dynamical effects. One of the latter concerns the presence of transverse order in smectic phases made of hard rods. In studies of smectics, one assumes that the orientational order parameter is high and that, as a result, the orientational distribution function should be highly peaked in the direction of the layer normal. The success (or not) of the parallel particle approximation is based on this expectation. Corrections to the free energy due to orientational freedom is expected to be quantitatively small and therefore the coupling between orientations and positions should be effectively weak, i.e. $\rho(\mathbf{r}, \hat{\Omega}) \simeq \rho(\mathbf{r})h(\hat{\Omega})$. This means that the extremely small fraction of rods located close to the interstitial region should also be highly oriented along the layer normal. However, already at the level of Onsager density functional theory, it was

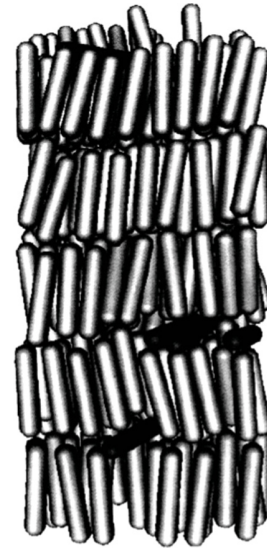


Figure 11. Configuration of hard spherocylinders in a smectic arrangement showing interstitial particles with transverse orientation (from simulations by van Roij *et al* [145]). Reprinted with permission from [145]. Copyright (1995) by the American Physical Society.

found by van Roij *et al* [145] that the orientational distribution function $h(\mathbf{r}, \hat{\Omega})$ is strongly modulated. Theory and simulations indicated that the interstitial particles are oriented parallel, instead of perpendicular, to the layers (see figure 11).

In more recent work, the related effect of interlayer diffusion has been studied. It has long been known that, in a nematic phase, diffusion constants along and perpendicular to the director are very different [146], with some peculiar effects found in simulations of the nematic phase of hard ellipsoids [147], where it was found that the longitudinal diffusion component increases with density in some density interval just above the isotropic–nematic transition. Longitudinal diffusion, which gives rise to interlayer diffusion or permeation in smectic phases, has been studied more recently. Lamellar phases made of rod-like viruses were seen to exhibit single particle hops, which occur by quasi-quantized steps of one rod length; this one-particle diffusion can be explained on the basis of a simple model based on the longitudinal diffusion of a nematic phase in a periodic potential that simulates the lamellar ordering. Diffusion mechanisms in smectics has been studied in detail, using computer simulation, by Cinacchi and de Gaetani [148].

The theories for nonuniform liquid-crystalline phases discussed so far were devised with a view to describing the transition from the nematic to the smectic phase since the latter is the simplest nonuniform phase, exhibiting spatial order along only one coordinate. An additional level of nonuniformity is presented by the columnar phase, where the local density depends on two spatial coordinates. Using computer simulation, Stroobants *et al* [90] studied a fluid of hard parallel spherocylinders and observed the formation of a columnar phase (consisting of a 2D hexagonal lattice of fluid columns) between the smectic and crystal phases for sufficiently large values of L/D . This phase was later shown to be an artefact of the small system size of the samples [100]. In fact, there are good reasons to expect that the columnar phase cannot be stable: in the large

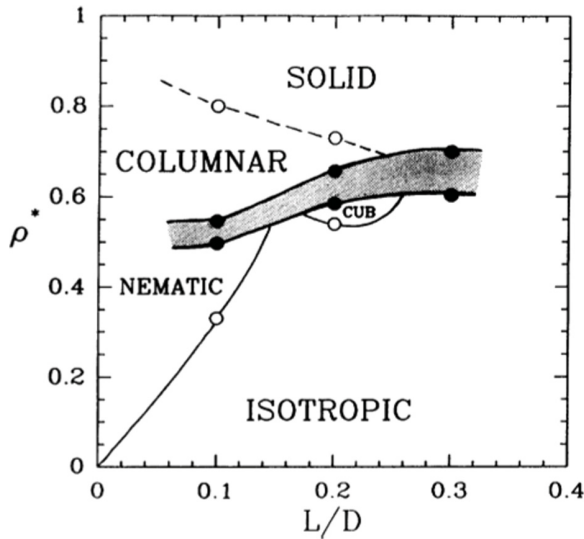


Figure 12. Phase diagram of the hard cut sphere model from computer simulation (from Veerman and Frenkel [152]). Reprinted with permission from [152]. Copyright (1992) by the American Physical Society.

L/D regime, hard parallel spherocylinders resemble hard parallel cylinders and these behave exactly as hard discs if scaled along the long particle axis. Since hard discs directly freeze from the fluid into the crystal, there should be no intermediate phase with partial order in the system of parallel cylinders. In the corresponding freely rotating model, rotational entropy plays against columnar ordering and the columnar phase is not stabilized either.

Therefore, except in mixtures of rods with different lengths [150] (see section 3.5.1) where columnar ordering (generated by length bidispersity) was found, we do not expect to find columnar phases in fluids of (prolate) hard rods. This is why columnar phases were searched for in fluids of oblate particles. However, for this purpose the choice of particle is not simple. The first model of oblate or discotic particle, the infinitely thin circular platelet discussed by Onsager, exhibits nematic ordering [85, 151], but it possesses a vanishing excluded volume as particles become increasingly ordered and, consequently, there is no mechanism to generate spatially nonuniform phases beyond the nematic. Another model considered, that of oblate hard ellipsoids, again shows no mesogenic phases different from the nematic [57, 147], since already the parallel model scales to the hard-sphere model. To circumvent these problems, Frenkel [149] studied a particle model that favours the piling-up of particles to form columns. This is the hard cut sphere model, consisting of a sphere of diameter D where two opposite parts have been removed, leaving a particle of thickness $L < D$ with two flat surfaces; when $L = D$ a full sphere is recovered. Frenkel [149] and Veerman and Frenkel [152] studied this model in detail by computer simulation. Their complete phase diagram is shown in figure 12. As expected, a columnar phase, intermediate between the nematic and the crystal phases, was formed for $L/D \lesssim 0.25$. Interestingly, an exotic nematic phase, the *cubic* phase, was stabilized in a small region of density and aspect ratio. This

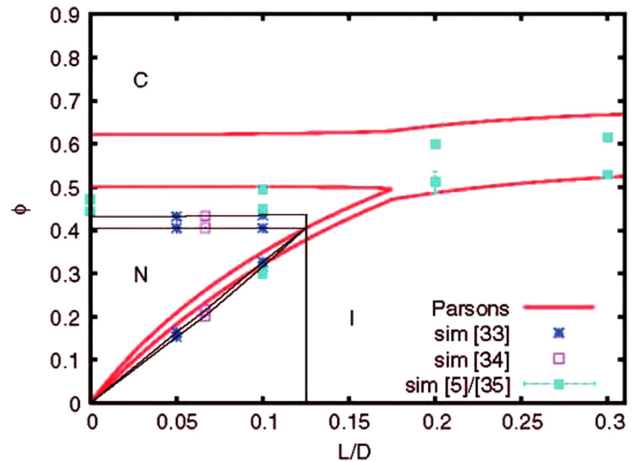


Figure 13. Phase diagram of oblate cylinders of aspect ratio L/D as obtained in [153]. The packing fraction of the system is represented in the vertical axis. Red lines are results from the theoretical approximation. Symbols correspond to different computer simulation studies (see original paper for details). Reprinted with permission from [153].

phase possesses no positional order but exhibits orientational order with cubic symmetry.

More recently, further studies on the columnar phase stability in systems of oblate hard particles have been carried out by Wensink and Lekkerkerker [153] and by Marechal *et al* [154]. Wensink and Lekkerkerker mapped out the complete liquid-crystal phase diagram of oblate cylinders of different aspect ratios $L/D < 1$. They used PL theory to describe isotropic and nematic phases and a Lennard-Jones–Devonshire cell model to address the question of the stability of nonuniform phases (namely, columnar and solid) at high packing fractions. At low enough aspect ratio ($L/D < \kappa_t \simeq 0.175$) the system shows I–N and N–C transitions upon increasing its packing fraction. For aspect ratios $L/D > \kappa_t$ the anisometry of the particles is too small to produce a stable nematic phase and the system shows a direct transition from the isotropic to the columnar phase. Results compare satisfactorily with computer simulations, particularly in the region $L/D > \kappa_t$, as can be seen in figure 13.

It is interesting to note that, within this model, the N–C transition does not depend appreciably on the aspect ratio. By using a Gaussian ansatz for the orientational distribution function and taking advantage of the fact that nematic order is very strong close to the N–C transition, Wensink and Lekkerkerker were able to show that the nematic-columnar transition is, in fact, universal and independent of particle shape.

Marechal *et al* [154] used Monte Carlo free energy calculations to obtain the phase diagram of oblate hard spherocylinders (OHSC) as a function of their aspect ratio. Their result has been reproduced in figure 14. Apart from the crystal phases, the topology of the phase diagram is qualitatively similar to that obtained by Wensink and Lekkerkerker for oblate cylinders using PL theory (figure 13). At low aspect ratios the system undergoes I–N and N–C phase transitions as packing fraction is increased. Above a particular value of aspect ratio, the N phase is no longer stable and a direct I–C phase transition

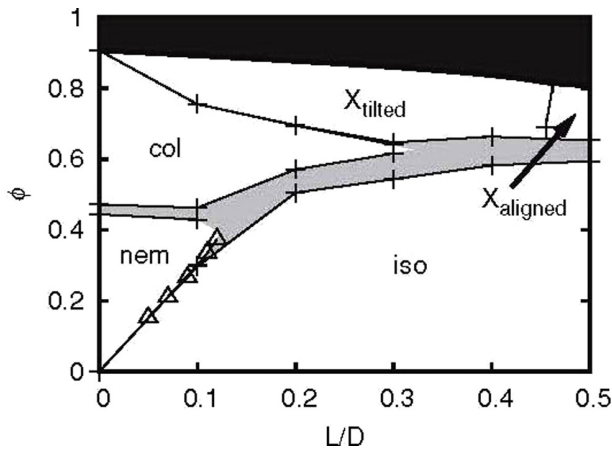


Figure 14. Phase diagram of oblate hard spherocylinders in the aspect ratio packing fraction plane as obtained by Marechal *et al* [154]. The shaded regions at high packing fraction are states above the close packing limit. Crystalline phases X_{tilted} and X_{aligned} , N and C mesophases and the I phase are stable. Symbols are coexistence points obtained from the simulations, while lines are only guides to the eye. Reprinted with permission from [154]. Copyright (2011), AIP Publishing LLC.

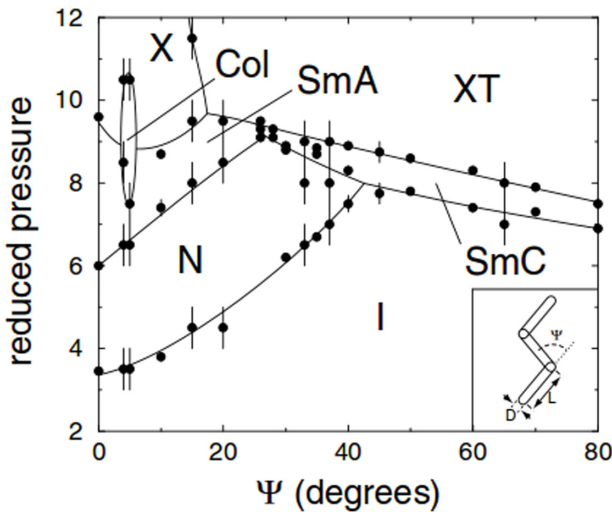


Figure 15. Phase diagram of zigzag molecules made out of hard spherocylindrical sectors with aspect ratio $L/D = 2$ as a function of angle between the sectors Ψ , from [157]. Labelled phases are: isotropic (I), nematic (N), smectic A (Sm A), smectic C (Sm C), columnar (C), tilted crystal (XT) and crystal (X). Reprinted with permission from [157]. Copyright (2004) by the American Physical Society.

takes place. Moreover, the similarity between both phase diagrams applies also to the N–C transition at low aspect ratios: like in the case of oblate cylinders, this transition seems to be almost independent of L/D .

There have been some studies on phase behaviour in fluids of rigid particles formed by linked rods. The resulting particles possess non-convex shapes and nonstandard liquid-crystalline phases may be stabilized due to nontrivial packing restrictions. For example, banana-shaped or V-shaped particles are biaxial bodies and consequently they have been used to investigate the stability of the biaxial nematic phases (see next section). However, these particles have been conjectured [155]

to be able to also form smectic phases with antiferromagnetic arrangement, an effect originating in their polar character (here polarity has a steric origin associated to the shape). A very detailed simulation study of zigzag particles was performed by Maiti *et al* [157], who considered particles with three sectors made from three hard spherocylinders attached by their ends. An amazingly large number of stable phases were found, including isotropic, nematic, smectic A, smectic C, columnar and two crystal phases (see figure 15, where the phase diagram is represented in the plane pressure versus angle between sectors Ψ). Figure 16 shows typical configurations of these phases. The presence of the smectic C phase and a transition from the smectic A to the smectic C phase is particularly interesting since it shows, as already demonstrated by Somoza and Tarazona using density functional theory [109, 110], that hard-body interactions alone can stabilize different types of smectic phases and drive transitions between them.

3.3. Biaxial particles

Up to now we have discussed the appearance of liquid-crystalline order as the direct consequence of the anisotropy along a single axis of common nematogens. Simple entropic arguments rapidly lead to the conclusion that the equilibrium uniform configuration of the system should be a nematic phase when the density is high enough, as was simply and elegantly shown by Onsager [16]. But it is clear that molecules of most liquid-crystal forming substances are not cylindrically symmetric and, therefore, it should be possible, as first predicted by Freiser [158] in 1970 in the context of an extended Maier–Saupe model for thermotropic liquid crystals, to find a stable biaxial nematic (N_B) phase, i.e. a nematic phase that shows not only long-range orientational order of the long molecular axis along one direction (the director), as it is the case in common uniaxial nematics, but also shows long-range order of the shorter molecular axes along two other mutually perpendicular directors. In other words, a nematic phase with three directors about which three molecular axes tend to align. In figure 17 we have shown common uniaxial nematic phases N_U^+ and N_U^- which are usually formed by rod-like molecules and disc-like molecules, respectively, and a biaxial nematic phase formed by board-like molecules.

In the case of the uniaxial nematic phases (a) and (b) shown in figure 17, all the directions perpendicular to \hat{n} are equivalent. Therefore, if we look at the system from a direction parallel to the director, we will find that the molecules have, on average, a circular cross section while they will show an elliptical cross section if we look at the system in a direction perpendicular to \hat{n} . This leads to an axially symmetric ellipsoid and, hence, this kind of nematic phase is optically uniaxial. In (a) the largest polarizability is parallel to \hat{n} and, as a consequence, this uniaxial nematic phase has positive birefringence. In case (b), however, the largest polarizability is perpendicular to \hat{n} , resulting in a negative birefringence. But in case (c) there is another possibility: the existence of a secondary director \hat{m} perpendicular to \hat{n} (and, therefore, a third one \hat{l} perpendicular to the other two). In this case molecules will show a non-circular (elliptical) averaged cross section if they are viewed either parallel to the main director \hat{n} or parallel to the secondary one \hat{m}

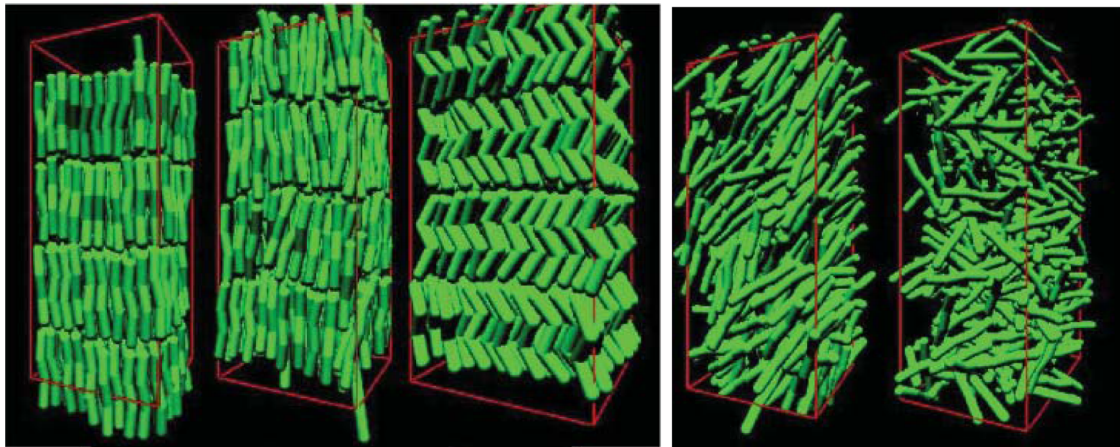


Figure 16. Typical configurations in different Monte Carlo simulations of a system of 400 zigzag molecules, from [157]. From left to right and top to bottom: crystal (reduced $p^* = 11$ and angle between consecutive sectors $\Psi = 15^\circ$), smectic A ($p^* = 9$ and $\Psi = 15^\circ$), smectic C ($p^* = 8$ and $\Psi = 65^\circ$), nematic ($p^* = 5$ and $\Psi = 15^\circ$) and isotropic ($p^* = 1$ and $\Psi = 15^\circ$) phases. Reprinted with permission from [157]. Copyright (2004) by the American Physical Society.

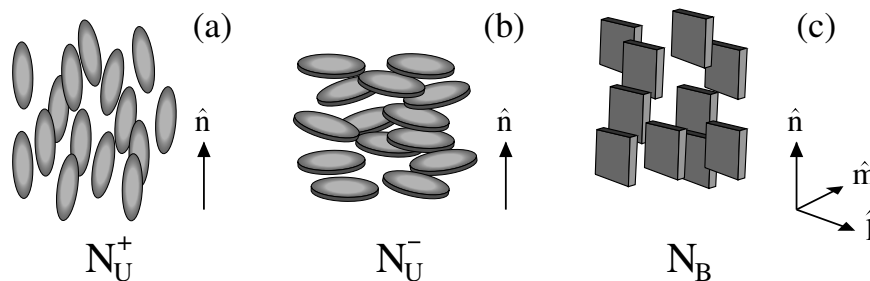


Figure 17. Uniaxial nematic phases of (a) prolate and (b) oblate particles and (c) biaxial nematic phase. See text for discussion.

(or $\hat{\mathbf{i}}$). Therefore, this nematic phase has reduced symmetry and is optically biaxial. In other words, molecules in the uniaxial phase are rotationally disordered around the long axis while in the biaxial phase this rotation is restricted in such a way that the molecules show a time averaged board-like shape. From the macroscopic point of view, the biaxial nematic has two optical axes, i.e. directions along which the optical properties appear to be cylindrically symmetric [159–161].

The theoretical prediction of the N_B phase in 1970 triggered its search since it was immediately recognized that the existence of N_B phases is a problem of great interest, not only theoretical but also practical, due to the fact that these phases could be used in the development of fast electro-optical devices (see the excellent review by Tschierske and Photinos [161, 164]). Consequently, after its prediction by Freiser, a great effort has been devoted to their theoretical analysis, experimental observation and computer simulation. The first experimental observation of the N_B phase, in a lyotropic system, was done in 1980 by Yu and Saupe [165], although their system was a ternary mixture rather than a pure compound. The occurrence of the N_B phase in mixtures will be reviewed in section 3.5.1. More recently biaxial nematics have been observed in thermotropic liquid crystals made of bent-core organic molecules [166–169]; however, in this case controversial issues about the correct identification of the biaxial phase still remain [159, 160, 168–170]. Direct experimental evidence of the existence

of the biaxial nematic phase in a system of particles that can be considered hard bodies is that found in 2009 by van den Pol *et al* [171] in a system of board-like particles. These authors found both biaxial nematic and biaxial smectic phases in a colloidal dispersion of goethite particles. The particles are so big ($254 \times 83 \times 28$ nm on average, with a polydispersity of 20%–25% in all directions) that they can be regarded, to a very good approximation, as hard particles. Small angle x-ray scattering was used to study the structure of the macroscopic domains formed. Biaxiality is found in a system whose particles have a shape that is almost exactly in between rod-like and plate-like, in agreement, as we shall review below, with the predictions of theoretical models. The results of this experimental study suggest that biaxial phases can be indeed easily obtained by a proper choice of the particle shape. Molecular asymmetry is also expected to have some other influences on the macroscopic phase behaviour of the system, involving transitions between non-biaxial phases as has been shown, for example, by Somoza and Tarazona [172] who used the decoupling approximation to investigate the isotropic-nematic transition as a function of particle biaxiality in a system of hard spheroplatelets. Their conclusion is that the first-order character of this phase transition is significantly weakened by the molecular asymmetry.

To our knowledge, the first hard-body model approximation to the biaxial nematic phase is that of Shih and Alben [173, 174]. They used a generalization of Flory's lattice model to compute the phase diagram of rectangular plate-like

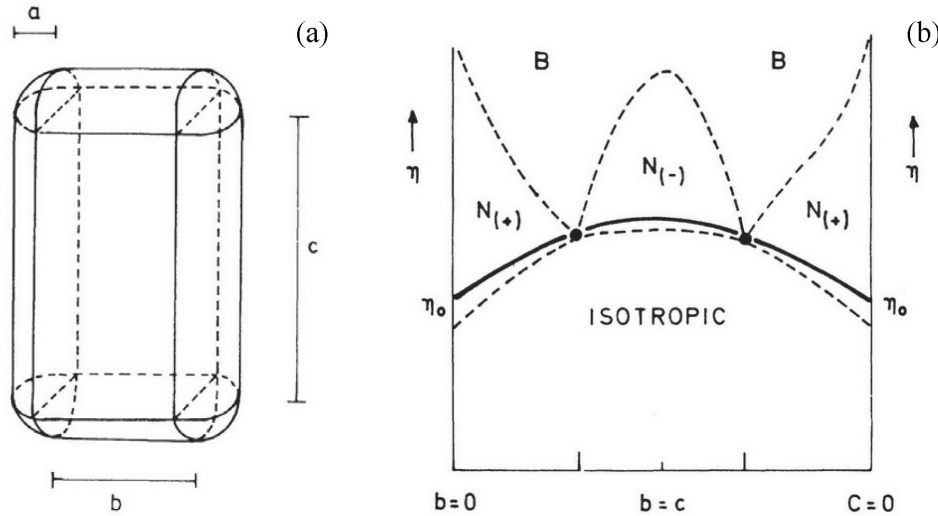


Figure 18. (a) Spheroplatelet. (b) Conjectured phase diagram for a system of spheroplatelets from Onsager’s theory as a function particle geometry and system’s packing fraction. Reprinted with permission from [175]. Copyright (1989) by the American Physical Society.

particles of any length and width. The system consists in a simple cubic lattice formed by M cells. N rigid rectangular plates are then dispersed through the lattice. Each one of these plate-like particles is w cells wide, l cells long and one cell thick and it is required that the two sides of the plates lie along mutually perpendicular base-vector directions. Therefore, there are six possible molecular orientations in this model. There are no interactions between particles except for the hard-core interaction needed in order to avoid overlapping between plates. The thermodynamic behaviour of the system is then obtained by considering the number of distinct ways $g(\{\alpha\}, N, M)$ of packing N molecules into M cells under the restriction that given fractions α_i ($i = 1, \dots, 6$) of the plates have each of the six possible orientations. In the limit of very large N the Helmholtz free energy of the system is related to g evaluated at the set $\{\bar{\alpha}\}$ for which it takes its maximum value:

$$F = -kT \ln g(\{\bar{\alpha}\}, N, M) \quad (60)$$

Details of the calculation of $g(\{\bar{\alpha}\}, N, M)$ are to be found in the original paper of Shih and Alben [173]. The results from the model are that a biaxial nematic phase is obtained at high pressure for plates which are neither very square nor very rod-like in shape. In this phase both the long axes and the flat faces of the particles tend to be parallel. At lower pressure the biaxial phase undergoes a second-order phase transition to a uniaxial phase. The model shows two different uniaxial nematics: prolate uniaxial states ($N_{\bar{U}}^+$) in which the long axes tend to be parallel and oblate uniaxial states ($N_{\bar{U}}^-$) in which the flat faces tend to be parallel. Prolate uniaxial nematics are stable for rod-like particles (length/width $\gtrsim 0.3$) at intermediate densities and oblate uniaxial states take place for plate-like particles (length/width $\lesssim 0.3$) also at intermediate densities. At even lower pressure the uniaxial nematic phase undergoes a first-order transition to an isotropic phase showing discontinuities in the density and the orientational order in going through the transition. The size of these discontinuities depends strongly on the aspect ratio of the plates.

A different kind of plate-like particles, namely spheroplatelets (see figure 18(a)), was considered in 1989 by Mulder [175] who used, taking advantage of the knowledge of the explicit expression for the excluded volume between two spheroplatelets, Onsager’s approximation to investigate the phase behaviour of a system of such particles. His results are not conclusive with respect to the precise topology of the phase diagram since a complete free energy minimization was not carried out. Instead, a bifurcation analysis with respect to particle geometry was performed and a conjectured phase diagram was presented (see figure 18(b)), which showed a biaxial nematic phase for high enough packing fractions. For moderate packing fractions, the biaxial phase was assumed to be stable for particles shaped not too rod- or plate-like.

Spheroplatelets of all possible values of their elongation c were also analyzed the following year, in 1990, by Hołyst and Poniewierski [176] using the smoothed density approximation. A Landau bicritical point, at which a direct transition from the isotropic phase to the biaxial phase occurs (and as conjectured by Mulder, figure 18), was found. In fact, a whole line of these points is obtained when the spheroplatelets elongation is allowed to vary. A line of bicritical points was also found for a system of hard biaxial ellipsoids of axes $a < b < c$ for elongations $c/a \leq 7$. Both spheroplatelets and biaxial ellipsoids show similar scaling at the Landau bicritical point: $b/a \sim (c/a)^{1/2}$, where b/a is the breadth of the ellipsoid or the spheroplatelet.

The phase diagram of a system of spheroplatelets was calculated later, in 1991, by Taylor and Herzfeld [177], this time making use of the scaled particle approximation. In order to further simplify the calculations, the resulting scaled particle equations were solved in the Zwanzig approximation, as in the previous work of Shih and Alben discussed above. Figure 19 shows the phase diagram obtained by Taylor and Herzfeld for a system of spheroplatelets with $c/2a = 5$. In the vertical axis the packing fraction of the system is shown, while the horizontal axis represents the particle geometry. Panel (a)

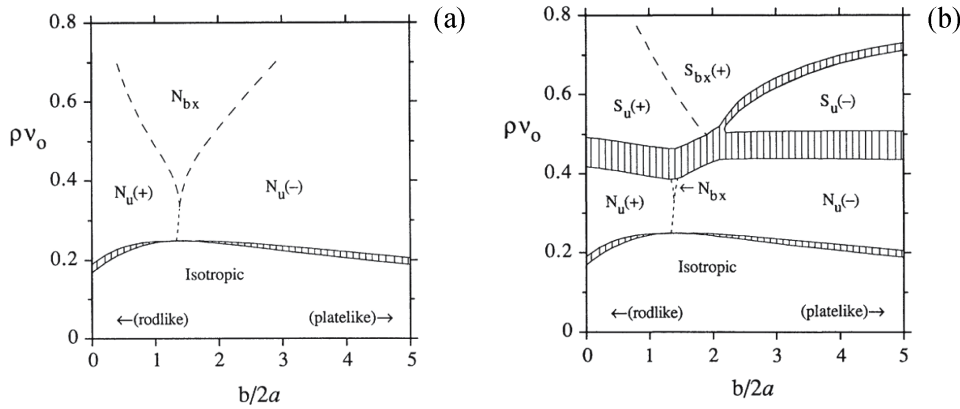


Figure 19. (a) Phase diagram of spheroplatelets with $c/2a = 5$ from the scaled particle of Taylor and Herzfeld [177]. (b) Same as (a) but including translationally ordered smectic phases (see text for discussion). Reprinted with permission from [177]. Copyright (1991) by the American Physical Society.

shows the result obtained from the scaled particle theory solved in the Zwanzig approximation, considering only the possible formation of nematic phases. The shaded areas correspond to first-order phase transitions while dashed lines correspond to second-order transitions. Two uniaxial nematics are stable, namely the rod-like uniaxial nematic $N_U(+)$ and the plate-like uniaxial nematic $N_U(-)$. For particles that are not too rod- or plate-like a biaxial nematic, N_{bx} , is found when the packing fraction is high enough, in agreement with previous models.

The elusiveness of the biaxial nematic phase led Taylor and Herzfeld to wonder about the possibility that the biaxial nematic were pre-empted by translationally ordered phases, namely by the smectic phase. In order to shed some light on that issue, they considered the stability of a smectic by using a cell model to treat the translational order. In that model, smectic order was imposed by introducing impenetrable cell walls which divide the system into smectic layers. Each layer is then treated as a 2D liquid confined within the 1D cell corresponding to the thickness of the smectic layer, the 2D density of this fluid being coupled to the 1D cell entropy through their mutual dependence on the smectic layer spacing. Three smectic A phases are then possible, depending on which of the three spheroplatelet principal axes is associated with the smectic ordering axis. Figure 19(b) shows the phase diagram obtained when this description of the smectic A ordering is combined with the scaled particle theory for the isotropic and nematic phases. Stable smectic A phases are found in the full range of particle biaxiality (as measured by the value of $b/2a$) for packing fractions $\gtrsim 0.5$. In the rod-like limit ($b \rightarrow 0$) there is a first-order transition from the uniaxial nematic to the uniaxial smectic $S_U(+)$ in which the rod axes are aligned perpendicular to the smectic layers. In the other extreme, for plate-like particles in the limit $b \rightarrow c$, a first-order transition between the uniaxial nematic $N_U(-)$ and a uniaxial smectic A phase $S_U(-)$ is found. In this smectic phase the short molecular axes are oriented perpendicular to the smectic layers. In an intermediate molecular biaxiality region of the phase diagram, a stable biaxial smectic phase, $S_{bx}(+)$, is obtained. In this phase the long molecular axes are aligned perpendicular to the smectic layers, like in the uniaxial $S_U(+)$ phase, but an in-layer second-order transition as the molecular biaxiality is increased

leads to the ordering of the short molecular axes, resulting in the biaxial smectic phase. This in-layer order of the short molecular axes is lost again, via a first-order phase transition, upon increasing even further the molecular biaxiality, giving rise to the stable uniaxial smectic $S_U(-)$. There are two remarkable aspects in the phase diagram of figure 19(b). The first is the almost complete disappearance of the stable biaxial nematic island predicted by this model when no translationally ordered phases are taken into account (as shown in panel (a) of the figure). The second is the strong first-order character of all the nematic-smectic transitions as shown by the wide shaded areas that separate those phases in the phase diagram. Although it is expected that the phase diagram predicted in this paper could be qualitatively correct, one must bear in mind that two different theories are used to describe the translationally disordered phases and the smectic one. Moreover, the approximation used to describe smectic phases will probably overestimate the stability of the smectic phase since the translational order is imposed by hand.

A weighted density theory was employed by Somoza and Tarazona [109, 110] to investigate the phase diagram of a system of hard particles with a different biaxial shape, namely oblique cylinders. The phase diagram of the system was computed, for a system of parallel particles, as a function of the molecular asymmetry as measured by the parameter Δ (see figure 20). The transition densities, ρ^* , shown in the vertical axis of the figure are expressed in units of the close packing density $\rho_{cp} = 2/(3^{1/2}D^2L)$. Apart from a continuous nematic-smectic A phase transition for small values of Δ/L , i.e. for particles with small biaxiality, and a first-order nematic-smectic C transition, at intermediate molecular biaxialities, a stable biaxial nematic (region B in the figure) is obtained for large values of Δ/L . The predicted existence of a biaxial nematic phase in a system of asymmetric hard particles is in agreement with the results from previous theoretical models but, as pointed out by the authors in their conclusions, in this particular model the biaxial nematic phase could be an artefact due to the imposed perfect alignment of the cylinder's axes which may favour the biaxial order.

A hard-boomerang fluid, formed by hard particles each one made of two hard spherocylinders joined at their ends at

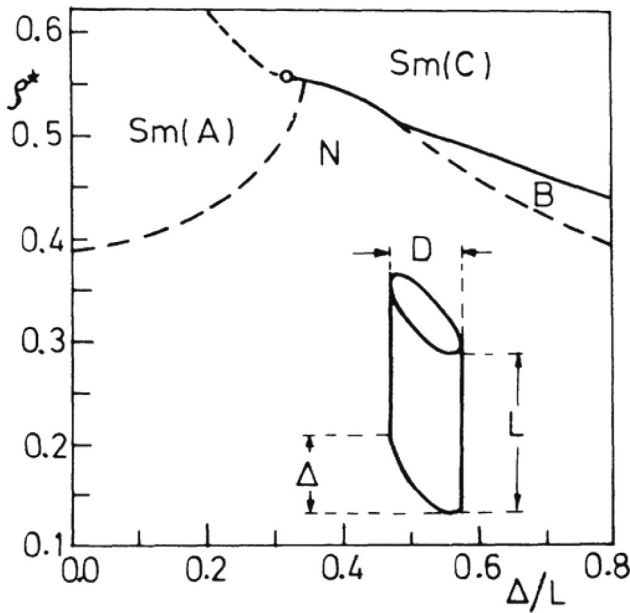


Figure 20. Phase diagram of a system of parallel oblique hard cylinders as obtained from the weighted density theory of Somoza and Tarazona [109]. Densities in the vertical axis are in units of the complete packing density. Reprinted with permission from [109]. Copyright (1988) by the American Physical Society.

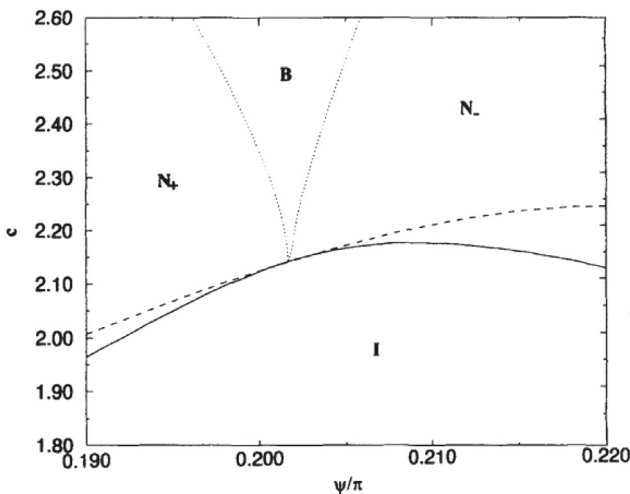


Figure 21. Phase diagram of a system of hard-boomerang particles as obtained from the Onsager theory by Teixeira *et al* [27]. Reprinted with permission from [27].

an angle ψ , has been studied by Teixeira *et al* [27]. In this way a biaxial particle is constructed, the value of ψ being a measure of its biaxiality. The Onsager approximation was then used to obtain the free energy of the system and bifurcation analysis was employed in order to study the relative stability of the isotropic and nematic phases as a function of the molecular biaxiality. The phase diagram of the system, in the vicinity of the Landau point where isotropic, uniaxial nematics and biaxial nematic meet, is shown in figure 21. In that figure $c = (\pi/4)DL^2\rho$ is the reduced density of the system while in the horizontal axis molecular biaxiality increases as we move to the right toward larger values of ψ . The solid line is the

locus of the lowest densities at which the model has uniaxial nematic solutions. The dotted lines are the loci of second-order uniaxial-biaxial transitions and the dashed line is the limit of stability of the isotropic phase with respect to nematic fluctuations. Therefore, at both sides of the Landau point the model predicts a first-order isotropic-uniaxial nematic transition, although coexistence was not calculated. At the Landau point the isotropic phase continuously transforms into the biaxial nematic upon increasing the density of the system. The phase diagram qualitatively resembles closely that obtained by Taylor and Herzfeld for hard spheroplatelets (left side of figure 19) and, as in that case, a uniaxial N_+ phase is obtained in the limit of rod-like particles and a uniaxial nematic N_- is stable in the opposite limit of plate-like particles. A simulation study of a bent-core molecule made from HSC sectors was performed by Lansac *et al* [156]. No biaxial nematic phase was found in this study, although other interesting features of the model were discovered, in particular the formation of a new class of smectic phase characterized by the spontaneous formation of macroscopic chiral domains (even though the particles are achiral).

A closed model for biaxial particles, composed of hard spherocylindrical sectors attached by their ends at an angle and forming a zigzag molecule, was studied by Maiti *et al* [157] by means of Monte Carlo simulations. This study, already discussed at the end of section 3.2, revealed the presence of isotropic, nematic, smectic A, smectic C, columnar and two crystal phases. Of interest here is the character of the smectic and crystal phases, which are biaxial, but not the nematic phase. Simulations have shown that a biaxial nematic phase made of hard biaxial ellipsoids require a high degree of biaxiality [162, 163]. Therefore, it is possible that the zigzag model may have a stable biaxial nematic phase for some specific molecular configuration.

Vanakaras *et al* [178] used Monte Carlo simulations and Onsager's theory of biaxial board-like particles with a frozen long axis and a freely rotating secondary axis. They calculated the phase diagram of the one-component fluid using simulation and compared the results with the Onsager theory. The phase diagram, in the packing fraction versus aspect ratio plane of the rectangular cross section perpendicular to the frozen axis (see figure 22) exhibited both uniaxial and biaxial nematic and smectic phases with phase boundaries all meeting at a single point. As discussed in section 3.5.1, they also studied a binary mixture, which was found to stabilize the biaxial nematic phase.

A more extensive theoretical study of the phase diagram of a system made of five different biaxial particles, differing in their cross sections, was done by Martínez-Ratón *et al* [179]. The orientation of the principal molecular axis was kept fixed along the z axis while the secondary axis can rotate freely. In this way, the system is able to show a uniaxial nematic phase with its director along the z axis, a biaxial nematic, with its secondary director in the xy plane (when long-range orientational order of the short molecular axes is present) and a tetratic nematic phase reminiscent of the corresponding tetratic nematic phase observed in 2D fluids of hard rectangles. Uniaxial, biaxial and tetratic smectic phases are also possible within this restricted-orientations model, their orientational

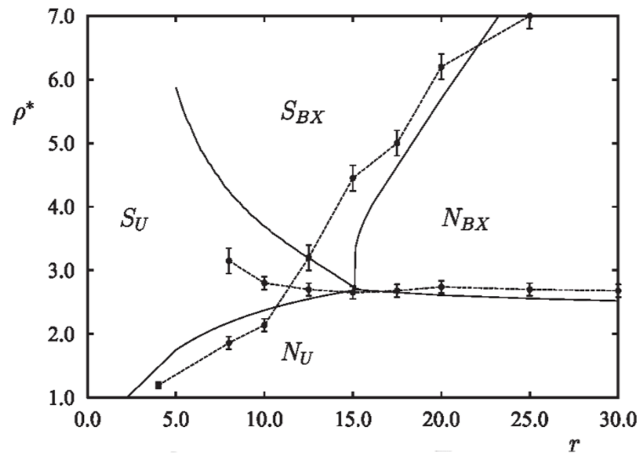


Figure 22. Phase diagram of the one-component fluid of hard biaxial board-like particles studied by Vanakaras *et al* [178] in the packing fraction versus particle aspect ratio plane. See text for a discussion. Reproduced from [178] with permission of the PCCP Owner Societies.

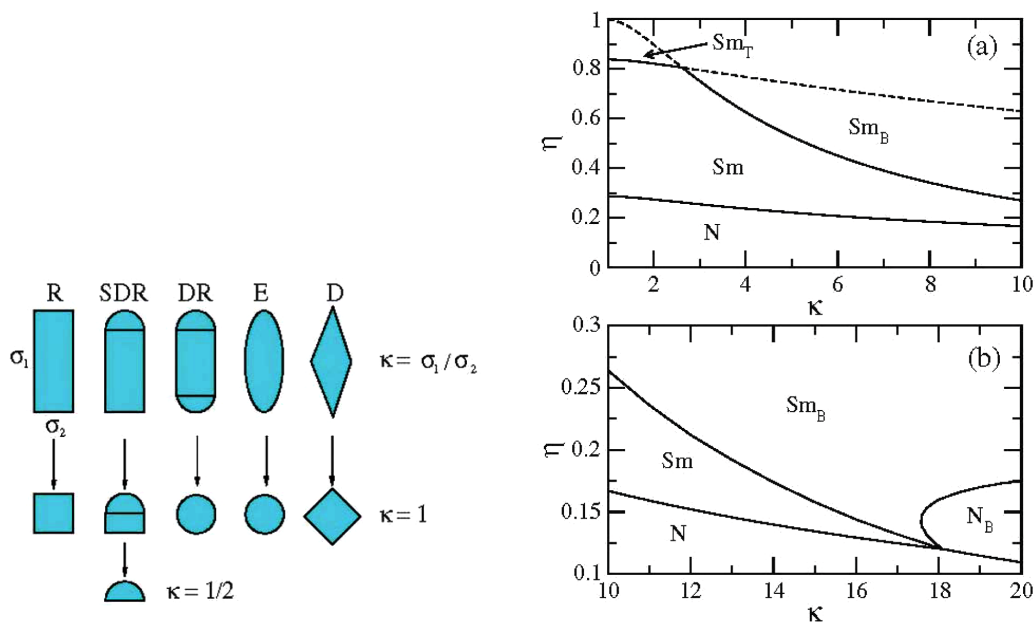


Figure 23. Left: cross section of biaxial particles studied in [179]. Right: phase diagram of a system of particles with R cross section. See text for a discussion. Reprinted with permission from [179]. Copyright (2008) by the American Physical Society.

properties being those of their nematic counterparts but showing long-range 1D translational order in such a way that particles arrange in layers perpendicular to the z direction. The theoretical approximation used was a fundamental measure density functional theory applied to parallel hard bodies, as reviewed in section 3.1.6. The model consists of hard biaxial particles with characteristic length L along the z axis and σ_1 and σ_2 in xy plane. Five different transverse sections (see figure 23) were considered: rectangle (R), semidiscrectangle (SDR, consisting of a rectangle capped with only one semidisc in one of its ends), discrectangle (DR, obtained from the previous one by adding another semidisc at the other end), ellipse (E) and deltoid (D, composed of an isosceles triangle and its reflection through its common base). Phase diagrams of one-component systems made of these particles were obtained as a function of particle biaxiality as measured by their cross section aspect ratio $\kappa = \sigma_1/\sigma_2$ (σ_1 being the largest size) and the system packing fraction η . The phase diagram of a system

of particles with R cross sections has been reproduced in figure 23 (a complete report of results is available in the original paper [179]). Cases (a) and (b) correspond to two different numerical minimizations of the free energy (a Gaussian parameterization in (a) and a Fourier expansion in (b) for the density profile). Continuous curves correspond to second-order phase transitions while dashed lines show the continuation of the Sm–Sm_B and Sm–Sm_T spinodals. For $\kappa = 18.101$ four second-order transition lines meet in a single point. The existence of this four-phase point at high enough values of κ is a common feature to all the systems of particles with different cross sections that have been studied. For aspect ratios of the cross section below the four-phase point, the system undergoes second-order N–Sm and Sm–Sm_B phase transitions upon increasing the packing fraction of the system. Beyond the four-phase point, for larger values of κ , the sequence of second-order phase transitions is N–N_B and N_B–S_B when packing fraction increases. In the case of the R cross section shown in

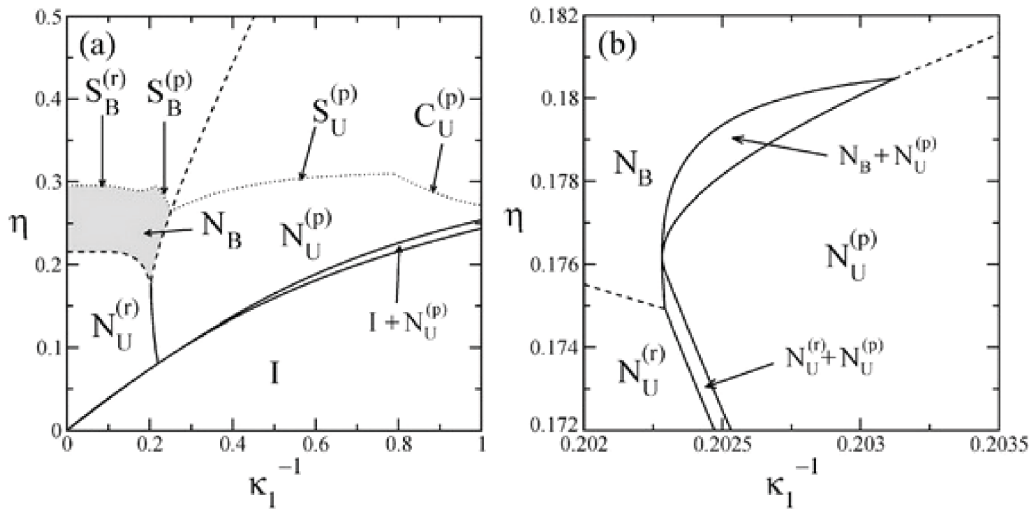


Figure 24. (a) Phase diagram of a system of hard board-like particles with $\kappa_2 = 5$ as obtained by Martínez-Ratón *et al* [180]. (b) A zoom around $\kappa_1^{-1} \sim 0.2$. Labels indicate regions of stability of the different phases, or the type of ordering with respect to which bifurcation curves are computed. Solid and dashed curves indicate first- and second-order phase transition, respectively. Dotted curves are bifurcation lines to the corresponding nonuniform phase from the stable bulk uniform phases. The shaded region in (a) corresponds to the estimated maximum region of stability of the biaxial nematic phase. Reproduced from [180] with permission of the PCCP Owner Societies.

figure 23, there is a region of κ just below the four-phase point where a re-entrant biaxial nematic is observed: the sequence of transitions in that region is $N-S_m$, S_m-S_{mB} , $S_{mB}-N_B$ and N_B-S_{mB} as η increases. The existence of this re-entrant behaviour of the biaxial nematic phase (also seen for some other cross sections studied, but not for all of them) is a genuine prediction of this fundamental measure approximation since Onsager’s theory predicts a monotonic phase boundary between N_B and S_{mB} phases [178].

An additional conclusion from this work is that the location of the four-phase point is highly sensitive to the shape of the particle’s cross section. As concluded by the authors, this fact suggests that the optimization of the particle geometry could be a useful criterion in the design of colloidal particles that can exhibit an increased stability of the biaxial nematic phase with respect to other competing phases with spatial order. Another relevant difference between different cross sections is the phase behaviour in the small κ and high η region where, as shown in figure 23 for the case of R particles, the S_{mT} phase could be stable. Not surprisingly, the region of stability of the tetratic smectic phase is found to strongly depend on the particle’s cross section, the reason being that the excluded volume involved in a T-configuration (two particles in a perpendicular configuration, needed in a stable tetratic phase) crucially depends on the particle cross section. In any case, the tetratic smectic phase is pre-empted by the crystalline phase, as the Monte Carlo simulations seem to show [178].

Inspired by the experimental finding by van den Pol *et al* [171] of a biaxial nematic phase in a system of goethite particles (see some details above), Martínez-Ratón *et al* [180] considered recently a system of board-like particles of sizes $\sigma_1 > \sigma_2 > \sigma_3$. As has been pointed out in the preceding paragraphs, there exists a general consensus among different approaches and also computer simulations, in that a biaxial nematic phase in systems of board-like particles (including spheroplatelets among them) could be stable for particles with $\sigma_1/\sigma_2 \approx \sigma_2/\sigma_3$

in such a way that they are not too rod-like or plate-like. In fact, this is also the case in the van den Pol *et al* experimental study: they found a stable biaxial nematic, as compared to the competing smectic and columnar phases, for board-like particles with $\sigma_1/\sigma_2 \approx \sigma_2/\sigma_3 = 3$. Martínez-Ratón *et al* used a fundamental measure density functional approximation, solved in the restricted-orientation approximation. The stability of the biaxial nematic with respect to smectic and columnar phases is studied as a function of the particle shape as measured by the two aspect ratios $\kappa_1 = \sigma_1/\sigma_2$ and $\kappa_2 = \sigma_2/\sigma_3$. A systematic study of the phase diagram of the system has been conducted by varying κ_1 while κ_2 is kept fixed. They have found phase diagrams which include all the uniform phases: isotropic, uniaxial rod- and plate-like nematics and biaxial nematic (see figure 24). Bifurcation analysis of the uniform phases with respect to fluctuations of the smectic, columnar and plastic solid types were also included in this study. According to their results for different values of κ_2 (see the original paper for other phase diagrams apart from that reproduced here), the biaxial nematic phase begins to be stable for $\kappa_2 \gtrsim 2.5$, in agreement with the experimental results of van den Pol *et al* [171]. Another feature of the phase diagram obtained from this theory, in agreement also with previous theories and simulations on biaxial hard particles, is the existence of a region of biaxiality centred at $\kappa_1 \sim \kappa_2$ which widens as κ_2 increases. The study of Martínez-Ratón *et al* was the first to apply fundamental measure theory to biaxial particles, going in this way beyond the second-order virial approximation. That allowed them to obtain a genuine result, not accounted for by previous studies based on second-order theories: the prediction that the phase diagram must be asymmetric in the neighbourhood of $\kappa_1 \sim \kappa_2$. Very recent computer simulations by Peroukidis and Vanakaras [181] for systems of board-like particles (namely, spheroplatelets) have confirmed the main conclusions of the work of Martínez-Ratón *et al*.

We end this section by noting that a big computer simulation effort has been done by different research groups to

shed some light on the problem of biaxial liquid-crystal phases. Some of these studies use hard-body models [162, 163]. An excellent and up-to-date review has been recently published in this journal by Berardi *et al* [164]. We refer the reader to this work for a more complete view on the current state-of-the-art in the field of biaxial phases in hard-body models.

3.4. Elasticity

Elasticity is a genuine property of liquid crystals and a crucial factor in determining the response of the material to external fields. A recent, general overview of the attempts to investigate liquid-crystal elasticity from the theoretical front has been written by Ferrarini [182]. Here we discuss the use of hard-body models to obtain qualitative and quantitative information on elastic constants of nematic and smectic materials.

Since the nematic phase has a broken rotational symmetry with respect to the isotropic phase, it presents elasticity. In practical terms this means that a spatial distortion of the local director field, $\hat{n} = \hat{n}(\mathbf{r})$, involves a cost in free energy. At the macroscopic level one expects this free energy cost to be related to the square gradient of the director field components, $\partial_\alpha \hat{n}_\beta$, where $\alpha, \beta = 1, 2, 3$ denote spatial coordinates. In an apolar nematic, i.e. one that does not distinguish between \hat{n} and $-\hat{n}$ (which is realized in practise when particles have head–tail symmetry), a general square–gradient expansion reduces, on applying the relevant symmetries, to the terms $(\nabla \cdot \hat{n})^2$, $[(\nabla \times \hat{n}) \cdot \hat{n}]^2$ and $[(\nabla \times \hat{n}) \times \hat{n}]^2$, meaning that there are three independent elastic distortion modes, splay, bend and twist, respectively, each associated to a particular elastic constant. The general expression for the elastic free energy, due to Frank [183], is

$$F_e = \frac{1}{2} \int_V d^3r \left\{ K_1 (\nabla \cdot \hat{n})^2 + K_2 [(\nabla \times \hat{n}) \cdot \hat{n}]^2 + K_3 [(\nabla \times \hat{n}) \times \hat{n}]^2 \right\}. \quad (61)$$

This is a purely macroscopic expression, giving the free energy that has to be added to the non-distorted nematic to obtain the complete free energy of the distorted nematic. It does not include any relaxation of the order parameter Q involved in the distortion, which will certainly exist. The study of this effect requires a microscopic theory.

The first microscopic theoretical calculations of elastic constants for model nematics were due to Priest [184], who used an Onsager theory for hard rods that incorporates a rotated director field in the long wavelength limit and an expansion in rotational invariants. Despite using hard rods as a model particle and Onsager theory (meant to reproduce hard needles), Priest obtained good agreement with experiment. The order of magnitude agreement with experimental values is remarkable, considering that the Onsager model strictly applies to very long rods. Shortly after this work, Straley [185] derived a more general expression for the elastic free energy directly from the Onsager density functional for hard rods, assuming a functional form for the distribution function but without any expansion. He obtained numerical values for the three constants close to the I–N phase transition, in agreement with the results of Priest.

In seminal work, Poniewierski and Stecki derived general expressions for the elastic constants of a nematic in terms of the direct correlation function [186, 187], $c^{(2)}(\mathbf{r}, \hat{\Omega}, \hat{\Omega}')$, of the undistorted nematic. For splay, bend and twist distortions, the elastic constants are given by:

$$\begin{aligned} K_1 &= \frac{1}{2} \int d\mathbf{r} x^2 \int d\hat{\Omega} \int d\hat{\Omega}' \rho'(\theta) c^{(2)}(\mathbf{r}, \hat{\Omega}, \hat{\Omega}') \rho'(\theta') \hat{\Omega}_x \hat{\Omega}'_x, \\ K_2 &= \frac{1}{2} \int d\mathbf{r} x^2 \int d\hat{\Omega} \int d\hat{\Omega}' \rho'(\theta) c^{(2)}(\mathbf{r}, \hat{\Omega}, \hat{\Omega}') \rho'(\theta') \hat{\Omega}_y \hat{\Omega}'_y, \\ K_3 &= \frac{1}{2} \int d\mathbf{r} z^2 \int d\hat{\Omega} \int d\hat{\Omega}' \rho'(\theta) c^{(2)}(\mathbf{r}, \hat{\Omega}, \hat{\Omega}') \rho'(\theta') \hat{\Omega}_x \hat{\Omega}'_x. \end{aligned} \quad (62)$$

Here $\rho(\mathbf{r}, \hat{\Omega}) = \rho(\theta)$ is the local density distribution of the undistorted nematic, with $\cos \theta = \hat{n} \cdot \hat{\Omega}$. Numerical values for the elastic constants were obtained for hard rods, using a direct correlation function from Onsager theory (i.e. the Mayer function, which is exact in the low-density limit). Equations (62) have later been rederived in more direct ways [188–190]. Also, the contribution from the relaxation of the distribution function was later evaluated [190] and the relative contributions from repulsive and attractive interactions have been assessed [191, 192]. The derivation of general expressions for K_i in terms of microscopic correlations was an important step, since it allowed the calculation of elastic constants from microscopic grounds: given a theory for $c^{(2)}$ for some particular molecular theory (e.g. a density functional theory, from which the direct correlation function can be obtained by functional differentiation), one can evaluate the constants K_i , which in turn can be plugged into the macroscopic Frank expression to give predictions about the behaviour of realistic models of distorted liquid crystals, something which is very important in technological applications.

Singh and Singh [193] calculated the elastic constants of hard ellipsoids, using series expansions for the direct correlation function. Bad convergence properties with respect to the number of terms in the expansion were found. Lee and Meyer [194] recalculated the elastic constants for hard rods using Straley’s method and Onsager theory (hard needles) and found general agreement with Poniewierski and Stecki. They used a more accurate orientational distribution function than previous authors. Also, they noted that reasonable predictions were obtained when comparing with real data for virus suspensions, but results were not so reasonable for solutions of more flexible colloidal particles. Shortly after, Lee [195] and Somoza and Tarazona [196] made calculations using different choices for the direct correlation function. Lee used PL theory to calculate the uniform nematic and obtained the direct correlation function not from the PL density functional, but from an independent prescription. Also, he neglected terms of order D/L and higher in the excluded volume expansion, which produced the equality $K_1 = 3K_2$, a result not supported by simulations. In contrast, Somoza and Tarazona obtained the direct correlation function in a consistent way, i.e. from the second functional derivative of the free energy density functional and the same theory was used to obtain the reference nematic state. Including contributions to all orders, they obtained much better agreement with simulations (figure 25).

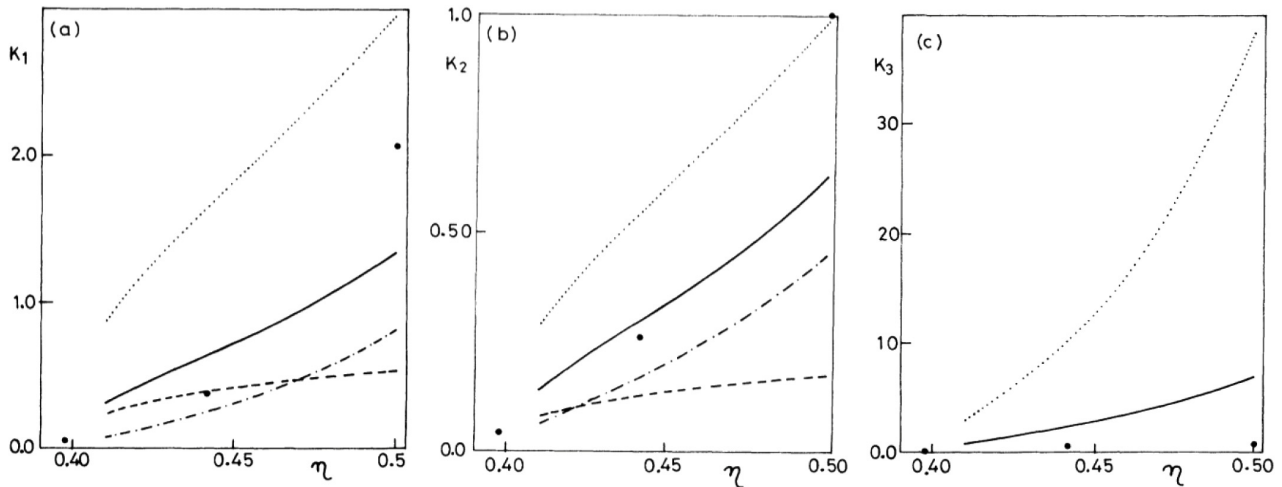


Figure 25. Results for the nematic elastic constants from the Somoza–Tarazona theory [196] (continuous line) and the Sin–Doo Lee theory [195] (dotted lines). Simulation results from [197] are given by circles. Reprinted with permission from [196]. Copyright (1989) by the American Physical Society.

Poniewierski and Hołyst [107] used their proposed version of DFT for hard spherocylinders to derive the necessary direct correlation function for the nematic fluid and to calculate the elastic constants, also in a consistent way. Their results were similar to those of Somoza and Tarazona and compared equally well with simulations. Finally, Somoza and Tarazona incorporated the relaxation of the nematic order parameter in the distorted nematic [190] and found that this effect reduces the values of the elastic constants.

On the simulation front, Allen *et al* used expressions for the elastic constants obtained from fluctuations of the order tensor [197] to compute values from simulations of the hard ellipsoid and hard spherocylinder models [198] (note the factor 9/4 missing in the results, corrected in [199]), finding moderate agreement with the then existing theories [193]. Tjipto-Margo *et al* [200] made a detailed analysis of the comparison between simulation results and the early theories for the direct correlation function; although order of magnitude agreement was found, discrepancies with simulation existed, which were attributed to the poor description of the function at long distances.

Later, Singh *et al* [201] presented a more systematic study of their expansion method to calculate numerical values for the elastic constants and included attractive contributions to the interactions via perturbation, concluding that the repulsive contribution of the pair interaction is dominant. These authors also used the same method to calculate values for the twelve elastic constants of a biaxial nematic fluid [202]. The relative values of the constants and their behaviour as the biaxial phase goes to the uniaxial phase were discussed. An interesting result is that the effect of biaxiality in the orientational ordering on the elastic constants is small.

The elastic behaviour of smectic phases has also been studied, although not so thoroughly as for nematic phases. In a smectic A phase, distortions of the director field must keep the integrity of the smectic layers intact, which means that bend and twist distortions are not allowed. Due to the broken translational symmetry of the smectic A along the director, there

exists an elastic modulus B , associated to layer compressibility, adding a term $\frac{1}{2}B \int_V d^3r (\partial u / \partial z)^2$ to the elastic free energy. u is the local displacement field of the layers (similar to the displacement field in 3D solids). Two derivations of expressions for the smectic elastic constants have appeared in the literature. Lipkin *et al* [189] derived expressions for the elastic constants of a smectic phase as a generalization of the corresponding expressions for the nematic and including the layer compressibility modulus B . Numerical values for the constants were not estimated. More recently, Singh *et al* [203] derived expressions for the constants in terms of order parameters and estimated their magnitude. The formalism included tilted smectic phases. However, in neither of these studies has a serious evaluation, related to a particle model, been made.

In this section we have mentioned works on elastic constants that make use of hard-body models to represent particle interactions. Many recent studies have been devoted to the effect of attractive interactions on the elastic properties of nematic liquids, mainly through perturbative treatments. In line with the spirit of the present review, these studies, more appropriate to establish contact with real materials, are not mentioned here and we refer the reader to the review works referenced in the introduction.

3.5. Multicomponent fluids

3.5.1. Binary mixtures. When hard-body particles of different shapes are mixed together in different concentrations, new phenomenology arises in the macroscopic phase behaviour of the system. Again, since particles are hard bodies, the new phenomena are due entirely to entropy. In the last 30 years or so there has been considerable interest in the study of entropy-driven transitions in mixtures.

Probably one of the first studies was due to Asakura and Oosawa [204], who showed that the addition of a small amount of non-adsorbing polymer to a dispersion of (hard) colloidal particles leads to an attractive interaction between these particles. The origin of this attraction is, of course,

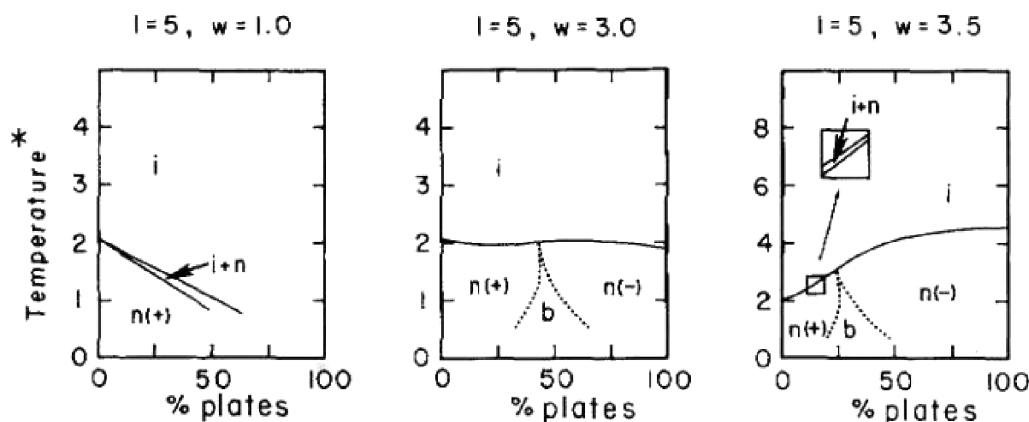


Figure 26. Phase diagrams of a mixture of rods and plates as obtained by Alben [209] using his mean field lattice model. The effective temperature shown in the vertical axis is proportional to the temperature divided by the pressure, as it corresponds to a system with hard-body interactions where the internal energy is, therefore, identically zero. Labels indicate isotropic (i), uniaxial nematics ($n(+)$ and $n(-)$) and biaxial nematic (b). Continuous lines correspond to first-order phase transitions while dotted lines are second-order phase transitions. Reprinted with permission from [209]. Copyright (1973), AIP Publishing LLC.

entropic: polymer molecules maximize their free volume when the large colloidal particles are close to each other, the so-called *depletion* effect. The mixture can be theoretically modelled in a simplified manner by getting rid of the polymer and considering this attraction as an effective depletion potential between the colloidal particles and one can then use all the theoretical tools available for simple fluids.

This route was followed by some authors in the last quarter of the last century to analyze the phase behaviour of different binary mixtures. For example, in 1999 Lekkerkerker and co-workers used an extension of the free-volume approximation to investigate the depletion-induced phase separation in mixed suspensions of colloidal spheres of diameter σ and colloidal rods of length L and diameter D , in the range $L \leq \sigma$ [205]. Later, the same group used the depletion approximation to conclude that the addition of a small amount of non-adsorbing polymer significantly modifies the I–N phase boundaries of a system of sterically stabilized colloidal platelets [206].

Mixtures of colloidal particles with non-adsorbing polymers and also mixtures of colloidal particles of different shapes, have been extensively studied not only from the theoretical point of view, but also experimentally, as shown, for example, in [207, 208] and references therein. Experimental studies have probably triggered the interest of many theoreticians in modelling mixtures in an effort to predict their macroscopic behaviour. Models based on the depletion approximation, like those mentioned above, have been applied to other mixtures of colloidal particles, but those models will not be treated in this review since they reduce the problem, at the end, to a simple system whose particles interact via an effective potential that is not a hard-body interaction, a subject not covered in this review.

One of the earliest approaches to describe theoretically binary mixtures of anisotropic particles with different shapes was presented in 1973 by Alben [209]. He made mean field lattice model calculations of a mixture of rod- and plate-like molecules. The model is a modification of that originally proposed by Flory to describe steric interaction in polymers. Space is represented by a cubic lattice of M cells. Dispersed on this

lattice there are a total of N molecules, a fraction $1 - c$ of which are rods, each occupying l consecutive cells along one of the lattice axes. A fraction c of the N particles are square plates, each occupying $w \times w$ coplanar cells in a plane defined by two of the lattice axes. Both types of particles are one cell thick. In this way, there are three possible orientations for each type of particle, making a total of six orientations. It is assumed that there are no interactions between particles, except for the hard-core interactions that prevent two particles from occupying the same cell. The thermodynamic properties of the system follow by approximating the configurational partition function corresponding to the ways of placing the N molecules into the M cells under the restriction that a fraction c are plates and a fraction $1 - c$ are rods. Details can be found in Alben's paper. The results indicate that the I–N transition can be continuously changed from first- to second-order and, also, that a biaxial nematic phase can be stabilized for an appropriate choice of the dimensions and concentrations of the two components of the mixture. Some of the results of Alben are reproduced in figure 26.

A formally exact theoretical approximation for a HS–HE mixture was developed in 1994 by Samborski and Evans [210]. They followed the standard route to express, in the framework of DFT, the free energy of the system in terms of a functional integral of the direct correlation function. Since there is no way to determine the direct correlation function of a system of hard anisotropic particles, even in the one-component case, Samborski and Evans approximated the direct correlation function from existing equations of state of fluid mixtures of hard convex bodies: integrating the pressure, the Helmholtz free energy of the system is obtained and from this the direct correlation function can be calculated upon functional differentiation. The theory was applied to different HS–HE mixtures, changing the HE elongation and the ratio between the HS and HE volumes. No demixing was found, even in cases where the HS volume was considerably smaller than the HE volume. At high enough density, a I–N transition was found, accompanied by phase segregation such that the N phase is richer in ellipsoids than the I phase. It was also found

that the N phase has a higher-order parameter and a higher pressure than the N phase of a one-component HE fluid.

Many of the hard-body models applied to binary mixtures of colloidal particles are extensions, at different degrees of sophistication, of the Onsager theory for one-component fluids. Each component i of a binary mixture ($i = 1, 2$) made of uniaxial particles is described in terms of a local density $\rho_i(\mathbf{r}, \hat{\Omega})$. For a uniform fluid $\rho_i(\mathbf{r}, \hat{\Omega}) = \rho_0 x_i h_i(\hat{\Omega})$, where $x_i = N_i/N$ is the fraction of species i , N_i its number of particles and $N = N_1 + N_2$ the total number of particles. $h_i(\hat{\Omega})$ are the orientational distribution functions. By substituting $\rho(\mathbf{r}, \hat{\Omega}) \rightarrow \rho_i(\mathbf{r}, \hat{\Omega})$ in the expression for the ideal free energy of a one-component system (8), summing over all species i and using Onsager excess free energy approximation (16) extended to all pairs of species ij , Lekkerkerker and co-workers [211, 212] extended Onsager's second virial theory to a mixture of hard particles. The resulting expression for the Helmholtz free energy per particle is

$$\frac{\beta F}{N} = \log(\rho_0 \Lambda_i^3) + \sum_{i=1}^2 x_i (\log x_i - s_{\text{or}}^{(i)}) + \rho_0 \sum_{i=1}^2 \sum_{j=1}^2 x_i x_j B_2^{(ij)} [h_i, h_j], \quad (63)$$

where Λ_i is the thermal wavelength of species i , $s_{\text{or}}^{(i)} = -\left\langle \log \left[4\pi h_i(\hat{\Omega}) \right] \right\rangle_{h_i}$ are the orientational entropies per particle of species i in units of the Boltzmann constant k [which is a functional of the orientational distribution function $h_i(\hat{\Omega})$], while

$$B_2^{(ij)} [h_i, h_j] = \frac{1}{2} \left\langle \left\langle v_{\text{excl}}^{(ij)}(\hat{\Omega}_i, \hat{\Omega}_j) \right\rangle \right\rangle_{h_i, h_j} = \frac{1}{2} \int_V d\hat{\Omega}_i \int_V d\hat{\Omega}_j v_{\text{excl}}^{(ij)}(\hat{\Omega}_i, \hat{\Omega}_j) h_i(\hat{\Omega}_i) h_j(\hat{\Omega}_j) \quad (64)$$

represents orientation-averaged excluded volumes of two particles of species ij . Three different entropy contributions are apparent in equation (63): mixing, orientation and excluded volume entropy terms, respectively. The phase behaviour of the system is the result of a delicate balance between the three entropic terms. The theory was first applied to a binary mixture of rods of different lengths [211]. A I–N transition was found, with the N phase being significantly richer in long rods than the I phase. The order parameter of the long rods was found to be larger in the coexisting N phase than in the one-component fluid made of equally long rods. The order parameter of the short rods first increased and then decreased with an increasing mole fraction of the long rods.

In another application, Stroobants and Lekkerkerker [212] used the theory for mixtures of rods and plates, modelled as hard cylinders of appropriate dimensions. The results obtained indicated that, depending on the total concentration of particles and the fraction of rods and discs, the mixture exhibits, in addition to the I phase, two uniaxial N phases and a biaxial N_B phase (see figure 27). One of the uniaxial N phases corresponds to a rod-rich mixture, with the rod director oriented along

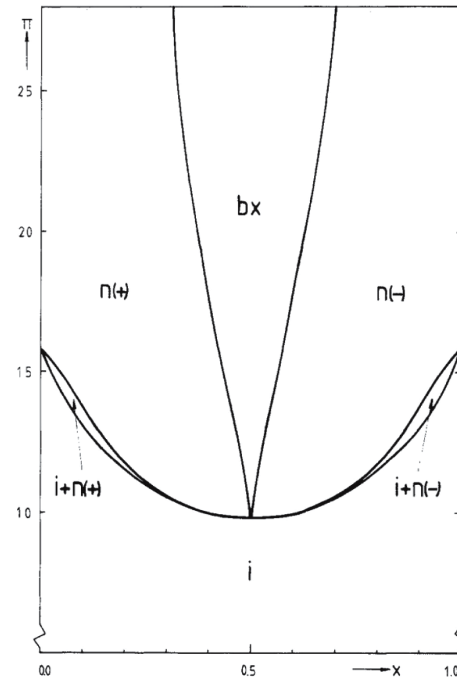


Figure 27. Osmotic pressure (Π)—fraction of discs (x) phase diagram of a mixture of rods and discs for the case $B_2^{(11)} = B_2^{(22)} = B_2^{(12)}$ obtained from the second virial Onsager theory of Stroobants and Lekkerkerker [212]. Reprinted with permission from [212]. Copyright (1984) American Chemical Society.

some direction and the plate director situated in the plane perpendicular to the rod director ($n(+)$ in the figure). The other uniaxial N phase is plate-rich with the rod director along the plane perpendicular to the plate director ($n(-)$ in the figure). In the N_B phase the two perpendicular directors are kept at a fixed orientation. If we take into account that in figure 27 the vertical axis is essentially the inverse of the effective temperature plotted in the vertical axis of figure 26, a remarkable qualitative agreement between results from the lattice model of Alben and the Onsager theory of Stroobants and Lekkerkerker is apparent.

In 1994, van Roij and Mulder [213] studied the relative stability of the N_B phase against N–N demixing as a function of aspect ratio in a symmetric binary mixture of plates and rods (meaning that the rod aspect ratio is the inverse of the plate aspect ratio), using the Onsager second virial theory in the Zwanzig approximation. They found that, for an aspect ratio equal to 5, the mixture separates into two uniaxial nematic phases, but with no biaxial nematic phase present. In contrast, for an aspect ratio equal to 15, a stable biaxial phase was found.

The same problem was analyzed, also using Onsager theory, by Vanakaras *et al* [214] (see also [178] where the N_B phase in mixtures of biaxial board-like particles is investigated using Onsager theory and MC simulations). They concluded that no stable N_B phase is found in mixtures of hard rods and plates for small aspect ratios (about 5, the typical value for usual nematogens). Stabilization was predicted, however, at much higher values of the aspect ratio (30 or higher).

The prediction of a biaxial N_B phase in fluids of uniaxial particles caught the attention of other researchers [215, 216]. In these investigations the rod-plate mixture was modelled by

prolate HE of finite aspect ratio $\kappa = e$ (rods) and oblate hard ellipsoids of aspect ratio $\kappa = 1/e$ (plates) and equal volume. Computer simulations were performed for $e = 10, 15$ and 20 . The same four distinct phases predicted by the theory were found: I, two uniaxial N and the biaxial N_B phases. However, the region of stability of the N_B phase was found to be severely limited by demixing into two coexisting uniaxial phases, N_U^+ and N_U^- , the N_B phase being stable only in a narrow region of elongation and mixture composition.

An extension of the Onsager theory to include, in the spirit of the PL approximation, the contribution from higher-order virial terms, was also carried out by Varga *et al* [217]. The Helmholtz free energy excess per particle of the mixture, giving the contribution from excluded volume interactions, is written as:

$$\frac{\beta F_{\text{ex}}[h_1, h_2]}{N} = \psi_{\text{HS}}(\eta) \frac{\sum_{i=1}^2 \sum_{j=1}^2 x_i x_j B_2^{(ij)}[h_1, h_2]}{B_2^{(\text{HS})}}. \quad (65)$$

The HS volume of the reference system, v_0 , is obtained as a mole-fraction-weighted sum of the particle volumes of each species, $v_0 = x_1 v_1 + x_2 v_2$. This is, in essence, the generalization to mixtures of the procedure that improves Onsager theory to give PL theory for a one-component fluid. Again the density prefactor accounts for the contribution to the free energy arising from higher-order virial terms. Compared with the simpler Onsager's second virial approach, the application of this theory to the analysis of HE mixtures improved the theoretical predictions as compared to simulations [217]. However, in contrast to simulation results, the rescaled Onsager theory predicts a symmetric phase diagram with respect to the equally molar mixture of prolate and oblate ellipsoids, as a result of the prolate-oblate symmetry of the excluded volume.

The possible existence of the biaxial N_B phase in mixtures of uniaxial particles was further analyzed by other authors and not only for rod-plate mixtures. In 2000 Kooij and Lekkerkerker [218] came back to study the problem, this time experimentally. They used a combination of two systems, rod-like boehmite (AlOOH) and plate-like gibbsite ($\text{Al}(\text{OH})_3$) colloids, which can be approximated as hard bodies. For the particular particle sizes used (see original reference for details), the study ruled out the existence of a N_B phase with rods and plates orientationally ordered in mutually perpendicular directions. It was found that the biaxial N_B phase is unstable with respect to demixing into an isotropic and two uniaxial nematic phases, in line with the findings of [215, 216]. The origin of demixing is the larger excluded volume of a rod-plate pair compared to the rod-rod and plate-plate excluded volumes, an effect that compensates the mixing entropy, which favours the biaxial phase. As concentrations increase, the excess excluded volume becomes more important and the system demixes. Nevertheless, a word of caution is needed, because experimental systems are always polydisperse and its phase behaviour may be dramatically different from that of strictly binary mixtures (see section 3.5.2).

The PL theory for binary mixtures was applied in 2001 by Wensink *et al* [219] to study the phase behaviour of a mixture

of thin and thick platelets. I–N density inversion (where the I phase is heavier than the N phase) was found, in agreement with previous experimental results.

The same theory was applied to different kinds of mixtures by Jackson and co-workers in an extensive series of works in the period 2002–2005 [217, 220–222]. The phase behaviour of a mixture of rods and plates [217], both approximated by hard cylinders of appropriate dimensions, was studied. In all cases the plate volume was always orders of magnitude larger than the rod volume. The authors did not carry out systematic free energy minimization and phase coexistence calculations for all the mixtures investigated; instead, they used a combined analysis based on I–N bifurcation and spinodal demixing calculations to determine the geometrical requirements for the occurrence of a demixing transition involving two I phases. What they found (see figure 28) was that the I phase is unstable relative to demixing for a wide range of molecular parameters. The reason is the large excluded volume associated with the mixing of unlike particles. However, using stability analysis they found, for certain aspect ratios, that the I–N transition always pre-empts I–I demixing, irrespective of the particle diameters. On the other hand, when I–I demixing was found, it was accompanied by the existence of an upper bound at large size ratios (Asakura and Oosawa limit) and a lower bound at small size ratios (Onsager limit), beyond which the system showed a mixed I phase. The results of the stability analysis were confirmed by full phase diagram calculations for selected values of the particle geometrical parameters.

Mixtures of rod-like and disc-like particles were studied also by Jackson and co-workers [221] using MC computer simulations in the canonical ensemble and PL theory. Particles were modelled as HSC of aspect ratio 5 and hard cut spheres of aspect ratio 0.12, the ratio of diameters being chosen so that both particles had the same volume. Simulations starting from a mixed isotropic state showed that, at low total density, the I phase is stable with respect to ordered states. Coexistence between two uniaxial N phases and the stabilization of a disc-rich I phase was found. At high densities the mixture exhibits N–C and S–C phase coexistence. In agreement with simulations, no stable biaxial nematic phases were found. The PL theory used in this work is not suitable for the study of translationally ordered states, such as C or S phases and, consequently, the study was restricted to the I and N phases.

The last kind of mixtures studied by Jackson and co-workers were mixtures of hard rod-like particles. In a first paper [220], a mixture of HC of aspect ratios 15 and 150 was considered. The phase behaviour of the mixture was explored as a function of the ratio d between the diameters of the two cylinders using again the PL theory. The results obtained can be summarized as follows: for large enough values of the diameter ratio, for example $d = 50$, the mixture shows only a I–N phase transition driven by the excluded volume interaction between the large particles. In this case of very different sizes, big particles can be considered as large colloidal particles. Since exclusion interactions between particles of the other component and between unlike particles are significantly small compared to interactions between large particles, small particles play the role of a weakly interacting solvent and

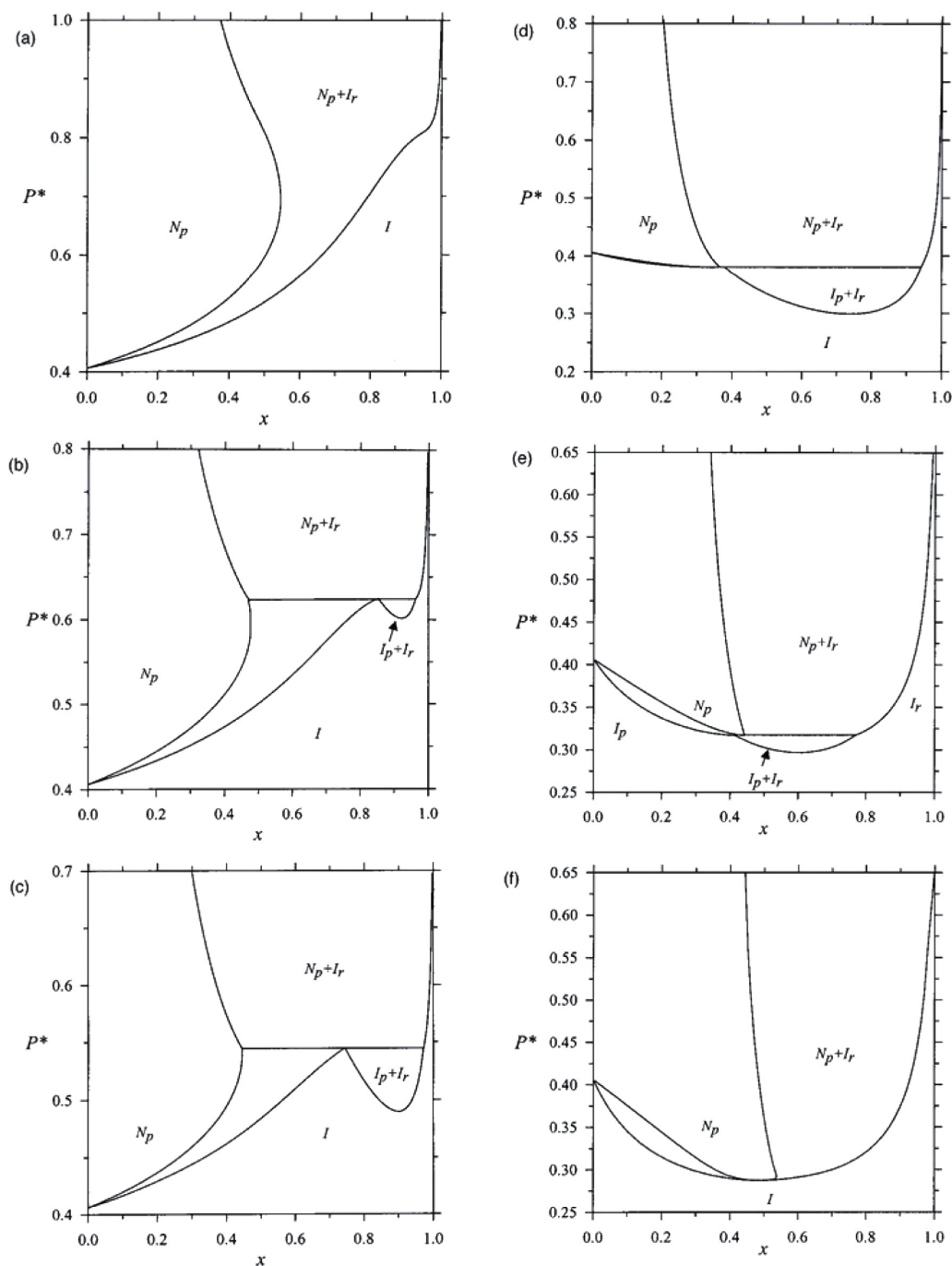


Figure 28. Pressure versus composition phase diagrams of mixtures of plates and rods with aspect ratios 50 and 1/50 and different plate/rod diameter ratios d , (a) $d = 80$, (b) $d = 60$, (e) $d = 50$, (d) $d = 25$, (e) $d = 18$ and (f) $d = 6$ as obtained by Jackson and co-workers using the Parsons–Lee theory [217]. The labels I_r , I_p , N_r , N_p denote the rod-rich isotropic, plate-rich isotropic, rod-rich nematic and plate-rich nematic phases, respectively. x is the mole fraction of rods. Reprinted with permission from [217]. Copyright (2002), AIP Publishing LLC.

I–I or N–N demixing is not to be expected. However, when the diameter ratio is reduced, excluded interactions involving small particles become more important, particularly those between unlike particles. As a consequence, I–I and N–N demixing transitions are indeed observed. The precise topology of the phase diagram of this particular mixture can be rather complicated and, in fact, it changes significantly with variations in the diameter ratio d . This is not surprising since the three excluded volume interactions become more and more

comparable as d is reduced and the final topology of the phase diagram is the result of a delicate free energy balance from these contributions. Detailed results can be found in the original paper [220].

In the last paper of their series [222], Jackson and co-workers again applied the PL theory of hard-rod mixtures to model an experimental mixture of thin and thick viral particles, consisting of charged semiflexible fd-virus (thin rods) and fd-virus irreversibly coated with the neutral polymer polyethylene

glycol, fd-PEG (thick rods). The geometrical parameters of the hard rods were chosen to mimic the experimental system. Thin and thick particles were modelled as rods of the same length $L = 24D_{\text{thick}}$, where D_{thick} is the diameter of the thick rods, and different diameters. This particular choice of L corresponds to the experimental aspect ratio of the thick particles. Phase diagrams of the mixture for diameter ratios $d = D_{\text{thick}}/D_{\text{thin}}$ ranging from 3.7 to 1.1 were considered in order to reproduce the experimental systems. The theory predicts a region of I–I coexistence which is not observed experimentally. Also, for small values of d , an I–N phase transition is found at low concentrations, while at high values of d a N–N coexistence region, ending in a lower critical point, is predicted. As d increases, the N–N lower critical point moves to lower rod concentrations and, upon increasing d even further, a parameter region is entered where the phase diagram shows an I–N–N coexistence region capped by a region of N–N coexistence bounded by an upper critical point and by an additional region of N–N coexistence bounded by a lower critical point. Finally, for very large d , these two regions of N–N coexistence coalesce to form a single N–N coexistence region (see figure 3 in [222] for details).

The mixture of thin and thick hard rods of the same length had been previously analyzed by van Roij *et al* in 1998 [223] using the simple Onsager theory. They found that the mixtures not only show an I–N transition and the previously predicted depletion-driven I–I demixing transition, but also a N–N demixing transition driven by the orientational entropy of the thin rods. Several cases, corresponding to different values of the diameter ratio d , were studied and phase diagrams exhibiting I–N, I–I and N–N coexistence, I–N–N and I–I–N triple points and I–I and N–N critical points, were obtained. When compared with experiments [222], these results showed that Onsager's second virial theory qualitatively reproduces the main features of the experimental phase diagram for large values of d . However, the theory is not able to account for the phase behaviour evolution from a totally miscible N phase to a demixed N–N state upon increasing d . The use of PL rescaling shows that an I–N–N coexistence region is not required for a region of N–N coexistence to exist, in contrast to the predictions of the second virial theory. But not everything is fully understood yet. For example, the N–N upper critical point, predicted for very long rods by both theories, has not been observed in the experiments. The effect of a small degree of flexibility was not taken into account in the theories, but fd-virus particles are not completely rigid. Therefore, direct comparison of theoretical predictions with experiments on mixtures of fd-virus has to be done with care.

All of the above theoretical studies on nematic ordering in mixtures of hard bodies use Onsager theory or variations thereof. In contrast, Schmidt [137] used his fundamental measure-based DFT to calculate the isotropic phase of a hard needle-hard sphere mixture for different values of the aspect ratio L/D , where D is the diameter of the spheres. The phase diagrams produced by the theory were similar to those obtained from free-volume theory [224], which predicts a demixing transition ending in a critical point, with each of the demixed phases rich in one of the components. The sphere-sphere radial

distribution function, as obtained from the theory, was in good agreement with the Monte Carlo simulation results performed by the same author [137].

This functional was further extended by Schmidt and von Ferber [225] to incorporate an amphiphilic-like hard-body particle formed by a HS with a radially attached hard needle. The resulting ternary mixture constitutes a simple model for a water (HS)-oil (needle)-amphiphilic (HS+needle) mixture where particles interact only via non-overlapping excluded volumes. While the Mayer functions for a pair of HS or a pair of hard needles are exactly obtained by convolutions of weight functions, for a HS and amphiphilic particle or two of the latter the Mayer functions are only approximate, due to their non-convex excluded volumes. However, the authors showed that the deviations of the second virial coefficients with respect to the exact result are relatively small. Equations of state for the pure amphiphilic fluid and for the amphiphilic-needle, amphiphilic-HS and HS-needle binary mixtures (all of them in the isotropic state) were calculated and compared with canonical MC simulations carried out by the same authors. The theory is in remarkable agreement with simulations for total packing fractions less than 0.3. Also, the equations of state for a ternary mixture of a particular composition compare very reasonably, figure 29. The authors calculated analytically the demixing spinodals of all possible binary mixtures and of the ternary mixture and showed that the amphiphilic-needle and amphiphilic-HS binary mixtures are more miscible than the HS-hard needle mixture, a property exhibited by real amphiphilic molecules due to their simultaneous hydrophilic and hydrophobic tendencies.

The same formalism was used by Schmidt and Denton to treat a ternary mixture of colloidal HS-hard needle-ideal polymer mixture [226]. The ideal polymer was approximated by a sphere that interacts via excluded volume with the colloidal spheres, but there is no interaction between the polymers. The effect of the polymer-needle interaction on the phase behaviour of the ternary mixtures was studied and different phase diagrams were calculated by solving the conditions for mechanical and chemical equilibrium of the isotropic coexisting phases. Calculations were carried out for the case where the HS diameter, the polymer diameter and the needle length are equal. In the case of no polymer-needle interaction, demixing between colloid-rich and colloid-poor phases is found. When the hard needle-polymer interaction is included, rich phase diagrams, exhibiting three-phase coexistence and re-entrant demixing behaviour, were obtained. The addition of needles to the HS-polymer mixture stabilizes the ternary mixture, an effect due to the competition between the polymer- or needle-mediated depletion effect and the interaction between them.

More recently, FMT functionals have been devised and applied to more complicated mixtures. A functional developed for a ternary mixture of HS, hard needles and hard platelets of vanishing thickness obtained by Esztermann *et al* [140], was later generalized by Philips and Schmidt [227] to study the phase behaviour of binary mixtures of infinitely thin platelets with different diameters D_1 and D_2 . Different phase diagrams were produced for $\kappa = D_1/D_2$ ranging from 1 to 5. For $\kappa = D_1/D_2 < 1.7$ the phase diagram includes the usual

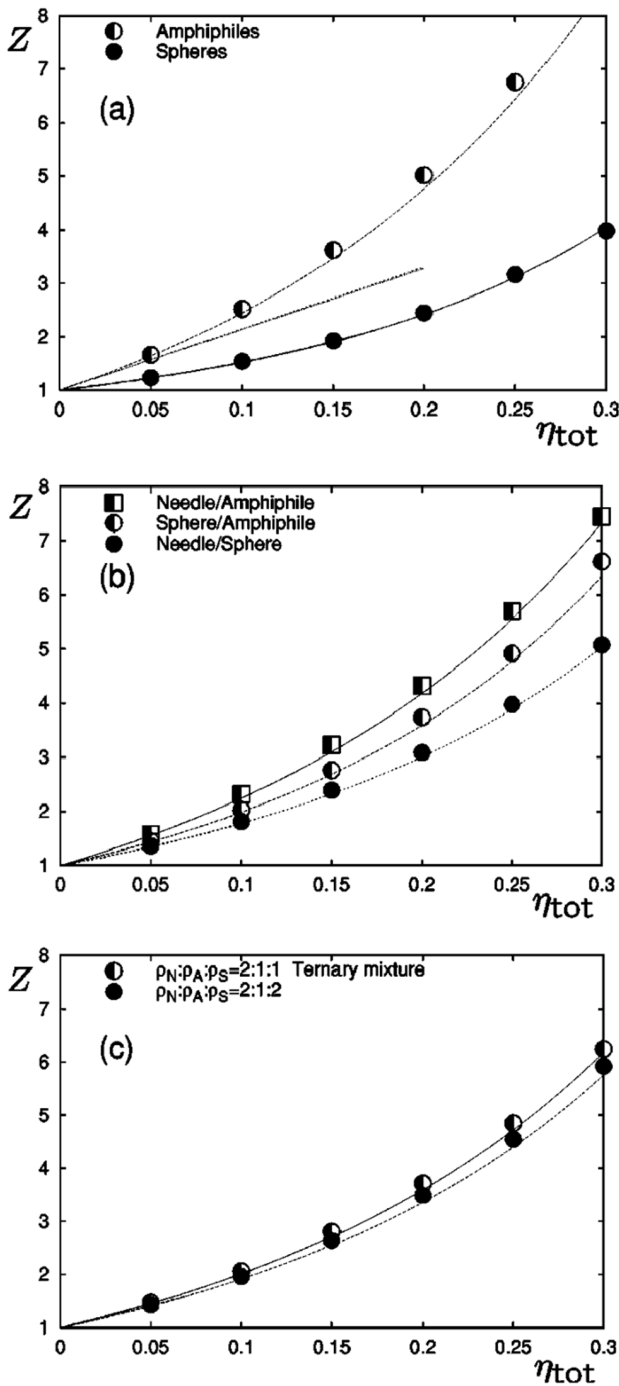


Figure 29. Compressibility factor Z as a function of total packing fraction η_{tot} of an amphiphilic mixture, according to the theory of Schmidt and von Ferber [225]. MC simulations (symbols) are compared with the theory (lines). Straight lines show the low-density limit governed by the second virial theory. (a) Pure systems; (b) binary mixtures; (c) ternary mixtures. Reprinted with permission from [225]. Copyright (2001) by the American Physical Society.

I–N transition, which becomes wider as κ is increased. For $\kappa > 2$ there appears N–N demixing and an associated I–N–N triple point. No I–I demixing was found. The results from the present theory were compared with those from the Onsager theory and three major differences were found: (i) the FMT predicts a smaller I–N biphasic region, (ii) the transitions

obtained by FMT are located at lower densities as compared to the Onsager model and (iii) for the same κ , the N–N demixing region obtained from FMT spans a larger range of compositions. However, the general phase diagram topologies predicted by both theories were similar. Fractionation between coexisting phases increases with κ and big particles in each of the coexisting phases are more orientationally ordered.

de las Heras and Schmidt [228] reformulated the FMT functional of Esztermann *et al* [140] for a binary mixture of HS and hard platelets of vanishing thickness, calculating the phase behaviour of the mixture. They found a strong broadening of the I–N biphasic region upon increasing the pressure. Also, for large values of the aspect ratio $\kappa = D_P/D_{HS}$, N–N demixing with different platelets concentrations was found. In the same work, the authors formulate a FMT-based functional for mixtures of hard platelets of vanishing thickness and overlapping hard spheres as an approximate model to study the phase behaviour of platelet-polymer mixtures. For low platelet-polymer size ratios, aside from I–N and N–N phase coexistences, the mixture exhibits I–I demixing (not found in hard-core platelet-sphere mixtures).

In addition to the more or less systematic studies on positionally disordered phases of mixtures reviewed in the previous paragraphs, there have been studies of very particular mixtures using both computer simulations and theoretical models. For example, Seara *et al* [229] used Onsager theory to study the phase behaviour of a binary mixture of rods with different aspect ratios. By choosing particle sizes adequately, the values of second-order virial coefficients were adjusted to be equal. Since virial coefficients are the same, phase diagrams of the one-component fluids are, at least in the framework of Onsager theory, identical and independent of the particle aspect ratio in the hard-needle limit. Therefore, the paper focuses on the case of mixtures where one component is longer and thinner than the other and the evolution of the phase diagram topology is studied as a function of the shape difference between the two components. The main result is the occurrence of I–I demixing, with an associated critical point and N–N demixing is also obtained. There is a N–N critical point that shifts as the shape difference increases, eventually reaching the I–N transition and giving rise to a four-phase region (for binary mixtures Gibbs phase rule permits a maximum of three phases in simultaneous coexistence, except in special cases of symmetric particles like the present one).

So far we have discussed the uniform I and N phases of binary mixtures. When positionally ordered phases, in particular S and C phases, are considered, it is easy to understand that the already complicated phase diagram topologies previously discussed will become even more complex. In particular, part of the phase equilibria involving I and N phases could be preempted by nonuniform phases and become metastable. Moreover, Koda *et al* [230] performed constant-pressure Monte Carlo simulations of binary mixtures of hard disc-like particles with diameter-to-thickness ratios 2.5 and 5.0 and found strong tendency of the large discs to form clusters with columnar ordering, induced by strong depletion effects due to the small discs.

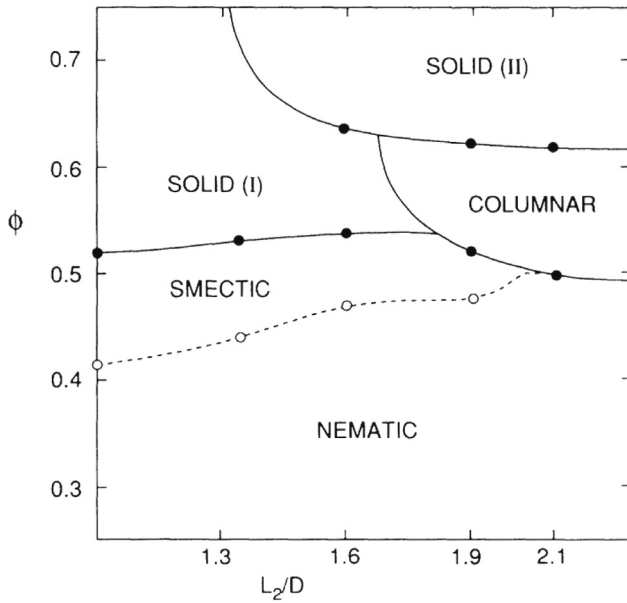


Figure 30. Monte Carlo results of Stroobants [150] for the phase diagram of a mixture of HSC. One of the species has fixed aspect ratio $\kappa_1 = L_1/D = 1$. The aspect ratio $\kappa_2 = L_2/D$ of the second species of the mixture is shown in the horizontal axis. The mixture's concentration is kept fixed at the equivalence point (i. e. the point at which partial volume fractions of both components are equal). The total packing fraction is represented in the vertical axis. Labels are as follows: Solid (I): substitutionally disordered binary crystal. Solid (II): phase separated pure component crystals. Open circles: continuous transition. Solid circles: first-order transition. Lines are guides to the eyes. Reprinted with permission from [150]. Copyright (1992) by the American Physical Society.

To simplify the analysis, the first attempts to deal with positionally ordered phases in hard-body binary mixtures assumed perfect orientational order (i. e. systems of parallel molecules). In 1992, Stroobants [150] performed MC simulations of binary mixtures of parallel HSC. Different mixtures were considered, keeping the aspect ratio of one of the species fixed, $\kappa_1 = L_1/D = 1$ and varying the aspect ratio of the other in the range $\kappa_2 = L_2/D = 1.3 - 2.1$. The diameter of both particle species was the same. In all cases the composition of the mixture was adjusted so that the partial volume fractions of both components were equal. A stable C phase was observed when $\kappa_2 \gtrsim 1.6$. Moreover, for $\kappa_2 \gtrsim 2.1$, the N–S phase transition was found to be pre-empted by a N–C transition (see figure 30). Since no stable C phase exists in the one-component systems, the conclusion was that bidispersity favours C over S order, at least for these particular mixtures.

Two years later, Cui and Chen [231] extended the third virial coefficient free energy functional approximation of Mulder for parallel one-component cylinders [93] to mixtures of the same diameter and different lengths. The theory is trivially extended by considering two local densities $\rho_i(z)$, where the z axis is along the director. The Helmholtz free energy functional is written as $F[\rho_1, \rho_2] = F_{id}[\rho_1, \rho_2] + F_{ex}[\rho_1, \rho_2]$, with

$$\frac{\beta F_{id}[\rho_1, \rho_2]}{A} = \sum_{i=1}^2 \int dz \rho_i(z) [\log(\rho_i(z) \Lambda_i^3) - 1]. \quad (66)$$

The excess free energy part can be written as a virial expansion:

$$\begin{aligned} \frac{\beta F_{ex}[\rho_1, \rho_2]}{A} &= \sum_{i=1}^2 \sum_{j=1}^2 \int dz \int dz' \rho_i(z) \rho_j(z') B_2^{(ij)}(z, z') \\ &+ \sum_{i=1}^2 \sum_{j=1}^2 \sum_{k=1}^2 \int dz \int dz' \int dz'' \rho_i(z) \\ &\times \rho_j(z') \rho_k(z'') B_3^{(ijk)}(z, z', z'') + \dots \quad (67) \end{aligned}$$

where A is the area of the layers. The first virial coefficients are given by

$$\begin{aligned} B_2^{(ij)}(z, z') &= -\frac{1}{2} \int d\mathbf{r}'_{\perp} f_{ij}(\mathbf{r} - \mathbf{r}'), \\ B_3^{(ijk)}(z, z, z'') &= -\frac{1}{6} \int d\mathbf{r}'_{\perp} \int d\mathbf{r}''_{\perp} f_{ij}(\mathbf{r}') f_{jk}(\mathbf{r}' - \mathbf{r}'') f_{ik}(\mathbf{r}''). \end{aligned} \quad (68)$$

Cui and Chen [231] truncated the expansion beyond the third term and calculated $B_2^{(ij)}(z, z')$ and $B_3^{(ijk)}(z, z', z'')$ explicitly for parallel HC. Conclusions similar to those of Stroobants [150] were obtained.

At the same time, the simpler Onsager theory, containing only the $B_2^{(ij)}(z, z')$ function, was used by Koda and Kimura [232] to study the N–S phase transition in the same mixture. Different phase diagrams, in the packing fraction composition plane and for different values of the length of the long cylinders, were obtained. The main findings of this work were: (i) the region of S stability is suppressed or enlarged depending on the length of the long cylinders and, (ii) two types of smectic phases exist. In one, smectic layers consist of uniform mixtures of large and short particles. In the other, microsegregation occurs with alternate layers of short and long particles.

The stability of the N phase of mixtures of long and short parallel cylinders against S or C phase formation was also studied, using Onsager theory, by Sear and Jackson in 1995 [233]. In agreement with the previous studies summarized above, they found that the addition of cylinders of a different length decreases the tendency towards S ordering, to the extent that the N phase can coexist directly with the C phase without forming a S phase first.

The study of the interplay between N and S phase stability and the possible microphase segregation was continued with studies on mixtures of parallel HSC and HS in the second half of the 90s. In 1996, Koda *et al* [234] again used Onsager theory, together with constant-pressure MC simulations, to conclude that the addition of spherical molecules to a system of parallel HSC induces the formation of a microsegregated S phase with alternating layers of HSC and HS. Later on, in 2000, Dogic *et al* [235] revisited the problem using computer simulations. The conclusions of this study were the following: (i) entropy-driven microsegregation occurs in mixtures of parallel rods and spheres. (ii) Adding spheres smaller than the rod width decreases the total packing fraction needed for the formation of the S phase and therefore small spheres effectively stabilize the S phase; the opposite is true for large spheres. (iii) The degree of stabilization increases with increasing rod length.

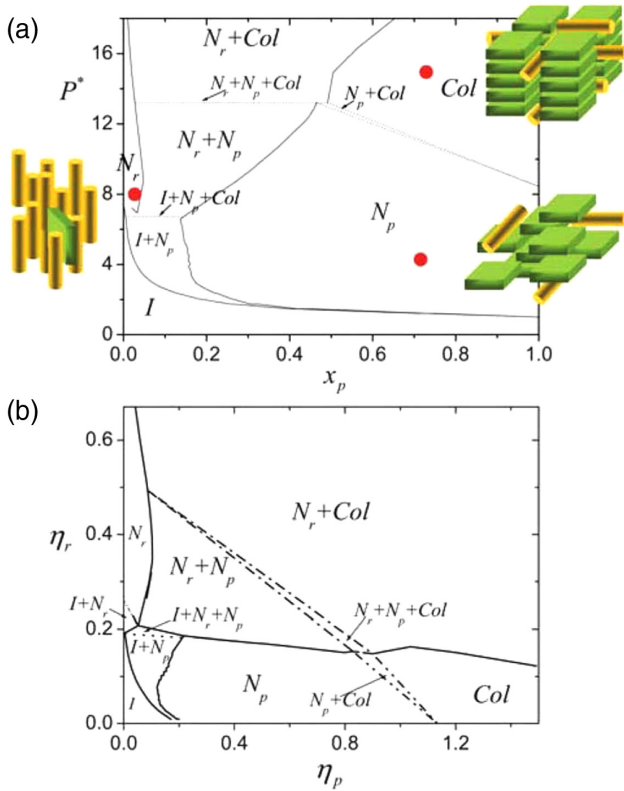


Figure 31. (a) Phase diagram of plate–rod binary mixtures of molecular sizes $L_p = 9$ and $L_r = 13$ in the pressure–plate concentration plane as calculated by Peroukidis *et al* [238]. Cartoons of molecular organization are shown for the marked points on the phase diagram. (b) Phase diagram in the packing fraction plane of rods (η_r)—packing fraction of plates (η_p) corresponding to the same case shown in (a). Reproduced from [238] with permission of the Royal Society of Chemistry.

An extra element was included in the contribution made by Martínez-Ratón *et al* [236] in 2006. In contrast to other works, these authors incorporated orientational order and carried out a more systematic study. Mixtures of rods of different aspect ratios and spheres of different diameters were considered and treated within Onsager theory (see below). The study concluded that depletion effects, and consequently S stability, decrease significantly as a result of orientational disorder in the S phase when compared with the corresponding data based on the frozen-orientation approximation.

The work of Koda *et al* on mixtures of parallel HSC and spheres was later extended by Vesely [237] to mixtures of other linear particles (fused spheres, ellipsoids and spher-ellipsoids) and HS. Mixtures of HS with shape-anisometric colloids, namely rod-like and plate-like particles, have been studied using a lattice model approach by Peroukidis *et al* [238] (see figure 31). Also, Varga and co-workers published results on further extensions of Koda’s theory to mixtures of equally long but differently wide cylinders [239] and HC of equal diameters but different lengths [240].

In 2004, the authors of this review and their co-workers published the first of a series of papers devoted to the phase behaviour of binary mixtures of freely rotating hard-body particles, paying special attention to the stability and properties of the S phase [241]. The approach used was a version of

the PL theory suitable for mixtures, but extended to deal with spatially ordered (nonuniform) systems. The local densities are now a function of the particle orientations, $\rho_i(\mathbf{r}, \hat{\Omega})$. Let us formulate the theory without assuming any special symmetry. The Helmholtz free energy functional is given by

$$\beta F_{id}[\rho_1, \rho_2] = \sum_{i=1}^2 \int_V d\mathbf{r} \int d\hat{\Omega} \rho_i(\mathbf{r}, \hat{\Omega}) \times [\log(\rho_i(\mathbf{r}, \hat{\Omega})\Lambda_i^3) - 1], \quad (69)$$

and

$$\beta F_{ex}[\rho_1, \rho_2] = -\frac{\Psi_{HS}(\eta)}{2B_2^{(HS)}} \sum_{i=1}^2 \sum_{j=1}^2 \int_V d\mathbf{r} \int d\hat{\Omega} \int_V d\mathbf{r}' \int d\hat{\Omega}' \rho_i(\mathbf{r}, \hat{\Omega}) \rho_j(\mathbf{r}', \hat{\Omega}') \times f_{ij}(\mathbf{r} - \mathbf{r}', \hat{\Omega}, \hat{\Omega}'), \quad (70)$$

where, as usual, $\eta = \rho_0 \sum_{i=1}^2 x_i v_i$ is the total packing fraction of the mixture (which is equal to that of the reference HS fluid). For uniform phases, $\rho_i(\mathbf{r}, \hat{\Omega}) = \rho_0 x_i h_i(\hat{\Omega})$, this theory reduces exactly to the PL approximation for mixtures and, consequently, all results pertaining to the I and N phases of previous sections apply here. Also, in the low-density limit and for strictly parallel particles with smectic symmetry, $\rho_i(\mathbf{r}, \hat{\Omega}) = \rho_i(z)\delta(\hat{\Omega} - \hat{z})$, the expression for $F_{ex}[\rho_1, \rho_2]$ reduces to equation (67) truncated at second-order. However, the generalized form of the theory can describe spatially ordered phases of any symmetry, including the S and C phases. In [241], the theory was applied to the S phase by making the simplification $\rho_i(\mathbf{r}, \hat{\Omega}) = \rho_i(z, \hat{\Omega})$. Computational details on free energy minimization to obtain the equilibrium density profiles and orientational distribution functions (from which N and S order parameters and thermodynamic and phase transition properties, can be easily derived) can be found in [241]. In this paper, binary mixtures of HSC of the same diameter but different lengths (and, therefore, different aspect ratios), were considered. Phase diagrams were found to depend strongly on the aspect ratio of each component and also on their length ratios. When the mole fraction of long rods is larger, it was found that layered phases present a S structure with short rods located at the layers, mixed with long rods. However, in the opposite case (short rods more abundant than long rods), a S_2 phase is obtained consisting of layers of short rods with long rods located parallel to the latter but in the interlayer region.

The same kind of mixture was analyzed by Cinacchi *et al* in [242]. The special case where one of the components is a HS was also considered. Particular emphasis was put on the interplay between S formation versus S–S segregation. It was found that, in general, S–S segregation occurs in a wide range of compositions and pressures, except when particles of both components have similar lengths in which case segregation appears only at high pressure. When lengths are very different and the mixture is poor in long molecules, a microsegregated (but macroscopically homogeneous) phase, where the minority species is expelled to the interlayer regions, was found to be stable.

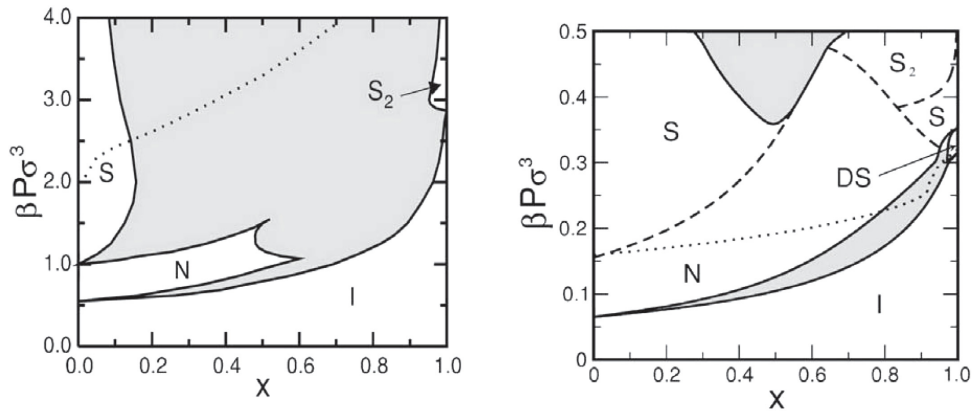


Figure 32. Phase diagrams in the pressure-composition plane (x being the fraction of shortest particles) for different mixtures, from [243]. (a) Mixture of HSC with the same diameter σ and aspect ratios $\kappa_1 = 4.5$ and $\kappa_2 = 8.0$, as obtained from an extended PL approach. (b) Phase diagram of a mixture of hard parallelepipeds of aspect ratios $\kappa_1 = 4.5$ and $\kappa_2 = 8.0$ and cross section σ^2 , as obtained from a FMT approach with a Zwanzig approximation. The continuous lines indicate first-order phase transitions. The shaded regions are two-phase regions of phase coexistence. The regions of stability are labelled by S (standard smectic formed by layers identical in composition), N (nematic), I (isotropic), S_2 (microsegregated smectic phase with long particles located in the interlayer space) and DS (discotic smectic). The dotted line is the spinodal line corresponding to the instability of the nematic phase with respect to columnar-type fluctuations. Reprinted with permission from [243]. Copyright (2005), AIP Publishing LLC.

A more general analysis of the phase behaviour of binary mixtures of hard rods of different lengths and diameters was published by Martínez-Ratón *et al* in 2005 [243]. Attention was focused on the formation of C phases and the relative stability between S and C phases. Once again the extended PL theory was used, this time complemented with a restricted-orientation (Zwanzig) approximation of the FMT for hard parallelepipeds. This strategy provided a complete picture of the problem: while the PL theory fully incorporates the orientational degrees of freedom, but treats spatial and orientational correlations in an approximate manner, the Zwanzig approximation of FMT theory considers only orientations along three mutually orthogonal axes, but correlations are more faithfully represented. Results for the phase diagram of a mixture of HSC using the extended PL theory have been reproduced in the left side of figure 32, results for a mixture of hard parallelepipeds obtained using FMT within the restricted-orientation Zwanzig approximation are shown on the right side of the same figure.

The main feature of the phase diagram obtained using PL theory is the very strong segregation of the smectic phase; it is in fact so strong that it pre-empts the I–N transition. Apart from the standard smectic phase, a second kind of smectic phase, S_2 , is found to be stable in the region of the phase diagram corresponding to mixtures rich in the short particles. In the microsegregated S_2 phase, layers of different composition alternate in such a way that the density distributions of the two species are shifted one with respect to the other by half a smectic period. In the case of the Zwanzig model (right side of the figure), the smectic segregation takes place at a much higher pressure (as compared, for example, with the location of the isotropic–nematic transition). As a result, the I–N transition is not pre-empted. There is no direct I–S phase transition like the one resulting from the PL theory for a mixture rich in short particles. Instead, we have continuous N–S transitions and a first-order S– S_2 transition at higher pressure. However, it has to be noted that when the stability of the nematic phase against columnar-type fluctuations is taken into account, these results

have to be modified considerably. The nematic–columnar spinodal line has been represented as a dotted line in figure 32. As is evident from the figure, the conclusion is that the FMT–Zwanzig approximation greatly enhances the stability of the C phase, pre-empting smectic order completely. By contrast, in the PL model, the C phase may pre-empt a large region of S phase stability in some mixtures, but some regions where the S phase is stable remain. Note that the stability against C-type fluctuations in the PL theory was estimated by computing spinodal lines; a proper calculation including binodal lines would probably result in enhanced stability of the C phase.

In a final study using the PL theory, Cinacchi *et al* [244] calculated the phase diagrams of a collection of binary mixtures of thin and thick HSC. Attention was paid to two cases: (i) binary mixtures where the two components have the same length and, (ii) binary mixtures where the two components have the same volume. Spherocylinders of the same total length and different diameter tend to demix considerably as soon as the diameter ratio deviates from unity, especially at (high) pressures such that at least the phase richer in the thicker component is S. In the case where the two components have equal volumes, demixing is further increased due to the disparity not only in particle diameter but also in particle length.

Many of the theoretical studies on mixtures of hard anisotropic bodies have been inspired by, or have inspired, experiments on colloidal suspensions of particles. When comparing the experimental results with the theories as regard the stable phases and the different regions of coexistence, it is important to pay attention to the possible effects of gravity, since the sedimentation profile is a cross result of phase behaviour and gravity effects. The sedimentation–diffusive equilibrium of colloidal liquid–crystal suspensions, either mixtures or poly-disperse systems, gives rise to a stack of distinct layers with different properties (such as particle composition). This problem has recently been discussed by de las Heras and Schmidt [245]. They used a Legendre transform on the FMT-based functional introduced by Esztermann *et al* [140] to study sedimentation

of a binary mixture of hard platelets with vanishing thickness and to account for the effect of gravity on the number of stacking diagrams. The authors found that even simple binary (not necessarily polydisperse) mixtures produce a stacking diagram containing six types of stacks with up to four distinct layers. The extended Gibbs phase rule that determines the maximum number (N_{\max}) of sedimented layers reads: $N_{\max} = 3 + 2(n_b - 1) + n_i$, where n_b is the number of binodals present in the bulk phase diagram, while n_i is the number of their inflection points.

3.5.2. Polydisperse systems. In this section we focus on continuously polydisperse mixtures, i.e. mixtures beyond binary and ternary that contain an arbitrarily large number of species, so large that in fact sizes can be characterized by a continuous distribution. Particle size polydispersity is now recognized as an important actor in the phase behaviour of real colloidal suspensions of anisotropic particles. Already in binary mixtures (section 3.5.1) interesting effects can be identified: (i) broadening of the coexistence gap, (ii) enrichment of coexisting phases in some species (an effect predicted to occur by Onsager in mixtures with a discrete number of species) and (iii) exotic phase equilibria, such as re-entrant nematic phases, nematic-nematic coexistence or even three-phase, isotropic-nematic-nematic coexistence. These effects have experimental evidence. Size polydispersity is a realistic feature of real fluids and has to be taken into account in theoretical treatments. Polydispersity adds an extra element of complexity which may entail richer phase diagrams. In particular, as the number of components increases without limit, Gibb's phase rule allows for the possibility of an unlimited number of phases to coexist. However, the theoretical analysis of polydisperse anisotropic fluids is not easy, as subtle questions arise concerning particle size distributions, lack of accuracy of perturbation treatments and numerical issues.

The experimental realization of polydisperse mixtures of hard particles consists of suspensions of colloidal synthetic particles (natural particles such as viruses are usually monodisperse) in an aqueous environment at high Coulomb screening conditions. The latter condition ensures that particle interactions will faithfully be represented by overlap or hard interactions. Many experimental procedures have been devised to synthesize colloidal particles with different geometries and shapes (a topic not covered in the present review). All of these procedures lead to samples containing particles of different sizes in all particle dimensions. Theoretical treatments of the resulting suspensions necessarily have to incorporate polydispersity. The polydispersities in each dimension are typically poorly controlled in the experiments and have to be measured by different means (dynamical light scattering, direct optical visualization, etc.)

Polydisperse fluids of hard rods were first considered in the context of Onsager theory. Onsager already outlined the possible generalization of his theory to discretely polydisperse systems in length and advanced the broadening effect on the coexisting gap for the isotropic-nematic transition. Later, several experimental studies motivated the analysis of these systems.

McMullen *et al* [246] generalized Onsager theory to polydisperse micelles (approximated by hard rods), considering a simple aggregation model where all rods are in chemical equilibrium and the distribution is obtained from the model itself. Later Odijk *et al* [247] and Sluckin [248] and Chen [249] further used Onsager theory with slight differences, considering an expansion valid for narrow size distributions. The first attempt to study continuously polydisperse fluids forming liquid-crystalline phases for general (not only small) polydispersity coefficient was made by Clarke *et al* [250]. More recently, an approximate but consistently more accurate procedure, the moment method, was used by Speranza and Sollich [251]. Before reviewing the results, we present the theory and then discuss the different implementations. Finally, we will review other works on polydispersity focused on particle shapes other than hard rods; these works use different versions of fundamental measure density functional in the Zwanzig approximation.

We consider hard rods of length L and breadth D and introduce the variables $\sigma_1 = L/\langle L \rangle$ and $\sigma_2 = D/\langle D \rangle$, denoted collectively by $\sigma \equiv (\sigma_1, \sigma_2)$. Here $\langle L \rangle$ and $\langle D \rangle$ are the averaged particle sizes (note that σ_i are dimensionless quantities, but the definition of polydisperse variables is not universal and some authors use different definitions). If one or more of these variables are continuously distributed, the local density distribution $\rho(\mathbf{r}, \hat{\Omega})$ has to be generalized to $\rho(\mathbf{r}, \sigma, \hat{\Omega})$. The present definition of polydisperse variables guarantees that the local distribution is a density, in the sense that its normalization is $\int d\sigma \int d\hat{\Omega} \rho(\mathbf{r}, \sigma, \hat{\Omega}) = N$. Assuming for the moment that there is no spatial dependence, we have $\rho(\mathbf{r}, \sigma, \hat{\Omega}) = \rho(\sigma, \hat{\Omega}) = \rho(\sigma)h(\sigma, \hat{\Omega})$. These functions satisfy the normalization conditions $\int d\sigma \rho(\sigma) = \rho_0$ (with ρ_0 the total mean density of the polydisperse mixture) and $\int d\hat{\Omega} h(\sigma, \hat{\Omega}) = 1$. It is also convenient to introduce $\rho_0(\sigma) = \rho_0 f(\sigma)$, the total density distribution function, where $f(\sigma)$ is the so-called *parent* distribution function, which reflects the particle size distribution obtained from the particular experimental procedure used to synthesize particles. Polydispersity is usually quantified in terms of polydispersity coefficients Δ_i which give the standard deviation of the size distribution function, $\Delta_i = \sqrt{\langle \sigma_i^2 \rangle / \langle \sigma_i \rangle^2 - 1}$ with $\langle \sigma_i^n \rangle = \int d\sigma \sigma_i^n f(\sigma)$.

The extended Onsager theory for the polydisperse mixture is [247, 248]

$$\begin{aligned} \frac{\beta \mathcal{F}[\rho]}{V} = & \int d\sigma \int d\hat{\Omega} \rho(\sigma, \hat{\Omega}) \left\{ \log \left[\rho(\sigma, \hat{\Omega}) \Lambda^3(\sigma) \right] - 1 \right\} \\ & + \frac{1}{2} \int d\sigma \int d\hat{\Omega} \rho(\sigma, \hat{\Omega}) \int d\sigma' \int d\hat{\Omega}' \rho(\sigma', \hat{\Omega}') \\ & \times V_{\text{exc}}(\sigma, \sigma', \hat{\Omega}, \hat{\Omega}'), \end{aligned} \quad (71)$$

where $V_{\text{excl}}(\sigma, \sigma', \hat{\Omega}, \hat{\Omega}')$ is the excluded volume between a pair of particles with dimensions σ, σ' and orientations $\hat{\Omega}, \hat{\Omega}'$, respectively and $\Lambda(\sigma)$ is the thermal wavelength of the species with dimensions σ . Minimization with respect to the function $h(\sigma, \hat{\Omega})$ provides the self-consistent equation

$$\begin{aligned} h(\sigma, \hat{\Omega}) = & \frac{e^{-\int d\sigma' \rho(\sigma') \int d\hat{\Omega}' h(\sigma', \hat{\Omega}') V_{\text{exc}}(\sigma, \sigma', \hat{\Omega}, \hat{\Omega}')}}{\int d\hat{\Omega}'' e^{-\int d\sigma'' \rho(\sigma'') \int d\hat{\Omega}''' h(\sigma'', \hat{\Omega}''') V_{\text{exc}}(\sigma, \sigma'', \hat{\Omega}, \hat{\Omega}''')}} \end{aligned} \quad (72)$$

from which the degree of orientational order for species σ can be obtained:

$$Q(\sigma) = \int d\hat{\Omega} P_2(\hat{\Omega} \cdot \hat{n}) h(\sigma, \hat{\Omega}). \quad (73)$$

Here \hat{n} is, as usual, the nematic director. Isotropic, $Q(\sigma) = 0$ and nematic, $Q(\sigma) \neq 0$, branches can be obtained from these equations.

The calculation of phase equilibrium for polydisperse mixtures is not a trivial task, since there is in general a whole region in the thermodynamic phase diagram where two or more phases can coexist and the density of particles of a given size changes depending on the coexistence point (giving rise to fractionation). Let $\rho_\alpha(\sigma)$ be the density of particles of size σ in phase α and $\mu_\alpha(\sigma)$ the corresponding chemical potential. If m phases are in chemical equilibrium, all chemical potentials of a given species σ should be equal to $\mu_0(\sigma)$, a function which is determined by the conservation of the number of particles (lever rule):

$$\rho_0(\sigma) = \sum_{\alpha=1}^m \gamma_\alpha \rho_\alpha(\sigma), \quad \sum_{\alpha=1}^m \gamma_\alpha = 1, \quad (74)$$

The coefficients γ_α , with $0 \leq \gamma_\alpha \leq 1$, represent the fraction of volume occupied by the phase α . Calculating the chemical potentials from equation (71) and using (72) and (74) gives

$$\begin{aligned} \rho_\alpha(\sigma) &= \rho_0(\sigma) \\ &\times \int d\hat{\Omega} e^{-\int d\sigma' \rho_\alpha(\sigma') \int d\hat{\Omega}' h_\alpha(\sigma', \hat{\Omega}') V_{\text{exc}}(\sigma, \sigma', \hat{\Omega}, \hat{\Omega}')} \\ &\times \left\{ \sum_{\beta=1}^m \gamma_\beta \int d\hat{\Omega}' e^{-\int d\sigma'' \rho_\beta(\sigma'') \int d\hat{\Omega}'' h_\beta(\sigma'', \hat{\Omega}'') V_{\text{exc}}(\sigma, \sigma'', \hat{\Omega}', \hat{\Omega}'')} \right\}^{-1} \end{aligned} \quad (75)$$

Fixing ρ_0 and solving (75) and (72) for each phase α we can find all the functions $h_\alpha(\sigma, \hat{\Omega})$ and $\rho_\alpha(\sigma)$. The latter gives information on particle fractionation. The $m - 1$ independent coefficients γ_α are calculated through the mechanical equilibrium conditions

$$p_1[\rho_1; \{\gamma_\tau\}] = p_2[\rho_2; \{\gamma_\tau\}] = \dots = p_m[\rho_m; \{\gamma_\tau\}], \quad (76)$$

with $\beta p_\alpha[\rho_\alpha; \{\gamma_\tau\}] = \rho_\alpha + \beta F_{\text{ex}}[\rho_\alpha]/V$ (valid for Onsager's second virial theory). Here $\rho_\alpha = \int d\sigma \rho_\alpha(\sigma)$ is the number density of phase α . For the case of two-phase coexistence, say between I and N phases, the onset of order is calculated by fixing $\gamma_N = 0$ (a vanishingly small amount of N phase, with the I phase occupying the whole volume). Solving the equations for chemical and mechanical equilibrium, the so-called I-cloud and N-shadow densities, $\rho_I^{(c)}$ and $\rho_N^{(s)}$ respectively, can be found. In the other limit, $\gamma_N = 1$ (vanishingly small amount of I phase), the same coexistence equations provide the N-cloud and I-shadow densities, $\rho_N^{(c)}$ and $\rho_I^{(s)}$, respectively. Usually phase diagrams are presented plotting the total number density ρ_0 as a function of the polydisperse coefficients. In the case where only the particle length L is polydisperse, the I-cloud and N-cloud curves in the $\rho_0 - \Delta_L$ plane define the boundaries of the two-phase I-N coexistence.

The calculation of coexistence parameters, even for the simplest two-phase transition, is a daunting task: equations (72) and (75), which include integrations on angular and polydispersity variables, have to be discretized and a huge number of grid points (and, therefore, of unknowns) have to be used. Therefore, some approximations are needed. Sluckin [248] and later Chen [249] were the first to study the effect of a small amount of polydispersity (i.e. the limit $\Delta \rightarrow 0$) on the coexistence densities of the I-N transition and the pressure values at the cloud and shadow points. They used the Onsager model for length-polydisperse hard rods, i.e. rods with $L_0/D_0 \rightarrow \infty$, fixed D_0 and polydisperse length L , with $L_0 = \langle L \rangle$ the mean length. Sluckin [248] used the Gaussian parameterization for the orientational distribution function proposed by Odijk,

$$h(\sigma, \hat{\Omega}) = \begin{cases} \frac{\alpha(l)}{4\pi} \exp\left[-\frac{\alpha(l)}{2}\theta^2\right], & 0 \leq \theta \leq \frac{\pi}{2} \\ \frac{\alpha(l)}{4\pi} \exp\left[-\frac{\alpha(l)}{2}(\pi - \theta)^2\right], & \frac{\pi}{2} \leq \theta \leq \pi, \end{cases} \quad (77)$$

with $l \equiv L/L_0$ and considered the polydispersity coefficient Δ as a perturbation parameter, obtaining transition densities, orientational order parameter and fractionation in terms of Δ . As in binary mixtures, he obtained a broadened density gap (more evident in the I-cloud-N-shadow boundary) and an enrichment of long rods in the nematic phase. Chen [249] developed a second-order perturbation theory without assuming any particular parameterization. Results were somewhat in disagreement with those of Sluckin, in that, for small Δ , the biphasic gap was predicted to be narrower than in the monodisperse fluid, a result attributed to the fact that the theory was valid only for small polydispersity. It might be that this apparent disagreement is due to the fact that Chen focused on the I-shadow-N-cloud boundary.

Speranza and Sollich [251] reconsidered the problem of length-polydisperse hard rods in the Onsager limit, in an effort to generalize the theory to general size distributions (not necessarily narrow). Also, they calculated the whole phase diagram and discussed the conditions for the appearance of exotic features such as three-phase I-N-N coexistence regions and N-N transitions. In order to make the problem tractable, Speranza and Sollich used a spherical harmonic expansion, truncated to second-order, of the excluded volume $V_{\text{exc}}(l, l', \hat{\Omega}, \hat{\Omega}') = 2L_0 D_0^2 l l' |\sin \gamma|$, (with γ the angle between the unit vectors $\hat{\Omega}$ and $\hat{\Omega}'$). Within this approximation, the free energy depends only on two generalized one-particle moments, n_0 and n_2 , where

$$n_k = \int_0^\infty dl l \int_0^\pi d\theta \sin \theta P_k(\cos \theta) \rho(l) h(l, \theta), \quad (78)$$

and $\rho(l)$ is the density distribution function scaled by the factor $\pi L_0^2 D_0 / 4$. Speranza and Sollich used the *moment method* to calculate the I-N phase coexistence. In this method the ideal free energy is projected onto a subspace generated by a finite set of moments. For a truncatable (with respect to the moments)

excess free energy density $\Phi_{\text{ex}}(\{n_k\})$, the ideal part of free energy density in reduced thermal units

$$\Phi_{\text{id}} = \int_0^\infty dl \int_0^\pi d\theta \sin \theta \rho(l, \theta) \left[\log \frac{\rho(l, \theta)}{f(l)} - 1 \right], \quad (79)$$

is minimized with respect to $\rho(l, \theta)$, with the constraint of having fixed values for the generalized moments n_k . Note that the factor $f(l)$ (the parent size distribution) inside the logarithm does not affect the phase behaviour but it is useful to derive the coexistence equations. The constrained minimization results in the following expression for the total free energy density

$$\Phi(\{n_k\}) = \sum_k \lambda_k n_k - n_0 + \Phi_{\text{ex}}(\{n_k\}), \quad (80)$$

where λ_k are the Lagrange multipliers that guarantee the constraints. As can be seen from (80), the total free energy depends on the generalized moments n_k , which can be viewed as densities of *quasiparticles* corresponding to a multicomponent mixture. Thus, if the excess part of the free energy density depends on two moments, the usual thermodynamic formalism for binary mixtures can be applied to calculate the phase coexistence between the I and N phases. We should note that the method is exact for the calculation of coexistence between a phase that occupies a vanishingly small part of the volume (shadow phase) and another that spans the whole volume (cloud phase). For a more formal discussion on the method of moments see [252–256].

Speranza and Sollich analyzed the consequences of assuming both unimodal and bimodal length distribution functions in the phase behaviour. The latter was written as a combination of two Schultz distributions of variance Δ_0 centred at two lengths L_1 and L_2 , with $r = L_2/L_1$. The phase diagram was calculated in the $\rho_0 - \Delta_0$ plane. For a unimodal distribution, broadening of the density gap between the I and N cloud curves as Δ_0 is increased was obtained. Also, strong fractionation was observed, with the N-shadow phase being more populated by long rods (first moment n_1 much higher than that in the I-cloud phase). For high enough Δ_0 , the zeroth moment (number density) of the N-shadow phase becomes lower than that of the I-cloud phase, i.e. the vanishingly small coexisting N phase has less rods (although they are longer). Also, three-phase I–N–N coexistence did not occur in fluids with unimodal (Schultz) length distributions, according to the truncated Onsager theory.

The results for a bimodal length distribution were compared with those for a binary mixture (for which the distribution function is a sum of two delta functions and I–N–N and N–N coexistences occur) of the same length asymmetry r . When the polydispersity Δ_0 is large enough, the I–N–N and N–N coexistencies disappear, while the re-entrant N phase is still present. The authors concluded that the bimodal distribution function should be sufficiently asymmetric and with two clearly visible peaks for the three-phase coexistence to exist [251].

In another work, Speranza and Sollich [257] used the same model but with a parent distribution function exhibiting

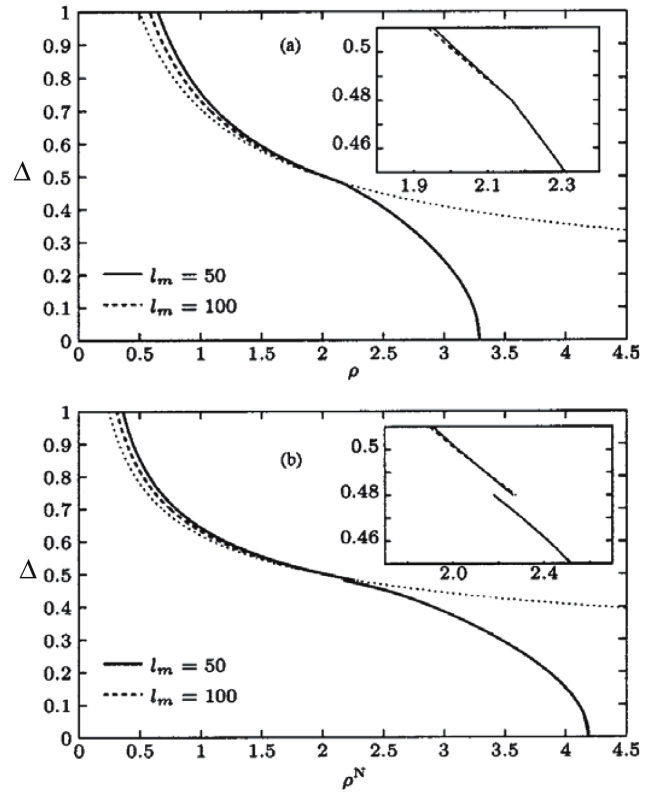


Figure 33. (a) I-cloud and (b) N-shadow curves in the polydispersity versus scaled density plane for length-polydisperse rods with Schultz distribution function truncated at $l_{\text{max}} = 50$ (solid) and 100 (dashed), from [258]. The dotted lines in both figures represent the limiting case $l_{\text{max}} \rightarrow \infty$. Insets in (a) and (b) show details of the main figures about the kink (a) and the discontinuity (b) of the cloud and shadow curves respectively. Reprinted with permission from [258]. Copyright (2003) by the American Physical Society.

a so-called fat-tail (i.e. a lower-than-exponential decay at large lengths, which needs to be truncated at a cut-off l_{max} to avoid divergences of the mean length in the N-shadow distribution function).

Now the phase behaviour in the $\rho_0 - \Delta$ plane is different: for small Δ the fluid exhibits the usual I–N phase transition, but beyond some value Δ^* the I-cloud curve possesses a kink. At this point the N-shadow curve has a discontinuity, since the coexisting N becomes bimodal with a second maximum at l_{max} that moves to lower values as γ_N is increased. Above but close to Δ^* , the fluid exhibits a narrow region of three-phase I–N–N coexistence, limited above by I–N coexistence. When the cut-off l_{max} is increased, the value of Δ^* decreases [257].

To confirm the results given by the truncated Onsager theory, Speranza and Sollich [258] also obtained the exact numerical solution to the I-cloud–N-shadow coexistence equations. The other set, the N-cloud–I-shadow equations, was not solved due to its inherent numerical complexity. Only unimodal (fat-tailed and Schultz) length-distributions were used. The existence of kinks and discontinuities in the cloud and shadow curves confirmed the existence of three-phase coexistence in a narrow interval of polydispersities for both distributions, while the cloud-point density at the kink was seen to decrease to zero as the cut-off length tends to infinity in the case of the fat-tail distribution. Contrary to the

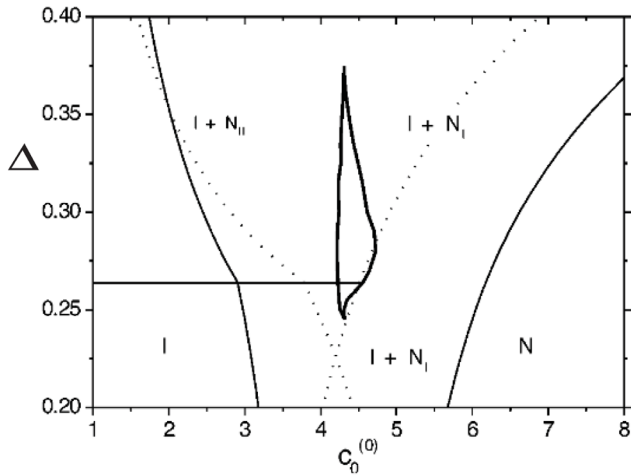


Figure 34. Phase diagram in the scaled density $c_0^{(0)} = \rho_0 \pi D_0 L_0^2 / 4$ -polydispersity Δ plane for length-polydisperse rods with a log-normal density distribution function truncated at $l_{\min} = 0.01$ and $l_{\max} = 10$, from [259]. Thin solid and dotted lines correspond to the I-N-cloud and the I-N-shadow curves, respectively. Thick lines enclose the region where one of the nematic phases loses stability with respect to the second nematic (so that the three-phase I-N₁-N₂ coexistence should be inside this region). The horizontal line represents the polydispersity at which the I-cloud curve exhibits a kink. Reprinted with permission from [259]. Copyright (2003), AIP Publishing LLC.

truncated Onsager model, the Schultz distribution predicts both a kink in the I-cloud curve (implying I-N-N coexistence) and a finite value for the cloud-point density at the kink as the cut-off length increases. Figure 33 is a plot of the I-cloud and N-shadow curves in the $\rho_0 - \Delta$ plane resulting for the truncated Schultz distributions with two different cut-offs $l_{\max} = 50, 100$. These results indicate that exponentially decaying distributions separate the functional space of size distribution functions in those that give three-phase I-N-N coexistence for finite l_{\max} and those which do not.

Although three-phase I-N-N coexistence was confirmed for fat-tail distributions, explicit calculation of coexistence boundaries was not carried out in the above works. In order to do this, the three-phase coexistence equations have to be solved well inside the I-N coexistence region. Taking $\gamma_{N_1} = \gamma \neq 0$ ($\gamma_1 = 1 - \gamma$) and taking $\gamma_{N_2} = 0$, the point in the $\rho_0 - \Delta$ phase diagram for which there appears a vanishingly small fraction of the coexisting N₂ phase in the already phase separated I-N₁ mixture can be calculated. The other point is calculated by setting $\gamma_{N_2} = \gamma \neq 0$ and $\gamma_{N_1} = 0$. This region was approximately obtained by Wensink and Vroege [259] by plotting the pressure p at the two-phase I-N coexistence as a function of γ_N , searching for the two values of $\gamma_N^{(i)}$ ($i = 1, 2$) for which $dp/d\gamma_N = 0$. When γ_N is between these values, the pressure is a decreasing function of γ_N , indicating the instability of the original N phase with respect to phase separation between two different nematics. The I-cloud and N-cloud curves and the phase diagram calculated by Wensink and Vroege is shown in figure 34. A Gaussian function for the orientational distribution was used in the I-N phase coexistence calculations, with an analytic expression obtained for the free energy in the limit of high order. The approximate

three-phase coexistence is delimited by two consolute points, the lower one located at a value of polydispersity below the kink of the I-cloud curve. Use of a Schultz distribution did not produce any indication for three-phase I-N-N coexistence. It can be concluded that the calculations with exponential distribution functions are very sensitive to the approximation used for the angular distribution function.

The study of freely rotating polydisperse particles other than rods has not been carried out yet due to the inherent numerical difficulties involved in solving the coexisting equations in the context of the presently available DFT approaches. To circumvent this problem, restricted-orientation (Zwanzig) approximations have been used for particles with different shapes. For example, the FMT-based DFT can be recast into a form where the weighted densities depend only on one-particle weights, which makes the problem numerically tractable. Within this approximation, the bulk behaviour of polydisperse plate-like particles has been analyzed [35, 260, 261]. Also, bimodal polydisperse mixtures of rods and plates [262, 263], polydisperse fluids of biaxial board-like particles [264] and parallel hard cylinders [265, 266] have been studied. In general, studies of this type aim at calculating the limits of two- or three-phase coexistences between uniform phases and in some cases also their instabilities against spatial density fluctuations with different liquid-crystal symmetries.

The FMT formalism for hard board-like, biaxial particles, in the Zwanzig approximation, can be easily generalized for the polydisperse case. The theory is written in terms of the density profiles $\rho_{\mu\nu}^{(i)}(\mathbf{r}, \boldsymbol{\sigma})$ ($\mu \neq \nu = x, y, z$), which gives the density of particles in the i th phase at point \mathbf{r} with the main axis pointing along the Cartesian axis μ and secondary axis pointing along ν . The edge lengths $\boldsymbol{\sigma} = (\sigma_1, \sigma_2, \sigma_3)$ are continuously polydisperse. The particle weights have to be redefined in order to consider the particle biaxiality. The constrained minimization of the total free energy per unit of volume $\beta\mathcal{F}^{(i)}/V$ corresponding to the phase i (in coexistence with the other $m - 1$ phases) with respect to the density profiles $\rho_{\mu\nu}^{(i)}(\mathbf{r}, \boldsymbol{\sigma})$, together with the lever rule constraint (74), provides an equation for these profiles, which is solved numerically. Use of Fourier transforms usually simplifies the problem. To find the spinodal instability of a uniform phase, say a biaxial nematic phase, with respect to nonuniform periodic modulation of a given wave vector q , one may apply a standard bifurcation analysis. Onsager theory has also been used in the Zwanzig approximation to treat hard-board particles in the polydisperse case.

Using these techniques, some effort has been devoted to the study of the biaxial nematic phase N_B in polydisperse fluids. As mentioned in section 3.3, binary mixtures of uniaxial hard rods and plates with high enough asymmetry can stabilize the biaxial nematic phase with respect to the occurrence of N_U⁺-N_U⁻ demixing. The N_B phase has not been observed in experimental rod-plate colloidal suspensions. Although particles can be prepared to closely resemble hard bodies, they are inevitably polydisperse, not only in size, but also in geometry. In a series of two papers, the effect of polydispersity on the stability of the N_B phase with respect to N_U⁺-N_U⁻ demixing has been investigated by Martínez-Ratón and Cuesta [262, 263],

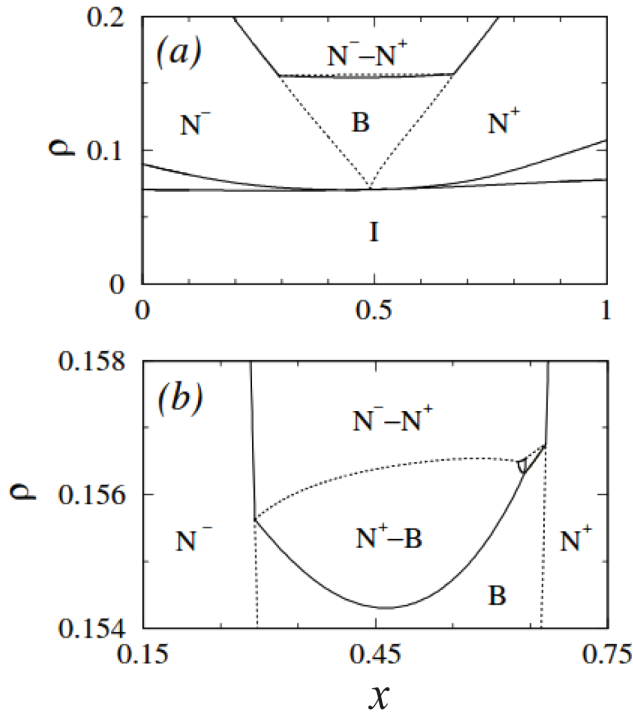


Figure 35. (a) $x - \rho$ phase diagram of a polydisperse mixture of Zwanzig rods and plates for $\kappa_0 = 5$, with x the fraction of rods [262]. The thickness and width polydispersities are $\Delta_{2/3} = 0.610$ and $\Delta_{-1/3} = 0.302$ respectively. Different stable phases and two-phase coexistences are correspondingly labelled. (b) A detail of the phase diagram shown in (a). Reprinted with permission from [262]. Copyright (2002) by the American Physical Society.

using hard board-like particles of square cross section and dimensions (L, σ, σ) . The volume of particles was set to unity and the polydispersity variable was the aspect ratio $\kappa = L/\sigma$, which accounts for both size and geometry polydispersity and a bimodal parent probability distribution function was chosen, with peaks at $\kappa_0 > 1$ (rod sector) and κ_0^{-1} (plate sector). The phase behaviour of the mixture was studied as a function of the aspect ratio κ_0 and polydispersity. The main result of this model is the enhanced stability of the N_B phase with polydispersity. For example, for $\kappa_0 = 5$ in the bidisperse limit, the binary mixture, just above the Landau point, exhibits a $N_U^+ - N_U^-$ demixing. However, when some polydispersity is added, the N_B becomes stable against $N_U^+ - N_U^-$ demixing [262] (see figure 35). For $\kappa_0 = 15$, for which the binary mixture exhibits a region of N_B phase stability, polydispersity gives rise to a rather complex phase diagram. Above the N_B there appears a region of three-phase $N_U^+ - N_U^- - N_B$ coexistence surrounded by a stable N_B phase (below), a two-phase $N_U^+ - N_U^-$ coexistence region (above), a $N_U^+ - N_B$ two-phase region (left) and finally a $N^- - N_B$ coexistence region (right) [263]. The coexisting phases also exhibit strong fractionation, more pronounced in the shadow coexisting phases. In both studies the instability of the uniform phases with respect to density modulations of given symmetries (like C and S) were estimated via the calculations of spinodal curves in the $x - \rho$ plane [262, 263].

Van den Pol *et al* [171] have recently managed to obtain experimentally the elusive biaxial nematic phase in colloidal suspensions of mineral board-like biaxial particles, polydisperse

in the three lengths $L > W > T$ (length, width and thickness, respectively) but with approximately the same shape. The effect of polydispersity on the stability of the N_B phase has been studied theoretically by Belli *et al* [264], focusing on the previous experimental results and using Onsager theory in the Zwanzig approximation. Belli *et al* showed that, under certain conditions, polydispersity can enhance N_B stability. The conditions are: (i) the shape parameter $\nu = L/W - W/T$ for all particles should be approximately the same and close to zero (the value for a perfect particle biaxiality) and (ii) polydispersity is taken on the particle volume. To match the experimental conditions, the authors chose $L/T = 9.07$ and $W/T = 2.96$ (which results in $\nu = 0.1$) for all species. 21 species with different Gaussian-distributed lengths T , characterized by mean value $\langle T \rangle$ and polydispersity coefficient Δ (again fixed in accordance with experiments), were chosen and the phase diagram in the total packing fraction polydispersity plane was calculated, neglecting the fractionation of particles between different coexisting phases (this is justified if phase transitions are continuous or of weakly first-order). While the one-component fluid exhibits the sequence $I - N_U^+ - S$ (where N_U^+ is a uniaxial nematic phase with the longest side of particles pointing on average along the nematic director), polydispersity (see phase diagram in figure 36) stabilizes the N_B phase in a region bounded below and above by the N_U^+ and S phases, respectively. At some particular polydispersity, a tetracritical point appears, where I, N_U^+ , N_B and a new N_U^- phase (with the shortest particle axes pointing in the direction of the nematic director) meet. For larger values of Δ , the N_B phase is bounded below and above by the N_U^- and S phases, respectively.

The smectic phase is usually found to be stable at high density in colloidal suspensions of close-to-monodisperse rod-like particles. It is known from theory and experiment that length-polydispersity in suspensions of particles with close-to-monodisperse widths can destroy smectic ordering and favour columnar ordering [267]. Intuitively one would expect that plate-like particles of approximately constant thickness will not form the columnar phase if the polydispersity in diameter is sufficiently high and that smectic ordering will result instead. The elusive platelet smectic phase was recently obtained in colloidal suspensions of mineral plate-like particles made of α -Zirconium phosphate [35]. These particles are completely monodisperse in thickness L , while their polydispersity in diameter σ is high and interact through a complex long-range repulsive interaction due to the surface charges and solvent effects. The suspensions exhibit a first-order I-N transition with a wide density gap at low densities and a continuous or possibly weak first-order N-S transition at high density [35]. A DFT in the Zwanzig approximation was used by the same authors to rationalize these experimental findings, considering polydisperse hard cylinders of constant effective thickness L_{eff} and mean diameter σ_0 . A second virial approximation was used to study the I-N transition, as the experimental mean aspect ratio L/σ_0 of the particles was very small. The effective thickness L_{eff} was chosen to match the volume fraction η of the experimental I-cloud point. For diameter polydispersities Δ between 0.3 and 0.5, both the density gap and the curvature of the function $\gamma_N(\eta_0)$ (the fraction of the sample volume

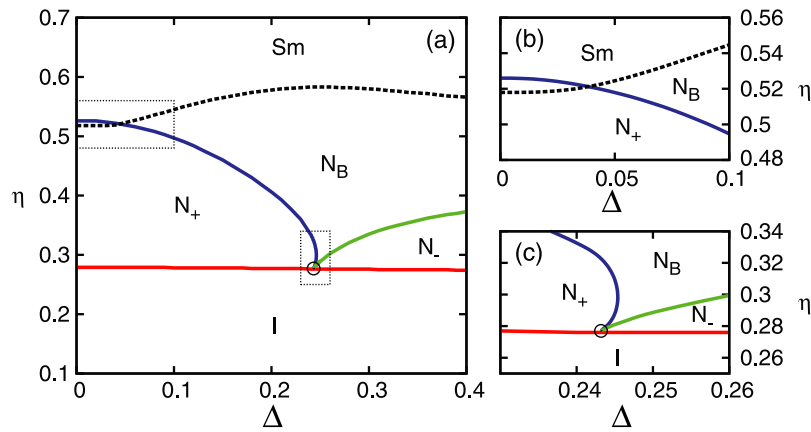


Figure 36. (a) Phase diagram in the packing fraction polydispersity plane of a polydisperse fluid of hard board-like biaxial particles with $L/T = 9.07$, $W/T = 2.96$ and polydispersity in the length T , according to Onsager theory in the Zwanzig approximation [264]. The solid lines show the boundaries limiting the stability regions of uniform phases (I, N_U^\pm and N_B , accordingly labelled in the figure). The dashed line shows the instability of uniform phases with respect to periodic modulations with smectic symmetry (the smectic phase is denoted Sm in the figure). (b) and (c) details of (a) around the crossing point between the N_U^+ – N_B transition curve and the N–S spinodal curve and (b) around the tetracritical point shown with circle. Reprinted with permission from [264]. Copyright (2011) by the American Physical Society.

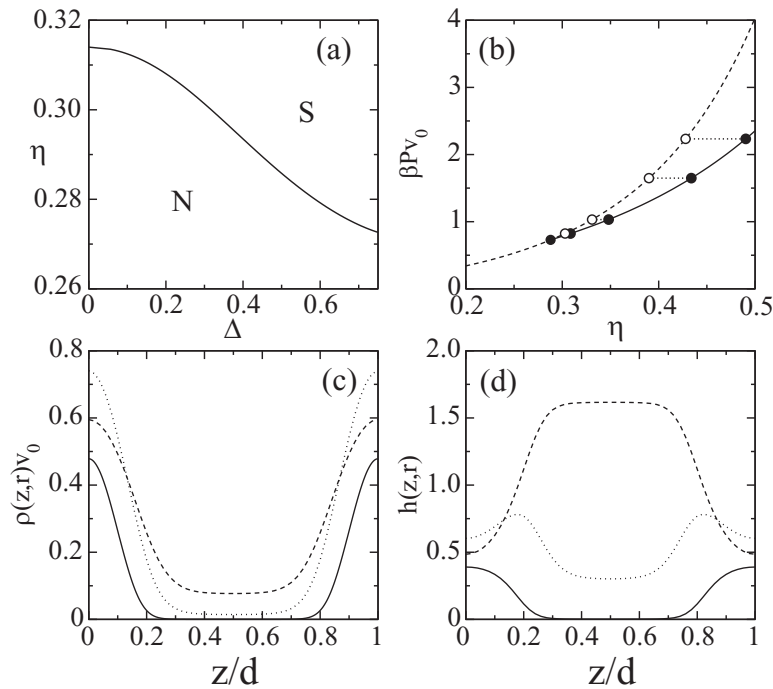


Figure 37. Theoretical results for a suspension of length-polydisperse hard cylinders of the same thickness [35]. (a) N–S spinodal packing fraction η_0 as a function of diameter polydispersity Δ . (b) Equation of state (reduced pressure versus packing fraction) of the N and S phases for $\Delta = 0.52$. Open circles represent the relative, experimental values of the packing fractions of the N phase with respect to the bifurcation point, while black circles correspond to the S phase with the same osmotic pressure. (c) Density profiles $\rho(z, r)$ as a function of z in reduced units for $r = 1.5$ (solid line), 0.4 (dashed line) and 0.8 (dotted line). (d) Normalized density distribution function, defined in the text, as a function of z/d for the same values of r as in (c) and with lines having the same meaning. In (c) and (d) the packing fraction and the period of the S phase are $\eta_s = 0.452$ and $d/L_{\text{eff}} = 1.211$, respectively. Reprinted with permission from [35]. Copyright (2009) by the American Physical Society.

occupied by the N phase as a function of the packing fraction) were correctly estimated [35]. As regards the N–S transition, a parallel hard-cylinder model treated with a FMT approach, suitably extended to consider polydispersity in diameter, was used. The parallel alignment approximation is justified here due to the high nematic ordering of colloidal particles at packing fractions close to that of the N–S transition. Setting Δ to the experimental value, equations of state for nematic and

smectic phases were calculated. The N–S transition was found to be continuous, while the packing fraction at the transition turned out to be a decreasing function of Δ (see figure 37 (a)). The experiment provided the value of packing fraction η_0^* at which there first appears a small amount of smectic. Slow kinetics prevents one from observing fully developed smectic domains when the sample packing fraction η_0 is increased and the smectic packing fraction η_s as a function of the sample

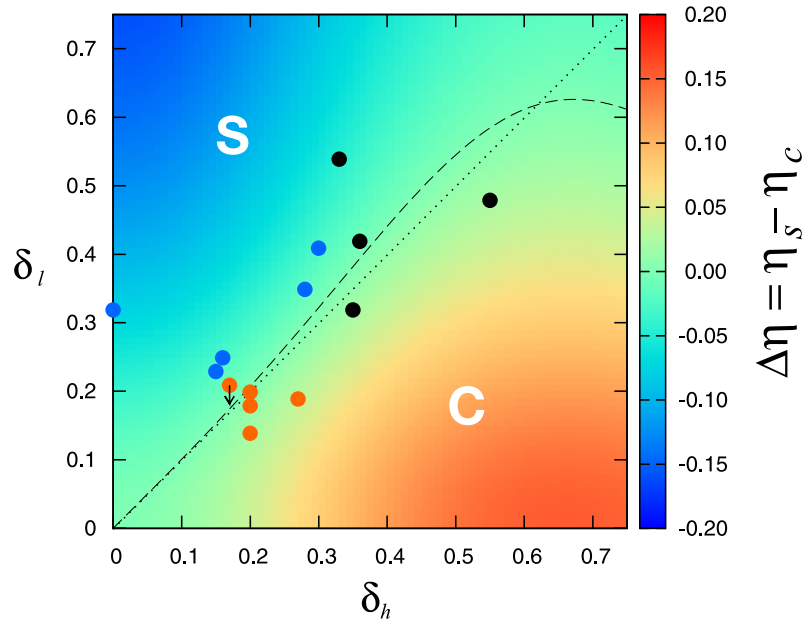


Figure 38. Regions of stability of the S (blue) and C (orange) phases as obtained from a bifurcation analysis of a fundamental measure theory of polydisperse hard platelets [261]. The difference $\Delta\eta = \eta_s - \eta_c$ between the packing fractions of S and C bifurcations from the N phase is plotted as a function of polydispersities in side-length δ_l and thickness δ_h in colour code (scale bar at right). Blue, orange and black circles represent the values of polydispersities corresponding to experimental samples in the S (blue), C (orange) and S–C (black) phases. Reproduced from [261] with permission of the PCCP Owner Societies.

packing fraction could not be directly measured. However, it was indirectly estimated from the theoretical equations of state for the nematic and smectic phases, figure 37(b). The ratio L_{eff}/L was determined as a function of η_0 from the knowledge of L/d from experiments (with d the smectic period) and d/L_{eff} given from the theory. The extrapolation of L_{eff}/L as a function of η_0 to the value for the I–N transition provides a value almost identical to the one giving the best fit of the curve $\gamma_N(\eta_0)$. Finally, the theory predicted a strong microsegregation in the S phase, with maxima of the local fraction of wider particles located at the layers and maxima of small particles located at interstitials. This is shown in figure 37(d), where this effect is illustrated through the function $h(z, r) = \rho(z, r) / \int_0^\infty dr \rho(z, r)$, where $r = \sigma/\sigma_0$ and $\rho(z, r)$ is the smectic density profile of species with relative diameter r .

Mejia *et al* [84] performed further studies on the above experimental system in order to study more systematically the effect of polydispersity on the two-phase I–N coexistence. Samples with different polydispersities and mean aspect ratios were prepared and phase diagrams in the total packing fraction, η_0 , versus fraction of the sample volume occupied by the N phase, γ_N , plane were calculated. The more polydisperse sample exhibits a huge coexistence gap and strong nonlinearity in the function $\gamma_N(\eta_0)$, results which were rationalized by Martínez-Ratón and Velasco [260] using a FMT-based theory for polydisperse oblate parallelepipeds in the Zwanzig approximation. A value for the effective aspect ratio L_{eff}/σ_0 was chosen to account for the effective repulsive interactions between platelets and the parent size-distribution function was chosen to be unimodal or bimodal. While samples with small polydispersity are well described by a unimodal distribution, large polydispersities require *marginally* bimodal distributions (i.e. distributions made from two overlapping peaks such that

no second maximum is visible). Bimodal distributions with two clearly separated maxima can give rise to a loop in the function $\gamma_N(\eta_0)$. Thus the fraction of total volume occupied by nematic exhibits a non-monotonic behaviour, not related to the presence of three-phase I–N–N coexistence, a genuine prediction of the model which is expected to be confirmed in future experiments.

As mentioned before, synthetic mineral particles cannot be made completely monodisperse in all their characteristic lengths. For example, in studies on colloidal platelets [267], particles are usually highly polydisperse in both diameter and thickness and, to our knowledge, only in one case [35] has the platelet thickness been perfectly controlled to exactly one monolayer. Diameter-polydispersity in platelets of equal thickness can destabilize the columnar phase with respect to the smectic phase, while rod-like, length-polydisperse particles exhibit the opposite behaviour. The effect of length-polydispersity on the relative stability of smectic and columnar phases in fluids of hard parallel cylinders was studied through coexistence calculations [265] and bifurcation analysis [266]. However, realistic models meant to reproduce experimental results must take into account both polydispersities, a programme recently followed by Velasco and Martínez-Ratón [261]. These authors considered hard board-like particles of square section $l \times l$ and thickness h , with main axes along a common direction and polydisperse in both lengths but with decoupled size distribution. A FMT theory, extended for a general polydisperse fluid, was adopted. Fixing the two polydispersity coefficients (δ_l, δ_h), bifurcation theory was used to obtain the N–(C,S) bifurcation packing fractions $\eta_{C,S}$, complemented with free energy calculations. Results are plotted in figure 38, with symbols representing experimental data collected from the literature. Colours of symbols represent the nature of the different phases obtained in experiments (blue for S, orange

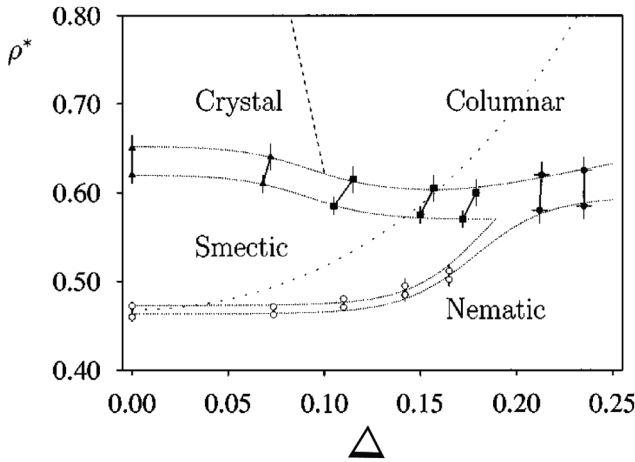


Figure 39. Phase diagram in the scaled density ρ^* versus polydispersity coefficient Δ for the freely rotating HSC model, as obtained from simulation [268]. Reprinted with permission from [268]. Copyright (1998), AIP Publishing LLC.

for C and black for S–C coexistence). The model correctly describes the interplay between C and S phase stability as a function of both polydispersities. Free energy relative differences between smectic and columnar phases confirm the scenario obtained from bifurcation theory: at high enough density and for $\delta_h \gg \delta_l$, the C is more stable than the S phase, while for $\delta_l \ll \delta_h$ their relative stability changes. There are values of (δ_l, δ_h) for which the two branches cross at a density ρ_0^* larger than the two bifurcation points: for $\rho_0 < \rho_0^*$ the smectic is more stable, with the opposite behaviour for $\rho_0 > \rho_0^*$. Finally, the microsegregation mechanism already observed in the smectic phase was also confirmed for the stable C phases: particles located at the sites of the square lattice have a side-length distribution similar to the global one, while particles at interstitial points exhibit a size distribution centred at much smaller values.

Computer simulations of polydisperse systems are technically difficult to perform and consequently there are very few studies. In 1998, Bates and Frenkel [268] studied the effect of length-polydispersity on the phase behaviour of freely rotating HSC in the limit of infinite aspect ratio. Their phase diagram in the density versus polydispersity coefficient plane is represented in figure 39. The authors found that when the polydispersity parameter Δ is less than 0.08, the phase behaviour is unchanged with respect to the one-component case, namely the phase transition sequence N–S–K is obtained. For polydispersities in the range $0.08 < \Delta < 0.18$ the window of stability of the S phase shrinks, while those of the N and C phases (bracketing the smectic region) become wider. Finally, for $\Delta > 0.18$, the S phase is no longer stable, since rods have a high dispersion in length and they are unable to arrange into periodic layers. The N phase exhibits a direct first-order transition to the C phase, which seems to be stable up to close packing. The same authors studied the I–N transition in a fluid of hard freely rotating platelets of vanishing thickness [269]. Semi-grand canonical Gibbs ensemble simulations were performed to study particle fractionation as a function of diameter-polydispersity. Larger particles tend to populate the coexisting N phase, while the I phase is richer in

small platelets. Also, large platelets are more orientationally ordered than small platelets in the N phase.

3.6. 2D fluids

2D systems have attracted a lot of interest for a long time, mainly because of their peculiar properties relating to their low dimensionality. Also, these systems are a simple realization of real materials forming monolayers adsorbed on a substrate or self-assembled structures on fluid interfaces. 2D fluids may also serve as models for biological or synthetic membranes and the understanding of the assembling properties of molecules of different shapes on a surface is becoming an increasingly important topic in condensed matter physics and cross-disciplines such as physical chemistry and biophysics.

The peculiar properties of 2D crystals and the associated liquid-crystal freezing transition (existence of bond-orientational order and the hexatic phase, absence of true long-range positional order, etc.) for fluids made of isometric or effectively isometric particles have their counterpart in mesophases possessing orientational order. There are indications that the I–N transition in 2D fluids might be governed by a Kosterlitz–Thouless mechanism, similar to the one thought to operate in the liquid-hexatic transition of an isotropic fluid. Since the order parameter of a nematic is a tensor quantity, there are subtle questions on the existence of order and its dependence on the dimensionalities of the order parameter matrix and of the physical space. A good introduction to these topics can be found in the book by Lubensky and Chaikin [270]. Another important difference with respect to the 3D case is the apparent nonexistence of smectic order in 2D, which is probably associated with the effect of 2D fluctuations on the emergence of spatial order along one direction.

The question of the existence and nature of orientational order in 2D fluids is an old one [271]. Evidence based on simulations [272] and experiments [273] indicate that, similar to spatial order in 2D crystals, true long-range orientational order does not exist in 2D nematics and that $D = 2$ is the lower critical dimensionality in nematics. As with many other 2D systems, the nematic state presents anomalously large thermal fluctuations which result in a highly fluctuating nematic director. Assuming that the free energy can be described by a Frank-type elastic model in the one elastic constant approximation,

$$F_e = \frac{1}{2} \int_A d^2r \left\{ K_1 (\nabla \cdot \hat{n})^2 + K_3 |\nabla \times \hat{n}|^2 \right\} = \frac{1}{2} K \int_A d^2r |\nabla \theta|^2, \quad (81)$$

(where $\hat{n} = (\cos \theta, \sin \theta)$), the fluctuations in θ , the director tilt angle with respect to a fixed reference direction, would depend on the number of particles N as $\langle \theta^2 \rangle \sim \log N$, with a vanishing order parameter in the thermodynamic limit, $q_2 = \langle \cos 2\theta \rangle \sim N^{-kT/2\pi K}$ and an orientational correlation function $g_n(r) = \langle \cos [n\theta(r)] \rangle \sim r^{-n^2 kT/2\pi K}$ that would decay algebraically rather than presenting long-range order. All of these results imply that, strictly speaking, the ordered nematic phase does not exist in the thermodynamic limit

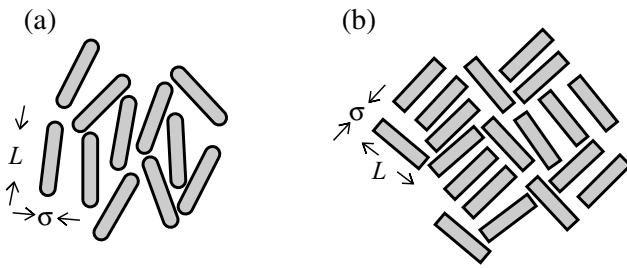


Figure 40. Typical models for 2D fluids made of anisotropic particles. (a) Hard discorectangles, with L the rectangle length and σ the width (note that the total length is $L + \sigma$). (b) Hard rectangles of length L and width σ .

$N \rightarrow \infty$, although the dependence is slow and even large nematic samples, or confined nematics, will be well ordered. This property, stemming from fluctuations, calls into question the very existence of the usual Frank elastic constants [271], which should be regarded to adopt values renormalized by fluctuations [274].

Concerning the nature of the I–N transition, an interesting property of 2D nematics is that, for apolar particles exhibiting head–tail symmetry, a general Landau expansion in the order parameter Q cannot depend on its sign, so that the I–N transition can be of first- or second-order; this is in contrast with 3D nematics, for which the Landau expansion contains cubic terms which drive the transition to be first-order (although weak as seen experimentally). Simulations of hard ellipses [275] have indeed found the presence of a tricritical point separating first-order from continuous I–N transition as a function of aspect ratio.

As in many other ordering phenomena in condensed matter physics, the role played by hard-body models in the investigations of orientational order in 2D has been crucial. Figure 40 shows two of the more popular particle models. The orientational transition in 2D was initially explained using entropy arguments. Straley [271] investigated Onsager theory for a 2D nematic and found it to predict a I–N transition. However, there is an important subtlety. The argument Onsager used to truncate the virial expansion at second-order for 3D rods is not valid in 2D since virial coefficients higher than the second are much more important in 2D than in 3D. Rigby [45] calculated higher-order virial coefficients for 2D isotropic fluids made of elliptical and discorectangular particles with a wide range of aspect ratios, including the hard-needle limit. He reported negative values for B_4 and B_5 for large elongations but, in the case of ellipses, B_5 becomes negative already for a length-to-breadth ratio of 1:6. Therefore, Onsager theory is not strictly valid even in the long-particle limit and results should always be taken with caution.

The first evidence by simulation of nematic ordering, due to Vieillard-Baron [56], was in fact in a 2D fluid. But the results were not conclusive. Later Frenkel and Eppenga [272] studied the same system and concluded that the nematic phase exhibits quasi-long-range order (with algebraically decaying orientational correlations). Cuesta *et al* [276] used density functional theory to describe the I–N and the freezing transitions. The theory was an extension of one used previously

for hard ellipsoids. For uniform phases it has the same structure as the PL theory for 2D fluids, but at low densities it does not reproduce the exact second virial coefficient, which is especially problematic for ellipses with large aspect ratio.

In more extensive work, Cuesta and Frenkel [275] investigated the transition by constant-pressure MC simulation. In these simulations the N phase appeared to be stable for aspect ratios $\kappa > 2$, with a crystal phase at high density. The order of the transition seemed to change from first-order to continuous as the aspect ratio increased, pointing to the existence of a tricritical point. For $\kappa = 6$ the transition proceeded via disclination unbinding. Cuesta and Frenkel also proposed a rescaling of the excluded volume to remedy the deficiencies of the Cuesta *et al* theory [276] and obtained a correct second virial coefficient. Comparison with the MC results was satisfactory for both the equation of state and the location of the transition. Figure 41 shows particle configurations of the system at different packing fractions for the case $\kappa = 4$, where isotropic, nematic and solid phases are stabilized. The configuration corresponding to the unstable nematic phase, panel (b), shows the presence of nematic domains, which herald the formation of a stable nematic phase at higher densities. It is also clear from the configuration pertaining to the solid phase that particles are not very localized and large positional fluctuations exist. One important point is that the computer simulations have not found a smectic phase in fluids of hard convex bodies [272, 275, 277], which is an important difference with respect to the 3D case and could be associated with the reduced dimensionality and the amplification of spatial fluctuations that destroy smectic order. 2D smectics have been observed, though, in adsorbed monolayers of molecules on graphite [278].

Bates and Frenkel [277] investigated in more detail the nature of the continuous isotropic–nematic transition using Monte Carlo simulation of a fluid of hard discorectangles. Analysis of the orientational correlations, which decay algebraically (quasi-long-range order) with distance, seemed to confirm a Kosterlitz–Thouless scenario for the continuous transition, governed by a disclination unbinding mechanism. For rods of low aspect ratio the isotropic phase changes to a crystal phase via a first-order transition. The isotropic phase exhibits strong short-ranged particle correlations in position and orientation. More recently, Khandkar and Barma [279] performed grand canonical Monte Carlo of hard needles and confirmed the quasi-long-range nature of the nematic phase.

The Onsager theory for 2D hard needles was investigated in more detail by Chrzanowska [280]. She made a careful analysis of the theory based on bifurcation theory and a detailed comparison of the order parameter and the thermodynamics with the available computer simulations of Frenkel and Eppenga [272] and Chrzanowska and Ehrentraut [281] and from her new MC data [280]. The agreement is very good, which is attributed to two causes: the small system size of the simulations, which prevents the appearance of director distortion and point defects and the fortuitous cancellation of virial coefficients due to some of them being negative. Also, it was conjectured that the disclination unbinding mechanism associated with the Kosterlitz–Thouless transition observed in the simulations takes place after the transition, i.e. in the nematic region.

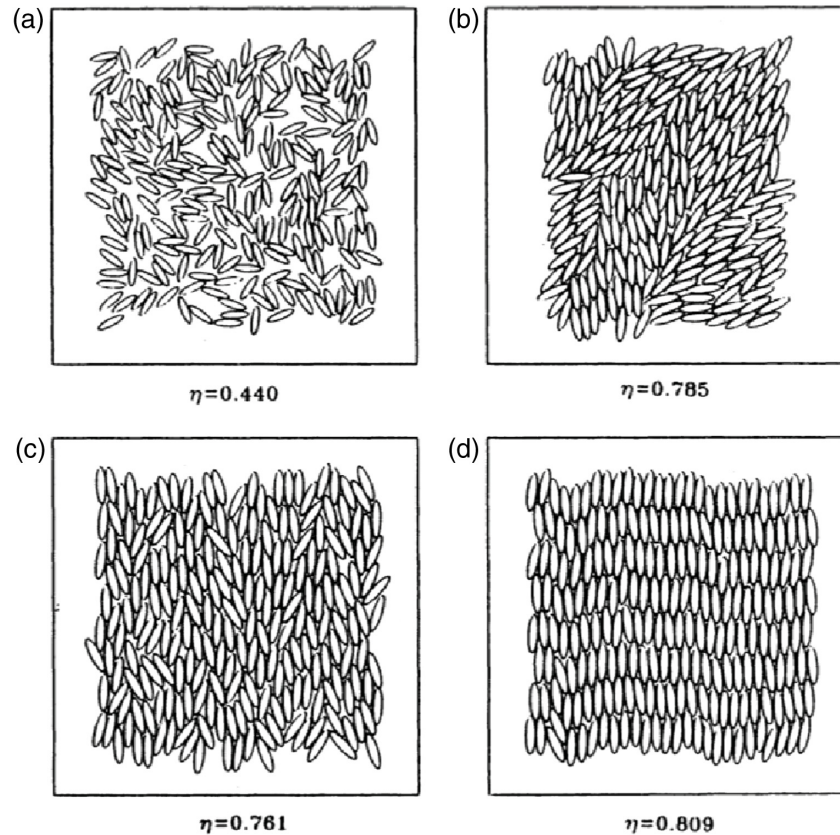


Figure 41. Snapshots of typical particle configurations of hard ellipses in different phases from simulations by Cuesta and Frenkel [275] for aspect ratio $\kappa = 4$. (a) Isotropic phase, at packing fraction $\eta = 0.440$; (b) unstable nematic phase, $\eta = 0.785$, obtained by compression from the isotropic phase; (c) stable nematic phase, $\eta = 0.761$; (d) solid phase, $\eta = 0.809$. The last two states were obtained by expanding a solid phase. Reprinted with permission from [275]. Copyright (1990) by the American Physical Society.

Extended Onsager theories à la Parsons–Lee have been proposed for hard rods in 2D. Varga and Szalai [282] studied the isotropic–nematic transition for hard ellipses using two versions of PL theory. In one, the reference fluid was taken to be the hard-disc fluid, whereas in the other the isotropic phase of hard ellipses was used. In general, PL theory gives reasonable agreement with MC data, but the order of the transition is not correct in the narrow range of aspect ratio about $\kappa = 4$. A PL theory for hard discorectangles was also proposed by de las Heras *et al* [283], using parallel hard ellipses as a reference fluid. Results were compared with the MC simulations of [277] for $\kappa = L/D = 15$ and very good agreement was found for the equation of state. In the case of the transition density the results were not in such an agreement, since the theory predicted an isotropic–nematic transition at a packing fraction $\eta = 0.257$, compared with 0.363 from the simulations. However, there is an interesting observation. de las Heras *et al* also calculated the two elastic constants of a 2D nematic (splay K_1 and bend K_3), using the same theory and expressions for the elastic constants similar to those for the 3D nematic. For $\kappa = 15$, the ratio K_1/K_3 decreases very quickly with density as the system goes into the nematic phase, which raised doubts about results based on the common one-constant approximation $K_1 = K_3$ (note that there are no estimations of elastic constants in 2D based on simulations). Also, Bates and Frenkel [277] estimated the transition density by assuming a Kosterlitz–Thouless-type transition and applying the condition $K_c = 8kT/\pi$ for the

value of the renormalized constant. Taking $K = (K_1 + K_3)/2$ and values from the DFT calculation, one obtains $\eta = 0.36$, in good agreement with the simulation value.

Hard ellipses and hard discorectangles have topologically similar phase diagrams, with I, N and K phases. The character of the I–N transition seems to depend delicately on the particle geometry and particle aspect ratio. However, beyond the type of transition, there are important subtleties associated with the particle shape. One example is the formation of oriented phases with different symmetries and recently interest has focused on the phase behaviour of particles with shapes different from the simple ellipsoidal or discorectangular shape. One of the most studied is the rectangular shape, which may be considered as a deformation of the ellipsoidal shape, given on the x,y plane by $(x/a)^n + (y/b)^n = 1$ with $n = 2$, in the limit when the exponent $n \rightarrow \infty$. The hard-rectangle model has received a lot of attention due to the possibility that the so-called *tetratic* phase might be stabilized. The tetratic phase is a nonstandard nematic phase possessing two, instead of one, equivalent and mutually orthogonal directors and it is equivalent to the cubatic phase in 3D. Therefore, the tetratic phase has four-fold symmetry, even though the particles possess two-fold symmetry. In the tetratic phase the angular distribution function $h(\varphi)$, with $0 \leq \varphi \leq 2\pi$, exhibits peaks not only at $\varphi = 0$ and π , but also at $\pi/2$ and $3\pi/2$ and all of these directions are equally probable. The formation of these nontrivial arrangements in self-assembled suspensions of colloidal rectangular particles

could be important in relation to the creation of patterned templates which could give rise to new layered materials of technological importance [284]. Therefore, the theoretical description of spontaneous ordering derived from packing (entropic) problems in nontrivial structures is a very relevant problem and the use of hard models is very adequate.

The first indication for the existence of a tetratic phase in fluids of rectangular particles came in 1998 from the work by Schlacken *et al* [285], who used SPT theory to study the orientational transition in fluids of hard ellipses and rectangles. For the case of ellipses they discussed the results for the equation of state and the transition densities and compared with the existing Monte Carlo results for ellipses of Cuesta and Frenkel [275]. In the case of hard rectangles they used the same theory, but with a different excluded area and a tetratic phase was found to be stable for low aspect ratios, in a small region in the density-aspect ratio plane. The phase diagram was found to depend on the value of aspect ratio. For $\kappa \equiv L/\sigma > 5.44$ (with L the length and σ the width of the rectangle) the isotropic fluid was predicted to change to a uniaxial nematic phase via a continuous phase transition. However, for $2.62 < \kappa < 5.44$ the transition changed to first-order. Finally, for $\kappa < 2.62$ a direct (continuous) transition from the isotropic phase to the tetratic phase was predicted to occur at a rather high density. At even higher densities the tetratic phase was conjectured to exhibit a second continuous transition to the uniaxial nematic phase (no explicit spinodal calculations were performed).

The reason why the tetratic phase can be stabilized lies in the existence of sharp corners in the particle shape. We do not expect to find tetratic phases for particles such as ellipses or discorectangles (the 2D version of spherocylinders). The reason is that there is a fundamental difference between rectangles and models with smooth corners. This difference can be appreciated by looking at the angular dependences of the excluded area, $v_{\text{exc}}(\varphi)$, of the two models, with φ the relative angle between the long axes of two particles. In the case of hard discorectangles there are minima at $\varphi = 0^\circ$ and 180° , but for hard rectangles there are additional, relative minima at $\varphi = 90^\circ$ and 270° , which the fluid can use in order to compensate for the loss of orientational entropy. The existence of tetratic order was ruled out for hard discorectangles in a Monte Carlo study by Bates and Frenkel [277].

Wojciechowski and Frenkel [286] studied the hard-square fluid in 2004. The fluid did not appear to freeze from the isotropic phase, but an intermediate phase with quasi-long-ranged (algebraic) orientational order and no positional (faster than algebraic) order appeared; this phase corresponds to a tetratic phase, although it cannot be considered a proper liquid-crystal phase since the particle does not differentiate the usual nematic phase from the tetratic phase.

A year later, Martínez-Ratón *et al* [287] performed a detailed study of the ordering properties of the hard discorectangle and the hard rectangle models using, as in the work of Schlacken *et al* [285], the SPT theory to describe spatially uniform phases, but extending and correcting the work of the latter authors. However, this theory predicts tetratic ordering at rather high values of packing fraction, $\eta \simeq 0.85$, in a region where phases with spatial order should be stable.

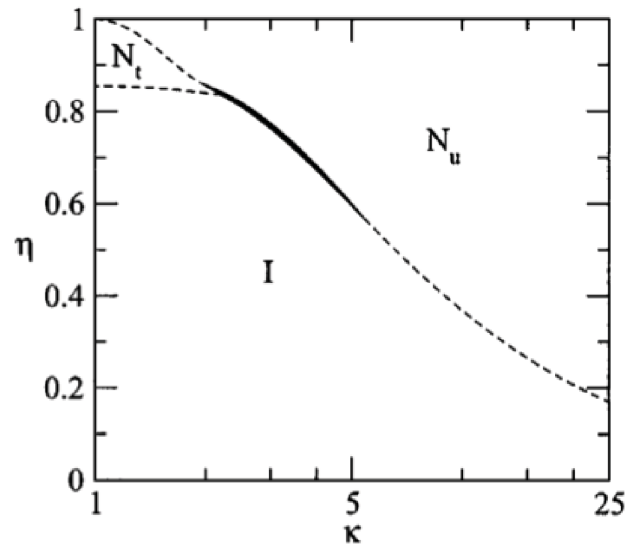


Figure 42. Phase diagram of the hard rectangle system in the packing fraction aspect ratio plane as obtained by Martínez-Ratón *et al* [287] using scaled particle theory. Reprinted with permission from [287]. Copyright (2005), AIP Publishing LLC.

Therefore, Martínez-Ratón *et al* also studied the formation of spatially nonuniform phases using an extended SPT theory that incorporated elements from fundamental measure theory, giving a reasonable account of spatial correlations. The results are shown in figure 42, which represents the SPT phase diagram of the model including only uniform phases. These results complement those of Schlacken *et al* [285] in that not only instability lines were calculated, but also the full phase equilibria. A complex phase behaviour in the region where the tetratic phase begins to be stable was found. In the interval $2.21 < \kappa < 5.44$ the isotropic-uniaxial nematic transition is of first-order. For $\kappa < 2.21$ the tetratic phase begins to be stable, with a stability region bounded by a continuous isotropic-tetratic transition below and by a tetratic-uniaxial nematic transition above; this transition is of first-order for $1.94 < \kappa < 2.21$ and continuous for $1 < \kappa < 1.94$. This means that there are two tricritical points: one at $\kappa = 5.44$, already predicted by Schlacken *et al* and a second one at $\kappa = 1.94$ whose calculation requires a proper bifurcation study from the tetratic to the uniaxial nematic phase. The spinodal line corresponding to the instability of the isotropic phase against spatial fluctuations was also calculated from this extended SPT theory. This line, not shown in the figure, is located in the range $0.5 \lesssim \eta \lesssim 0.6$, a long way below the predicted stability for the tetratic phase, which would mean that, even though tetratic correlations may be large, they are not sufficient to stabilize the tetratic phase.

The hard-rectangle system was explored in detail for the case $\kappa = 3$ by Martínez-Ratón [288]. His aim was to investigate layering and commensuration transitions in a confined set-up (hence the choice of an aspect ratio that ensured that the columnar phase was the stable phase at high density), but the bulk phase sequence was calculated as a preliminary step. The theory used was a FMT for hard rectangles in the Zwanzig approximation, considering orientations along two perpendicular axes. A number of phases were found: isotropic, nematic, two different smectic phases, a plastic solid,

a perfectly oriented crystal and a columnar phase (note that this theory cannot describe a tetratic phase). However, the equilibrium sequence of phases was isotropic and columnar, with a direct first-order transition between the two.

Parallel with these developments, experiments on vibrated quasi-2D monolayers made of (macroscopically-sized) granular rods have been performed. Vibration induces motion of the grains which is similar to thermal motion in statistical systems. Although the nature of vibrated granular matter is very different from that of thermal systems, they are both partially controlled by overlap (entropic or packing) interactions and in some regimes they are expected to generate similar types of structures, either steady (granular matter) or equilibrium (thermal matter) states. In fact, Narayan *et al* [289] performed experiments on vibrated monolayers of anisotropic grains, such as basmati rice, pinrolls and steel cylinders. Pinrolls exhibit nematic phases, while basmati rice grains have smectic ordering. But cylinders, which have sharp corners, form nematic phases with strong tetratic correlations. These conclusions were obtained directly from visible inspection of real images, but also from the proper orientational correlation functions. In particular, defining correlation functions by $g_n(r) = \langle \cos n\phi(r) \rangle$ (where $\phi(r)$ is the angle of the long axis of a particle at distance r relative to another particle fixed at the origin), nematic ordering is measured by $g_2(r)$, while $g_4(r)$ controls the presence of tetratic order. One interesting thing is that tetratic correlations were seen to be substantial for rather large aspect ratios ($\kappa = 12.6$). In contrast, SPT predicts that tetratic order should be small for aspect ratios $\kappa \gtrsim 2.21$.

At high packing fractions hard rectangles would be expected to crystallize with particles pointing in the same direction and with their centres of mass arranged on a rectangular lattice (the metastable phase obtained by Martínez-Ratón [288] in his density functional study mentioned above). But in the case $\kappa = 2$ two such rectangles can form a dimer with square shape and a definite axis (the long sides of the rectangles). A collection of such square dimers can arrange to form a crystal with dimers lying at the sites of a square lattice and with a close-packing limit at $\eta = 1$ (perfect packing), but with residual entropy associated with the random orientation of the dimer axis. Therefore, a nonperiodic degenerate solid phase could be the lowest free energy phase. This is an interesting scenario explored by Wojciechowski *et al* [290] in 1991 using hard-disc dimers. In effect, they identified a nonperiodic crystal at high density, but the underlying lattice was triangular.

In 2006 Donev *et al* investigated hard rectangles of aspect ratio $\kappa = 2$, i.e. particles that can form square dimers [291]. They demonstrated that this system exhibits both phases with tetratic order and nonperiodic solids at high density. The latter is a nonperiodic tetratic phase made of a random tiling of dimers forming a square lattice, with a residual entropy of 1.79k per particle and a possibly glassy character. The results of Donev *et al* are consistent with a two-stage transition scenario of the Kosterlitz–Thouless type, with an isotropic–tetratic liquid transition followed by a tetratic–solid transition. The robustness of these results was checked by using two complementary approaches: a Monte Carlo simulation on hard rectangles and a molecular dynamics simulation using rectangles with

rounded corners. These results suggest that hard-rectangle fluids show a strong tendency to form clusters and that theories based on two-body correlations [285, 287] should not give accurate results for their structure and thermodynamics.

Therefore, Martínez-Ratón, Velasco and Mederos [292] revisited the problem of the stability of the tetratic phase using a modified SPT theory that incorporates the third virial coefficient, thus including three-body correlations that should be important to describe clustering of hard rectangles. A phase diagram was calculated using a variational procedure. The range of stability of the tetratic phase was found to be increased with respect to the standard SPT approach based solely on two-body correlations, both in density and particle aspect ratio. The same group studied the problem with a focus on clustering [293], using Monte Carlo simulation as a guide to construct a model based on stable polydisperse clusters of rectangles. Clustering was seen to greatly enhance the relative stability of the tetratic phase with respect to the standard, uniaxial nematic phase. In particular, it was predicted that square clusters have a dominant contribution to the free energy.

An important experimental study on the issue of the tetratic phase was performed, using colloidal particles, by Zhao *et al* [294]. A solution of PMMA discs, with $\kappa \simeq 6.4$, were prepared standing on edge on a planar surface and their ordering properties were analyzed. The system should be similar to a fluid of hard rectangles. Almost smectic behaviour was observed at high densities but, more interestingly, a single Kosterlitz–Thouless transition from the isotropic to the nematic phase was found. Nematic order seems to be destroyed by wall defects, which lead to strong short-range tetratic order on the isotropic side of the transition.

More recently, Geng and Selinger [295] have investigated the conditions for tetratic order to appear. They used a soft-potential, Maier–Saupe-type model, analyzed with a mean field theory supplemented with Monte Carlo simulations. The model included an anisotropy coefficient that reflects the amount of two-fold symmetry breaking. Although a soft-potential model, the results are interesting also to interpret hard-body studies. An important finding is that the tetratic phase can exist up to a relatively high value of the anisotropy coefficient which, when transferred to a hard-particle view, points to rather high particle aspect ratios. Also, the phase diagram obtained is surprisingly close to that predicted by Martínez-Ratón *et al* [287] for the hard-rectangle fluid, including the different phases, the nature of the phase transitions and even the existence of tricritical points. This result indicates that the phase behaviour is very generic and independent of the particular interactions.

In a very complete MC simulation work, Triplett and Fichthorn [284] studied the hard-rectangle fluid with a range of aspect ratios and densities. For large aspect ratios the results compared even quantitatively with the results of [287] for the isotropic to uniaxial nematic transition. For a moderate value, $\kappa = 7.5$, a detailed study of angular correlations showed strong tetratic ordering, but not sufficiently large to give a stable tetratic phase with long- or quasi-long-range order.

The ordering properties of 2D hard squares have recently been revisited by Avendaño and Escobedo [296], who went

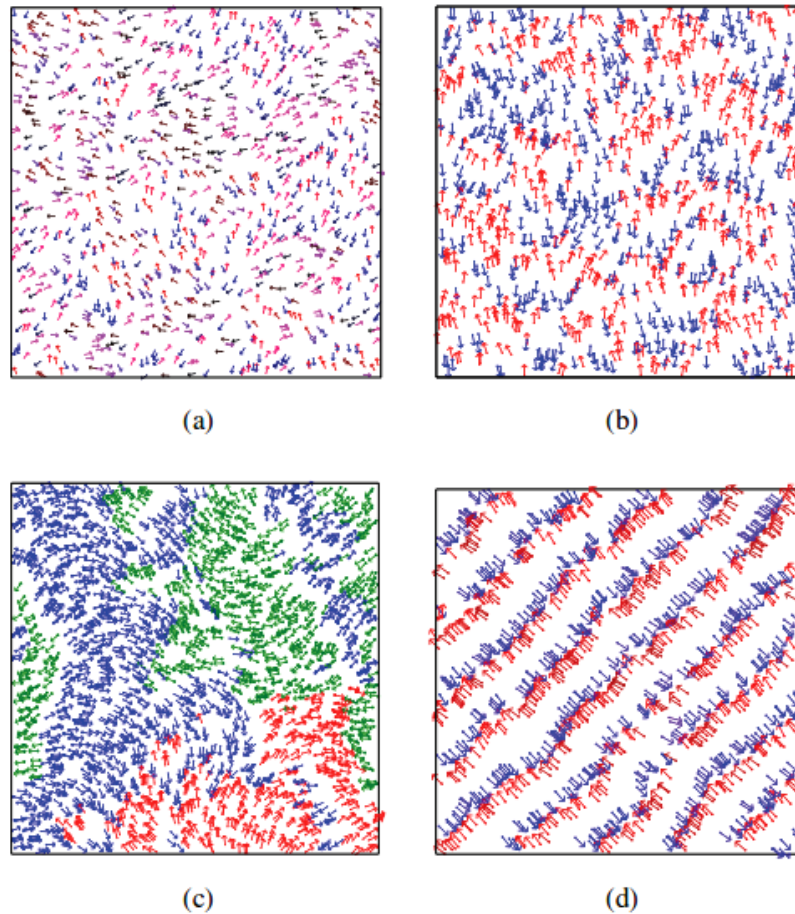


Figure 43. Typical configurations of V-shaped hard-needle particles in 2D as obtained from simulations [29]. (a) Isotropic (reduced pressure $p^* = 15$, number of particles in the simulations $N = 1000$); (b) nematic ($p^* = 40$, $N = 1000$). (c) deformed nematic ($p^* = 60$, $N = 2000$), all for a bending angle between the needles of $\alpha = \pi/8$ (linear configuration would have $\alpha = 0$). (d) Antiferroelectric smectic ($p^* = 55$, $N = 1000$) for $\alpha = 3\pi/8$. See original article for details.

a step further from the simulations of Wojciechowski and Frenkel [286] for hard squares. Avendaño and Escobedo considered a fluid of rounded hard squares and investigated the evolution of phase behaviour with respect to a roundness parameter, using rather large system sizes. For this system there is still some debate on the true mechanism of orientational and positional ordering, which in some sense parallels that around the freezing transition in the hard-disc fluid (a debate not completely closed, see [297]). Experimental studies on hard colloidal platelets of square and pentagonal shapes [298, 299] in part motivated this study, together with simulation work on pentagons [300]. In general, the crystal phases predicted by the simulations are not observed in the experiments, a result that has been associated with roundness effects and periodic boundary conditions. Avendaño and Escobedo found that the shape roundness is a very important factor and that the experimental phases can indeed be observed in the simulations. For a particular range of roundness parameter, the tetratic mesophase mediates the phase evolution from the isotropic to the crystal phase.

As mentioned before, there is evidence, based on computer simulations, that the smectic phase is not stable in 2D fluids of hard ellipses and hard discorctangles [272, 275, 277] and that, in these fluids, the only mesophase between the

isotropic and crystal phases is the nematic. In an effort to search for other mesophases in different, not necessarily convex, bodies, Varga *et al* [28] considered the fluid of zigzag needles introduced in [301] and applied Onsager theory. The study was motivated by computer simulations of Peón *et al* [302], who collected evidence for the stabilization of the smectic phase and the existence of isotropic-nematic, nematic-smectic and isotropic-smectic transitions. Crystal structures cannot be formed in this system, as in any other system of particles without volume. Varga *et al* included the rotational freedom of particles to describe the isotropic and nematic phases, but considered a parallel particle approximation for the smectic phase. The results were seen to agree reasonably with the simulations. The stabilization of the smectic phase was associated with the effect of increased particle terminal line segments or bent angle of the zigzag. Its structure is peculiar, since the central core of the zigzag is tilted with respect to the layer normal, an optimized arrangement that maximizes the free volume inside the layers.

Bisi *et al* [155], based on packing arguments, have speculated on the formation of antiferroelectric smectic phases in V-shaped particles due to a shape-polarity effect similar to that taking place in real dipolar molecules. More recently, Martínez-González *et al* [29] have considered the simpler

V-shaped needles and performed Monte Carlo simulation and calculations based on Onsager theory. They observed the formation of deformed, stable nematic phases consisting of orientationally ordered polar domains with bent director orientation, but with zero overall polarization. Using Onsager theory, it can be shown that the V-shaped particle geometry favours bend deformations due to a free energy reducing bend torque, while splay deformations have an associated free energy cost. As pressure is increased, these polar domains become smaller and transform into linear arrays with alternating polarity, i.e. an antiferroelectric smectic phase. The theoretical results were seen to be in good agreement with the simulations. A sequence of typical configurations can be seen in figure 43.

Mixtures of anisometric particles in 2D have also been investigated. One of the important issues is the possibility of nematic-nematic demixing phenomena. In 2005, Martínez-Ratón *et al* [303] used scaled particle theory to study binary mixtures of hard discorightangles and hard rectangles, with a view to exploring possible liquid-crystal demixing scenarios in two dimensions. Using a bifurcation analysis from the isotropic phase and coexistence calculations, it was shown that both isotropic-nematic phase separation and nematic-nematic demixing ending in a critical point was possible in a binary mixture of hard discorightangles and also in mixtures of hard discs and discorightangles. In addition, an isotropic-nematic-nematic triple point for a mixture of hard discs and hard discorightangles was found. Similar demixing phase diagrams were obtained when one or two of the species have an elliptical shape, as shown in [304]. The elliptical shape enhances the demixing gap since, for a given aspect ratio, the ellipse is the more convex body in two dimensions.

de las Heras *et al* [305] used scaled particle theory to study binary mixtures composed of hard rectangles and other particles not possessing stable tetratic order by themselves (either hard discorightangles or hard discs). Due to packing frustration associated with particle shape, the tetratic phase in hard rectangles of low aspect ratio is destabilized when the second component is added, leading to demixing involving a second phase (uniaxial nematic or isotropic). The effect is minimized for hard squares. The effect is also observed when the second component is a hard rectangle of different aspect ratio but the same particle area or different particle area but the same aspect ratio. When the size ratio is sufficiently large, isotropic-tetratic or tetratic-tetratic demixing was obtained in mixtures of hard squares. Figure 44 shows a pressure-composition phase diagram for a mixture of hard rectangles with aspect ratio $\kappa_1 = 1.5$ and width $\sigma_1 = 1$ and hard discorightangles of aspect ratio $\kappa_2 = 2$ and same particle area as a rectangle of aspect ratio equal to 2 and unit width. The phase diagram includes a lower critical point terminating a region of uniaxial nematic demixing, an azeotropic point and two tricritical points separating first-order from continuous phase transitions. Isotropic I, uniaxial nematic N_U and tetratic N_T phases were found, with corresponding regions of stability shown in the figure.

Finally, we mention some applications of hard-body models to systems whose properties are in the region between

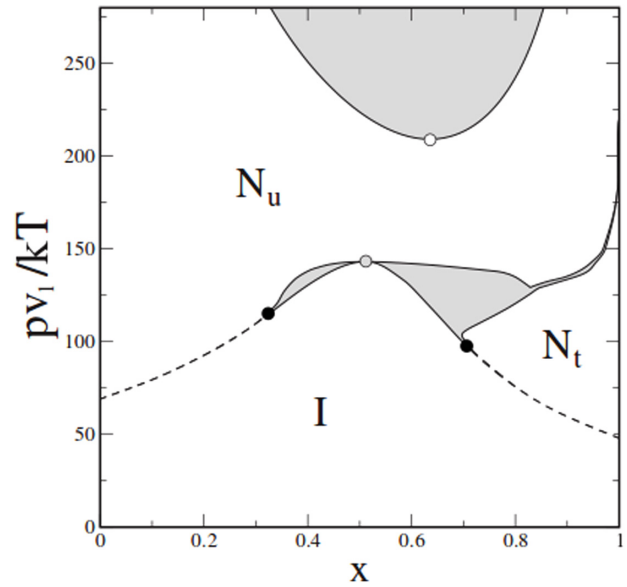


Figure 44. Phase diagram for a hard rectangle/hard discorightangle mixture in the scaled pressure versus composition of the hard-rectangle component, from [305]. Values of the shape parameters are: aspect ratio $\kappa_1 = 1.5$ and width $\sigma_1 = 1$ for the rectangles and aspect ratio $\kappa_2 = 2$ and same particle area as a rectangle of aspect ratio equal to 2 and unit width for the discorightangles. The open circle indicates the critical point, the shaded circle denotes an azeotropic point, while the filled circles indicate tricritical points. Two-phase regions are indicated by the grey areas. Reprinted with permission from [305]. Copyright (2007) by the American Physical Society.

two and three dimensions and that share some characteristics with 2D and 3D fluids. A very important example is that of Langmuir monolayers. These systems are composed of liquid-crystal-forming molecules located at an approximately 2D surface (usually flat but with possibly substantial thermal fluctuations in case the surface is a liquid interface) and with molecular axes that can freely rotate in 3D. Experimentally these monolayers are observed to undergo an amazingly complex variety of phase transitions [306], including positional ordering, chain freezing and expanded-to-condensed phase transitions and tilt transitions. These transitions are associated with orientational order of the molecules, conformational changes in the molecular chains and positional order of the centres of mass. Some of these transitions are possibly explained, partially or totally, in terms of excluded volume.

A model of hard rods (in the Onsager limit) grafted to a flat surface was analyzed by various authors [307–310]. Contrary to the full 3D case, this system does not possess a discontinuous nematic-like transition. Somoza and Desai [311] used the same model to examine the possibility that the fluid may exhibit a transition to a tilted nematic phase. In agreement with previous findings the totally repulsive model was not shown to exhibit such a tilt transition, although a bifurcation analysis to a phase with a broken azimuthal symmetry showed a tendency towards the tilted phase. In order to induce a phase transition, an external field [310] or interparticle attractive interactions had to be incorporated and Somoza and Desai [311] obtained a rich phase diagram using simple model attractions between the rods.

Table 2. Summary of hard-body models and applications.

Models	Theories	Applications
Hard ellipsoids	Onsager	Uniaxial & biaxial nematics
Hard Gaussian overlap	Extended Onsager	
	Simulation	
Hard cylinders	Onsager	Nematics
	Scaled-particle theory	Smectics
	Extended Onsager	Mixtures
	Bifurcation	Columnar
	FMT (parallel particles)	
	FMT (freely rotating with vanishing thickness)	
	Simulation	
Hard spherocylinders	Onsager	I-N-S-K transitions
	Scaled-particle theory	Plastic phase
	Bifurcation	Elastic constants
	Extended Onsager	Mixtures
	FMT	Polydisperse fluids
	Simulation	Columnar
Hard cut spheres	Extended Onsager	Cubic
	Simulation	Mixtures
Hard boards	Onsager	Uniaxial & biaxial nematics
	FMT (Zwanzig approx.)	Smectics
	Cell theory	Exotic phases
	Simulation	Polydisperse fluids
Hard ellipses (2D)	Scaled-particle theory	I-N-K transitions
	Extended Onsager	Nature of I-N transition
	Simulation	Effect of particle geometry
Hard discorectangles (2D)	Scaled-particle theory	I-N-K transitions
	Extended Onsager	Nature of I-N transition
	Simulation	Mixtures
Hard rectangles (2D)	Scaled-particle theory	Tetratic nematics
	Extended Onsager	I-N-T-K transitions
	Simulation	Clustering
		Mixtures
		Effect of particle geometry

More recently, Martínez-Ratón *et al* [312] used a fundamental measure density functional to study a monolayer of particles consisting of hard uniaxial boards of sizes $L \times \sigma \times \sigma$ with centres lying on a flat surface. The aim was to study the existence of a phase transition from a uniaxial to a biaxial nematic phase for both prolate ($L > \sigma$) and oblate ($L < \sigma$) geometries. Since the Zwanzig approximation (with three possible orientations of the distinct axis) was used, the 3D one-component fluid can be mapped onto a 2D fluid mixture of three components consisting of hard squares and two hard rectangles pointing along perpendicular directions (these 2D bodies are the projections of the 3D particles on the surface). The authors found that, for oblate particles and $\kappa^{-1} \equiv \sigma/L > 3.5$, there exists a planar N_U (with the same number of rectangles pointing along the two perpendicular directions) to N_B (with more rectangles pointing along one direction) continuous phase transition, which is bounded above by a stability region of a nonuniform phase (with some kind of spatial order, be it columnar, smectic or crystal). In contrast, for $\kappa < 3.5$, there is a direct transition from the N_U to a nonuniform phase. For prolate particles, but only for $\kappa = L/\sigma > 21.34$, is there a (re-entrant) N_B phase, surrounded by regions of N_U -phase stability.

4. Conclusions

For more than a century, hard-core models have been playing a crucial role in understanding the structure and phase behaviour of condensed phases of matter. In particular, since the pioneering work of Onsager, hard bodies have been used to qualitatively understand the formation of orientationally ordered phases (see table 2 for a summary of models and applications). Even though anisotropic hard interactions are enough to explain the stability of nematic, smectic, columnar and many other mesophases, this does not mean that they are essentially responsible for the stability of liquid-crystalline phases in real materials. However, their study is very important insofar as they play an essential role in theories that incorporate more realistic molecular interactions. Also, many real colloidal systems (e.g. naturally occurring virus particles) have interactions which can be approximated by hard interactions. The actual possibility to fabricate tailor-made colloidal particles of different shapes has recently revitalized the attention on hard-particle models and research on theories that quantitatively solve their statistical mechanics is still very active. Coupling between orientational and positional order, crucial in mesophases that exhibit partial-spatial order, gives rise to nontrivial issues that these theories have to face. Most theories proposed so far rely on Onsager theory, which only

considers two-body correlations and different schemes have been proposed to go beyond this approximation, with limited success. Perturbative treatments on hard-body models have reached some predictive power in some instances, but lack of knowledge on correlations functions of hard-particle fluids is a serious drawback in these applications. The recently developed FMT version of density functional theory as applied to freely rotating anisotropic particles opens up a promising avenue of research on hard-body models (as exemplified by a recently proposed hard-helix model producing screw-like nematic phases [313, 314]) and in the future we expect important activity both in the use of new hard-body models and in the development of new theoretical tools.

Acknowledgments

This work was partially supported by grants MODELICO-CM/S2009ESP-1691 (Comunidad Autónoma de Madrid, Spain) and FIS2010-22047-C05-01, FIS2010-22047-C05-02 and FIS2010-22047-C05-04 (MINECO, Spain).

Note added in proof. Since submitting this review, a new version of DFT in the FMT formalism that provides a correct scaling for extremely anisotropic hard bodies (which is not fulfilled by equation (58)) and simultaneously accounts for the right dimensional crossover, has recently been formulated by Wittmann *et al* [315]. Using this version, the phase diagram of the HSC model, including I, N, and S phases, has been calculated.

References

- [1] Reinitzer F 1888 Beiträge zur Kenntnis des Cholesterins *Monatsh. Chem.* **9** 421
- [2] de Gennes P G and Prost J 1995 *The Physics of Liquid Crystals* (Oxford: Oxford University Press)
- [3] Chandrasekhar S 1992 *Liquid Crystals* (Cambridge: Cambridge University Press)
- [4] Collings P J and Hird M 2009 *Introduction to Liquid Crystals—Chemistry and Physics* (London: Taylor and Francis)
- [5] Khoo I-C 2007 *Liquid Crystals* (Hoboken, NJ: Wiley)
- [6] Gray G W, Vill V, Spiess H W, Demus D and Goodby J W (ed) 2009 *Physical Properties of Liquid Crystals* (London: Wiley)
- [7] Chandrasekhar S and Ranganath G S 1990 Discotic liquid crystals *Rep. Prog. Phys.* **53** 57
- [8] Bahadur B (ed) 1991 *Liquid Crystals—Applications and Uses* (Singapore: World Scientific)
- [9] Rosenbluth M N and Rosenbluth A W 1954 Further results on Monte Carlo equations of state *J. Chem. Phys.* **22** 881
- [10] Alder B J and Wainwright T E 1957 Studies in molecular dynamics. II. Behavior of a small number of elastic spheres *J. Chem. Phys.* **33** 1439
- [11] Wood W W and Jacobson J D 1957 Preliminary results from a recalculation of the Monte Carlo equation of state of hard spheres *J. Chem. Phys.* **27** 1207
- [12] Tarazona P 1985 Free-energy density functional for hard spheres *Phys. Rev. A* **31** 2672
- [13] Hansen J-P and McDonald I R 2013 *Theory of Simple Liquids* 4th edn (Amsterdam: Academic)
- [14] Rascón C, Mederos L and Navascués G 1996 Perturbation theory for classical solids *Phys. Rev. Lett.* **77** 2249
- [15] Allen M P, Evans G T, Frenkel D and Mulder B M 1993 Hard convex body fluids *Adv. Chem. Phys.* **86** 1
- [16] Onsager L 1949 The effects of shape on the interaction of colloidal particles *Ann. N.Y. Acad. Sci.* **51** 627
- [17] Mederos L, Velasco E and Martínez-Ratón Y Hard-body models of interfacial liquid crystals (unpublished)
- [18] Boublík T and Nezbeda I 1986 P-V-T behaviour of hard body fluids. Theory and experiment *Collect. Czech. Chem. Commun.* **51** 2301
- [19] Allen M P, Frenkel D and Talbot J 1989 Molecular dynamics simulations using hard particles *Comput. Phys. Rep.* **9** 301
- [20] Vroege G J and Lekkerkerker H N W 1992 Phase transitions in lyotropic and polymer liquid crystals *Rep. Prog. Phys.* **55** 1241
- [21] Lekkerkerker H N W and Vroege G J 1993 Lyotropic colloidal and macromolecular liquid crystals *Phil. Trans.* **344** 419
- [22] Tarazona P 1993 Theories of phase behaviour and phase transitions in liquid crystals *Phil. Trans.* **344** 307
- [23] Berne B J and Pechukas P 1972 Gaussian model potentials for molecular interactions *J. Chem. Phys.* **56** 4213
- [24] Frenkel D, Mulder B M and McTague J P 1984 Phase diagram of a system of hard ellipsoids *Phys. Rev. Lett.* **52** 287
- [25] Padilla P and Velasco E 1997 The isotropic-nematic transition for the hard Gaussian overlap fluid: testing the decoupling approximation *J. Chem. Phys.* **106** 10299
- [26] Velasco E and Padilla P 1998 Nematic virial coefficients of very long hard molecules and Onsager theory *Mol. Phys.* **94** 335
- [27] Teixeira P I C, Masters A J and Mulder B M 1998 Biaxial nematic order in the hard-boomerang fluid *Mol. Cryst. Liq. Cryst.* **323** 167
- [28] Varga S, Gurin P, Armas-Pérez J C and Quintana-H J 2009 Nematic and smectic ordering in a system of 2D hard zigzag particles *J. Chem. Phys.* **131** 184901
- [29] Martínez-González J A, Varga S, Gurin P and Quintana-H J 2012 Spontaneously bended nematic and antiferroelectric smectic structures of banana-shaped hard particles in two dimensions *Eur. Phys. Lett.* **97** 26004
- [30] Baus M, Rull L F and Ryckaert J-P 1995 Phase transitions in colloidal suspensions of virus particles ed S Fraden *Observation, Prediction and Simulation of Phase Transitions in Complex Fluids (NATO-ASI Series C)* vol 460 (Boston: Kluwer) p 113
- [31] Dogic Z and Fraden S 2006 Ordered phases of filamentous viruses *Curr. Opin. Colloid Interface Sci.* **11** 47
- [32] Lemaire B J, Davidson P, Ferré J, Jamet J P, Panine P, Dozov I and Jolivet J P 2002 Outstanding magnetic properties of nematic suspensions of goethite (α -FeOOH) nanorods *Phys. Rev. Lett.* **88** 125507
- [33] Vroege G J, Thies-Weesie D M E, Petukhov A V, Lemaire B J and Davidson P 2006 Smectic liquid-crystalline order in suspensions of highly polydisperse goethite nanorods *Adv. Mater.* **18** 2565
- [34] van Der Kooij F M and Lekkerkerker H N W 1998 Formation of nematic liquid crystals in suspensions of hard colloidal platelets *J. Phys. Chem. B* **102** 7829
- [35] Sun D, Sue H J, Cheng Z, Martínez-Ratón Y and Velasco E 2009 Stable smectic phase in suspensions of polydisperse colloidal platelets with identical thickness *Phys. Rev. E* **80** 041704
- [36] Ding T, Liu Z, Song K, Tung C H 2009 Synthesis of monodisperse ellipsoids with tunable aspect ratios *Colloids Surf. A* **336** 29
- [37] Lutsko J F 2010 Recent developments in classical density functional theory *Adv. Chem. Phys.* **144** 1
- [38] Singh S 2000 Phase transitions in liquid crystals *Phys. Rep.* **324** 107
- [39] Lasher G 1970 Nematic ordering of hard rods derived from a scaled particle treatment *J. Chem. Phys.* **53** 4141

- [40] Kayser F and Raveche H J 1978 Bifurcation in Onsager's model of the isotropic-nematic transition *Phys. Rev. A* **17** 2067
- [41] Herzfeld J, Berger A E and Wingate J W 1984 A highly convergent algorithm for computing the orientation distribution functions of rodlike particles *Macromolecules* **17** 1718
- [42] Stroobants A, Lekkerkerker H N W and Odijk T H 1986 Effect of electrostatic interaction on the liquid crystal phase transition in solutions of rodlike polyelectrolytes *Macromolecules* **19** 2232
- [43] Zwanzig R 1963 First-order phase transition in a gas of long thin rods *J. Chem. Phys.* **39** 1714
- [44] Runnels L K and Colvin C 1970 Nature of the rigid-rod mesophase *J. Chem. Phys.* **53** 4219
- [45] Rigby M 1993 Virial coefficients of hard convex molecules in 2D *Mol. Phys.* **78** 21
- [46] Rigby M 1970 Virial expansion for hard nonspherical molecules *J. Chem. Phys.* **53** 1021
- [47] Rigby M 1978 Virial equation of state for rigid spherocylinders *Mol. Phys.* **35** 1337
- [48] Rigby M 1989 Hard ellipsoids of revolution. Virial coefficients for prolate and oblate molecules *Mol. Phys.* **66** 1261
- [49] Rigby M 1989 Hard Gaussian overlap fluids *Mol. Phys.* **68** 687
- [50] Cooney W R, Thompson S M and Gubbins K E 1989 Virial coefficients for the hard oblate spherocylinder fluid *Mol. Phys.* **66** 1269
- [51] Maeso M J and Solana J R 1993 An accurate equation of state for hard Gaussian overlap fluids from a generalized Carnahan–Starling method *Mol. Phys.* **79** 449
- [52] de Miguel E and Martin del Rio E 2003 Equation of state for hard Gaussian overlap fluids *J. Chem. Phys.* **118** 1852
- [53] You X-M, Vlasov A Y and Masters A J 2005 The equation of state of isotropic fluids of hard convex bodies from a high-level virial expansion *J. Chem. Phys.* **123** 034510
- [54] Frenkel D 1987 Onsager's spherocylinders revisited *J. Phys. Chem.* **91** 4912
- Frenkel D 1988 Erratum: Onsager's spherocylinders revisited *J. Phys. Chem.* **92** 5314
- [55] Perram J W and Wertheim M S 1985 Statistical mechanics of hard ellipsoids. I. Overlap algorithm and the contact function *J. Comput. Phys.* **58** 409
- [56] Vieillard-Baron J 1972 Phase transitions of the classical hard-ellipse system *J. Chem. Phys.* **56** 4729
- [57] Mulder B M and Frenkel D 1985 The hard ellipsoid-of-revolution fluid: I. Monte Carlo simulations *Mol. Phys.* **55** 1171
- [58] Zarragoicoechea G J, Levesque D and Weis J J 1992 Monte Carlo study of dipolar ellipsoids. II. Search for an isotropic-nematic phase transition *Mol. Phys.* **75** 989
- [59] Allen M P and Mason C P 1995 Stability of the nematic phase for the hard ellipsoid fluid *Mol. Phys.* **86** 467
- [60] Allen M P and Frenkel D 1987 Observation of dynamical precursors of the isotropic-nematic transition by computer simulation *Phys. Rev. Lett.* **58** 1748
- [61] Straley J P 1973 The Gas of long rods as a model for lyotropic liquid crystals *Mol. Cryst. Liq. Cryst.* **22** 333
- [62] Straley J P 1973 Third virial coefficient for the gas of long rods *Mol. Cryst. Liq. Cryst.* **24** 7
- [63] Tjpto-Margo B and Evans G T 1990 The onsager theory of the isotropic-nematic liquid crystal transition: incorporation of the higher virial coefficients *J. Chem. Phys.* **93** 4254
- [64] Barboy B and Gelbart W M 1979 Series representation of the equation of state for hard particle fluids *J. Chem. Phys.* **71** 3053
- [65] Mulder B M and Frenkel D 1985 The hard ellipsoid-of-revolution fluid: II. The y -expansion equation of state *Mol. Phys.* **55** 1193
- [66] Cotter M A and Martire D E 1970 Statistical mechanics of rodlike particles. I. A scaled particle treatment of a fluid of perfectly aligned rigid cylinders *J. Chem. Phys.* **52** 1902
- [67] Cotter M A and Martire D E 1970 Statistical mechanics of rodlike particles. II. A scaled particle investigation of the aligned-isotropic transition in a fluid of rigid spherocylinders *J. Chem. Phys.* **52** 1909
- [68] Reiss H, Frisch H and Lebowitz J L 1959 Statistical mechanics of rigid spheres *J. Chem. Phys.* **31** 369
- [69] Cotter M A 1974 Hard-rod fluid: scaled particle theory revisited *Phys. Rev. A* **10** 625
- [70] Flory P J 1956 Phase equilibria in solutions of rod-like particles *Proc. R. Soc. A* **234** 73
- [71] Alben R 1971 Pretransition effects in nematic liquid crystals: model calculations *Mol. Cryst. Liq. Cryst.* **13** 193
- [72] Barboy B and Gelbart W M 1980 Hard-particle fluids. II. General y -expansion-like descriptions *J. Stat. Phys.* **22** 709
- [73] Parsons J D 1979 Nematic ordering in a system of rods *Phys. Rev. A* **19** 1225
- [74] Pynn R 1974 Theory of static correlations in a fluid of linear molecules *Sol. State Commun.* **14** 29
- [75] Pynn R 1974 Density and temperature dependence of the isotropic-nematic transition *J. Chem. Phys.* **60** 4579
- [76] Wulf A 1977 Short-range correlations and the effective orientational energy in liquid crystals *J. Chem. Phys.* **67** 2254
- [77] Lee S-D 1987 A numerical investigation of nematic ordering based on a simple hard-rod model *J. Chem. Phys.* **87** 4972
- [78] Lee S-D 1988 The Onsager-type theory for nematic ordering of finite-length hard ellipsoids *J. Chem. Phys.* **89** 7036
- [79] Baus M, Colot J-L, Wu X-G and Xu H 1987 Finite-density Onsager-type theory for the isotropic-nematic transition of hard ellipsoids *Phys. Rev. Lett.* **59** 2184
- [80] Colot J-L, Wu X-G, Xu H and Baus M 1988 Density-functional, Landau and Onsager theories of the isotropic-nematic transition of hard ellipsoids *Phys. Rev. A* **38** 2022
- [81] Williamson D C 1995 The isotropic-nematic phase transition: the Onsager theory revisited *Physica A* **220** 139
- [82] McGrother S C, Williamson D C and Jackson G 1996 A re-examination of the phase diagram of hard spherocylinders *J. Chem. Phys.* **104** 6755
- [83] Langmuir I 1938 The role of attractive and repulsive forces in the formation of tactoids, thixotropic gels, protein crystals and coacervates *J. Chem. Phys.* **6** 873
- [84] Mejia A F, Chang Y-W, Ng R, Shuai M, Sam Mannan M and Cheng Z 2012 Aspect ratio and polydispersity dependence of isotropic-nematic transition in discotic suspensions *Phys. Rev. E* **85** 061708
- [85] Frenkel D and Eppenga R 1982 Monte Carlo study of the isotropic-nematic transition in a fluid of thin hard disks *Phys. Rev. Lett.* **49** 1089
- [86] Hosino M, Nakano H and Kimura H 1979 Nematic-smectic transition in an aligned rod system *J. Phys. Soc. Japan* **46** 1709
- [87] Hosino M, Nakano H and Kimura H 1979 Effect of orientational fluctuation on nematic-smectic a transition in the system of hard rod molecules *J. Phys. Soc. Japan* **47** 740
- [88] Wen X and Meyer R B 1987 Model for smectic-A ordering of parallel hard rods *Phys. Rev. Lett.* **59** 1325
- [89] Stroobants A, Lekkerkerker H N W and Frenkel D 1986 Evidence for smectic order in a fluid of hard parallel spherocylinders *Phys. Rev. Lett.* **57** 1452
- [90] Stroobants A, Lekkerkerker H N W and Frenkel D 1987 Evidence for 1D, 2D and 3D order in a system of hard parallel spherocylinders *Phys. Rev. A* **36** 2929

- [91] Frenkel D, Lekkerkerker H N W and Stroobants A 1988 Thermodynamic stability of a smectic phase in a system of hard rods *Nature* **332** 822
- [92] Wen X, Meyer R B and Caspar D L D 1989 Observation of smectic-A ordering in a solution of rigid-rod-like particles *Phys. Rev. Lett.* **63** 2760
- [93] Mulder B 1987 Density-functional approach to smectic order in an aligned hard-rod fluid *Phys. Rev. A* **35** 3095
- [94] Ree F H and Hoover W G 1964 Fifth and sixth virial coefficients for hard spheres and hard disks *J. Chem. Phys.* **40** 939
- [95] Ree F H and Hoover W G 1967 Seventh virial coefficients for hard spheres and hard disks *J. Chem. Phys.* **46** 4181
- [96] Bolhuis P and Frenkel D 1997 Tracing the phase boundaries of hard spherocylinders *J. Chem. Phys.* **106** 666
- [97] Esposito M and Evans G T 1994 Isotropic, nematic and smectic A phases in fluids of hard spherocylinders *Mol. Phys.* **83** 835
- [98] Evans G T 1992 Liquid crystal smectic-A phases and issues of geometry *Mol. Phys.* **76** 1359
- [99] Martínez-Ratón Y and Velasco E 2008 Nonuniform liquid-crystalline phases of parallel hard rod-shaped particles: from ellipsoids to cylinders *J. Chem. Phys.* **129** 054907
- [100] Veerman J A C and Frenkel D 1991 Relative stability of columnar and crystalline phases in a system of parallel hard spherocylinders *Phys. Rev. A* **43** 4334
- [101] Hoover W G and Ree F H 1968 Melting transition and communal entropy for hard spheres *J. Chem. Phys.* **49** 3609
- [102] Taylor M P, Hentschke R and Herzfeld J 1989 Theory of ordered phases in a system of parallel hard spherocylinders *Phys. Rev. Lett.* **62** 800
- [103] Xu H, Lekkerkerker H N W and Baus M 1992 Nematic-smectic A and nematic-solid transitions of parallel hard spherocylinders from density functional theory *Europhys. Lett.* **17** 163
- [104] Evans R 2010 *Density Functional Theory for Inhomogeneous Fluids I: Simple Fluids in Equilibrium (Lecture Notes at 3rd Warsaw School of Statistical Physics)* (Warsaw: Warsaw University Press) p 43
- [105] Poniewierski A and Hołyst R 1988 Density-functional theory for nematic and smectic-A ordering of hard spherocylinders *Phys. Rev. Lett.* **61** 2461
- [106] Tarazona P 1984 A density functional theory of melting *Mol. Phys.* **52** 81
- [107] Poniewierski A and Hołyst R 1990 Density-functional theory for systems of hard rods *Phys. Rev. A* **41** 6871
- [108] Hołyst R and Poniewierski A 1990 Smectic-A, crystalline and columnar ordering in the system of hard parallel cylinders *Mol. Phys.* **71** 561
- [109] Somoza A M and Tarazona P 1988 Nematic-Smectic-A-Smectic-C transitions in systems of parallel hard molecules *Phys. Rev. Lett.* **61** 2566
- [110] Somoza A M and Tarazona P 1989 Density functional approximation for hard-body liquid crystals *J. Chem. Phys.* **91** 517
- [111] Somoza A M and Tarazona P 1990 Nematic and smectic liquid crystals of hard spherocylinders *Phys. Rev. A* **41** 965
- [112] Poniewierski A 1992 Nematic to smectic-A transition in the asymptotic limit of very long hard spherocylinders *Phys. Rev. A* **45** 5605
- [113] Velasco E, Mederos L and Sullivan D E 2000 Density-functional theory of inhomogeneous systems of hard spherocylinders *Phys. Rev. E* **62** 3708
- [114] Graf H and Löwen H 1999 Density functional theory for hard spherocylinders: phase transitions in the bulk and in the presence of external fields *J. Phys.: Condens. Matter* **11** 1435
- [115] Graf H and Löwen H 1999 Phase diagram of tobacco mosaic virus solutions *Phys. Rev. E* **59** 1932
- [116] Rosenfeld Y 1988 Scaled field particle theory of the structure and the thermodynamics of isotropic hard particle fluids *J. Chem. Phys.* **89** 4272
- [117] Rosenfeld Y 1989 Free-energy model for the inhomogeneous hard-sphere fluid mixture and density-functional theory of freezing *Phys. Rev. Lett.* **63** 980
- [118] Rosenfeld Y, Schmidt M, Löwen H and Tarazona P 1997 Dimensional crossover and the freezing transition in density functional theory *J. Phys.: Condens. Matter* **8** L577
- [119] Rosenfeld Y, Schmidt M, Löwen H and Tarazona P 1999 Fundamental-measure free-energy density functional for hard spheres: dimensional crossover and freezing *Phys. Rev. E* **55** 4245
- [120] Roth R 2010 Fundamental measure theory for hard sphere mixtures: a review *J. Phys.: Condens. Matter* **22** 063102
- [121] Tarazona P and Rosenfeld Y 1997 From zero-dimension cavities to free-energy functionals for hard disks and hard spheres *Phys. Rev. E* **55** R4873
- [122] Tarazona P 2000 Density functional for hard sphere crystals: a fundamental measure approach *Phys. Rev. Lett.* **84** 694
- [123] Cuesta J A, Martínez-Ratón Y and Tarazona P 2002 Close to the edge of fundamental measure theory: a density functional for hard-sphere mixtures *J. Phys.: Condens. Matter* **14** 11965
- [124] Tarazona P, Cuesta J A and Martínez-Ratón Y 2008 Density functional theories of hard particle systems *Lect. Notes Phys.* **753** 247
- [125] Korden S 2012 Deriving the Rosenfeld functional from the virial expansion *Phys. Rev. E* **85** 041150
- [126] Korden S 2014 Density functional theory for hard particles in N dimensions (arXiv:1403.2054v1)
- [127] Marechal M, Korden S and Mecke K 2014 Deriving fundamental measure theory: reconciling the zero-dimensional limit with the virial approach (arXiv:1403.4505v1)
- [128] Cuesta J A 1996 Fluid mixtures of parallel hard cubes *Phys. Rev. Lett.* **76** 3742
- [129] Cuesta J A and Martínez-Ratón Y 1997 Dimensional crossover of the fundamental-measure functional for parallel hard cubes *Phys. Rev. Lett.* **78** 3681
- [130] Cuesta J A and Martínez-Ratón Y 1997 Fundamental measure theory for mixtures of parallel hard cubes. I. General formalism *J. Chem. Phys.* **107** 6379
- [131] Martínez-Ratón Y 2004 Bulk inhomogeneous phases of anisotropic particles: a fundamental measure functional study of the restricted orientations model *Phys. Rev. E* **69** 061712
- [132] Casey A and Harrowell P 1995 Monte Carlo simulations of a layering transition in hard parallelepipeds *J. Chem. Phys.* **103** 6143
- [133] John B S and Escobedo F A 2005 Phase behavior of colloidal hard tetragonal parallelepipeds (cuboids): a Monte Carlo simulation study *J. Phys. Chem. B* **109** 23008
- [134] Martínez-Ratón Y, Capitán J A and Cuesta J A 2008 Fundamental-measure density functional for mixtures of parallel hard cylinders *Phys. Rev. E* **77** 051205
- [135] Capitán J A, Martínez-Ratón Y and Cuesta J A 2008 Phase behavior of parallel hard cylinders *J. Chem. Phys.* **128** 194901
- [136] Cinacchi G and Schmid F 2002 Density functional for anisotropic fluids *J. Phys.: Condens. Matter* **14** 12223
- [137] Schmidt M 2001 Density functional theory for colloidal rod-sphere mixtures *Phys. Rev. E* **63** R050201
- [138] Brader J M, Esztermann A and Schmidt M 2002 Colloidal rod-sphere mixtures: fluid-fluid interfaces and the Onsager limit *Phys. Rev. E* **66** 031401

- [139] Esztermann A and Schmidt M 2004 Density functional theory for sphere-needle mixtures: toward finite rod thickness *Phys. Rev. E* **70** 022501
- [140] Esztermann A, Reich H and Schmidt M 2006 Density functional theory for colloidal mixtures of hard platelets, rods and spheres *Phys. Rev. E* **73** 011409
- [141] Rosenfeld Y 1994 Density functional theory of molecular fluids: free-energy model for the inhomogeneous hard-body fluid *Phys. Rev. E* **50** R3318
- [142] Hansen-Goos H and Mecke K 2009 Fundamental measure theory for inhomogeneous fluids of nonspherical hard particles *Phys. Rev. Lett.* **102** 018302
- [143] Hansen-Goos H and Mecke K 2010 Tensorial density functional theory for non-spherical hard-body fluids *J. Phys.: Condens. Matter* **22** 364107
- [144] Härtel A and Löwen H 2010 Fundamental measure density functional theory for hard spherocylinders in static and time-dependent aligning fields *J. Phys.: Condens. Matter* **22** 104112
- [145] van Roij R, Bolhuis P, Mulder B and Frenkel D 1995 Transverse interlayer order in lyotropic smectic liquid crystals *Phys. Rev. E* **52** R1277
- [146] Hess S, Frenkel D and Allen M P 1991 On the anisotropy of diffusion in nematic liquid crystals: test of a modified affine transformation model via molecular dynamics *Mol. Phys.* **74** 765
- [147] Allen M P 1990 Diffusion coefficient increases with density in hard ellipsoid liquid crystals *Phys. Rev. Lett.* **65** 2881
- [148] Cinacchi G and de Gaetani L 2009 Mechanism of diffusion in the smectic-A phase of wormlike rods studied by computer simulation *Phys. Rev. E* **79** 011706
- [149] Frenkel D 1989 Columnar ordering as an excluded-volume effect *Liq. Cryst.* **5** 929
- [150] Stroobants A 1992 Columnar versus smectic order in binary mixtures of hard parallel spherocylinders *Phys. Rev. Lett.* **69** 2388
- [151] Eppenga R and Frenkel D 1984 Monte Carlo study of the isotropic and nematic phases of infinitely thin hard platelets *Mol. Phys.* **52** 1303
- [152] Veerman J A C and Frenkel D 1992 Phase behavior of disklike hard-core mesogens *Phys. Rev. A* **45** 5632
- [153] Wensink H H and Lekkerkerker H N W 2009 Phase diagram of hard colloidal platelets: a theoretical account *Mol. Phys.* **107** 2111
- [154] Marechal M, Cuetos A, Martínez-Haya B and Dijkstra M 2011 Phase behavior of hard colloidal platelets using free energy calculations *J. Chem. Phys.* **134** 094501
- [155] Bisi F, Rosso R, Virga E G and Durand G E 2008 Polar steric interactions for V-shaped molecules *Phys. Rev. E* **78** 011705
- [156] Lansac Y, Maiti P K, Clark N A and Glaser M A 2003 Phase behavior of bent-core molecules *Phys. Rev. E* **67** 011703
- [157] Maiti P K, Lansac Y, Glaser M A and Clark N A 2004 Entropy-stabilized smectic C phase in a system of zigzag-shaped molecules *Phys. Rev. Lett.* **92** 025501
- [158] Freiser M J 1970 Ordered states of a nematic liquid *Phys. Rev. Lett.* **24** 1041
- [159] Luckhurst G R 2004 Liquid crystals: a missing phase found at last? *Nature* **430** 413
- [160] Luckhurst G R 2001 Biaxial nematic liquid crystals: fact or fiction? *Thin Solid Films* **393** 40
- [161] Tschierske C and Photinos D J 2010 Biaxial nematic phases *J. Mater. Chem.* **20** 4263
- [162] Allen M P 1990 Computer simulation of a biaxial liquid crystal *Liq. Cryst.* **8** 499
- [163] Camp P J and Allen M P 1997 Phase diagram of the hard biaxial ellipsoid fluid *J. Chem. Phys.* **106** 6681
- [164] Berardi R, Muccioli L, Orlandi S, Ricci M and Zannoni C 2008 Computer simulations of biaxial nematics *J. Phys.: Condens. Matter* **20** 463101
- [165] Yu L J and Saupe A 1980 Observation of a biaxial nematic phase in potassium laurate-1-decanol-water mixtures *Phys. Rev. Lett.* **45** 1000
- [166] Madsen L A, Dingemans T J, Nakata M and Samulski E T 2004 Thermotropic biaxial nematic liquid crystals *Phys. Rev. Lett.* **92** 145505
- [167] Acharya B R, Primak A and Kumar S 2004 Biaxial nematic phase in bent-core thermotropic mesogens *Phys. Rev. Lett.* **92** 145506
- [168] Galerne Y 2006 Comment on 'thermotropic biaxial nematic liquid crystals' *Phys. Rev. Lett.* **96** 219803
- [169] Madsen L A, Dingemans T J, Nakata M and Samulski E T 2006 Thermotropic biaxial nematic liquid crystals *Phys. Rev. Lett.* **96** 219804
- [170] Van Le K, Mathews M, Chambers M, Harden J, Li Q, Takezoe H and Jakli A 2009 Electro-optic technique to study biaxiality of liquid crystals with positive dielectric anisotropy: the case of a bent-core material *Phys. Rev. E* **79** R030701
- [171] van den Pol E, Petukhov A V, Thies-Weesie D M E, Byelov D V and Vroege G J 2009 Experimental realization of biaxial liquid crystal phases in colloidal dispersions of boardlike particles *Phys. Rev. Lett.* **103** 258301
- [172] Somoza A M and Tarazona P 1992 Liquid crystals of asymmetric hard body molecules *Mol. Phys.* **75** 17
- [173] Shih C S and Alben R 1972 Lattice model for biaxial liquid crystals *J. Chem. Phys.* **57** 3055
- [174] Alben R 1973 Phase transitions in a fluid of biaxial particles *Phys. Rev. Lett.* **30** 778
- [175] Mulder B 1989 Isotropic-symmetry-breaking bifurcations in a class of liquid-crystal models *Phys. Rev. A* **39** 360
- [176] Hołyst R and Poniewierski A 1990 Study of the Landau bicritical point in dense systems of hard biaxial molecules *Mol. Phys.* **69** 193
- [177] Taylor M P and Herzfeld J 1991 Nematic and smectic order in a fluid of biaxial hard particles *Phys. Rev. A* **44** 3742
- [178] Vanakaras A G, Bates M A and Photinos D J 2003 Theory and simulation of biaxial nematic and orthogonal smectic phases formed by mixtures of board-like molecules *Phys. Chem. Chem. Phys.* **5** 3700
- [179] Martínez-Ratón Y, Varga S and Velasco E 2008 Biaxial nematic and smectic phases of parallel particles with different cross sections *Phys. Rev. E* **78** 031705
- [180] Martínez-Ratón Y, Varga S and Velasco E 2011 Biaxial nematic phases in fluids of hard board-like particles *Phys. Chem. Chem. Phys.* **13** 13247
- [181] Peroukidis S D and Vanakaras A G 2013 Phase diagram of hard board-like colloids from computer simulations *Soft Matter* **9** 7419
- [182] Ferrarini A 2010 The theory of elastic constants *Liq. Cryst.* **37** 811
- [183] Frank F C 1958 I. Liquid crystals. On the theory of liquid crystals *Discuss. Faraday Soc.* **25** 19
- [184] Priest R G 1973 Theory of the Frank elastic constants of nematic liquid crystals *Phys. Rev. A* **7** 720
- [185] Straley J P 1976 Theory of piezoelectricity in nematic liquid crystals and of the cholesteric ordering *Phys. Rev. A* **14** 1835
- [186] Poniewierski A and Stecki J 1979 Statistical theory of elastic constants of nematic liquid crystals *Mol. Phys.* **38** 1931
- [187] Poniewierski A and Stecki J 1982 Statistical theory of the Frank elastic constants *Phys. Rev. A* **25** 2368
- [188] Singh Y 1984 Molecular theory of liquid crystals: application to the nematic phase *Phys. Rev. A* **30** 583
- [189] Lipkin M D, Rice S A and Mohanty U 1985 The elastic constants of condensed matter: a direct-correlation function approach *J. Chem. Phys.* **82** 472

- [190] Somoza A M, Tarazona P 1991 Density functional theory of the elastic constants of a nematic liquid crystal *Mol. Phys.* **72** 911
- [191] Gelbart W M and Ben-Shaul A 1982 Molecular theory of curvature elasticity in nematic liquids *J. Chem. Phys.* **77** 916
- [192] Singh S 1996 Elastic constants of uniaxial nematic liquid crystals: a comparison between theory and experiment *Liq. Cryst.* **20** 797
- [193] Singh Y and Singh K 1986 Density-functional theory of curvature elasticity in nematic liquids. I *Phys. Rev. A* **33** 3481
- [194] Lee S-D and Meyer R B 1986 Computations of the phase equilibrium, elastic constants and viscosities of a hard-rod nematic liquid crystal *J. Chem. Phys.* **84** 3443
- [195] Lee S-D 1989 Density-functional approach to curvature elasticity in a liquid-density nematic system *Phys. Rev. E* **39** 3631
- [196] Somoza A M and Tarazona P 1989 Frank elastic constants of a nematic liquid crystal of hard molecules *Phys. Rev. A* **40** 6069
- [197] Forster D 1975 *Hydrodynamic Fluctuations: Broken Symmetry and Correlation Functions (Frontiers in Physics)* vol 47 (Reading, Mass: Benjamin)
- [198] Allen M P and Frenkel D 1988 Calculation of liquid-crystal Frank constants by computer simulation *Phys. Rev. A* **37** R1813
- [199] Allen M P and Frenkel D 1990 Erratum: calculation of liquid-crystal Frank constants by computer simulation *Phys. Rev. A* **42** 3641E
- [200] Tjijto-Margo B, Evans G T, Allen M P and Frenkel D 1992 Elastic constants of hard and soft nematic liquid crystals *J. Phys. Chem.* **96** 3942
- [201] Singh Y, Singh S and Rajesh K 1992 Molecular theory of elastic constants of liquid crystals: application to uniaxial phases *Phys. Rev. A* **45** 974
- [202] Singh Y, Rajesh K, Menon V J and Singh S 1994 Molecular theory of elastic constants of liquid crystals. II. Application to the biaxial nematic phase *Phys. Rev. E* **49** 501
- [203] Singh Y and Ram J 2001 Molecular theory of elastic constants of liquid crystals. III. Application to smectic phases with tilted orientational order *Phys. Rev. E* **64** 051705
- [204] Asakura S and Oosawa F 1954 On interaction between two bodies immersed in a solution of macromolecules *J. Chem. Phys.* **22** 1255
- [205] Vliegthart G A and Lekkerkerker H N W 1999 Phase behavior of colloidal rod-sphere mixtures *J. Chem. Phys.* **111** 4153
- [206] van Der Kooij F M, Vogel M and Lekkerkerker H N W 2000 Phase behavior of a mixture of platelike colloids and nonadsorbing polymer *Phys. Rev. E* **62** 5397
- [207] Baus M, Rull L F and Ryckaert J-P 1995 Phase transition of spherical colloids *Observation, Prediction and Simulation of Phase Transitions in Complex Fluids (NATO-ASI Series C)* vol 460 ed W C K Poon and P N Pusey (Boston: Kluwer) p 3
- [208] Adams M, Dogic Z, Keller S L and Fraden S 1998 Entropically driven microphase transitions in mixtures of colloidal rods and spheres *Nature* **393** 349
- [209] Alben R 1973 Liquid crystal phase transitions in mixtures of rodlike and platelike molecules *J. Chem. Phys.* **59** 4299
- [210] Samborski A and Evans G T 1994 Binary hard sphere, hard ellipsoid liquid crystal mixtures *J. Chem. Phys.* **101** 6005
- [211] Lekkerkerker H N W, Coulon P H, Van Der Haegen R and Deblieck R 1984 On the isotropic-liquid crystal phase separation in a solution of rodlike particles of different lengths *J. Chem. Phys.* **80** 3427
- [212] Stroobants A and Lekkerkerker H N W 1984 Liquid crystal phase transitions in a solution of rodlike and disklike particles *J. Phys. Chem.* **88** 3669
- [213] van Roij R and Mulder B 1994 Demixing in a hard rod-plate mixture *J. Phys. II France* **4** 1763
- [214] Vanakaras A G, Terzis A F and Photinos D J 2001 On the molecular requirements for the stabilisation of thermotropic biaxial ordering in rod-plate nematics *Mol. Cryst. Liq. Cryst.* **362** 67
- [215] Camp P J and Allen M P 1996 Hard-ellipsoid rod-plate mixtures: Onsager theory and computer simulations *Physica A* **229** 410
- [216] Camp P J, Allen M P, Bolhuis P G and Frenkel D 1997 Demixing in hard ellipsoid rod-plate mixtures *J. Chem. Phys.* **106** 9270
- [217] Varga S, Galindo A and Jackson G 2002 Global fluid phase behavior in binary mixtures of rodlike and platelike molecules *J. Chem. Phys.* **117** 7207
- [218] van der Kooij F M and Lekkerkerker H N W 2000 Liquid-crystalline phase behavior of a colloidal rod-plate mixture *Phys. Rev. Lett.* **84** 781
- [219] Wensink H H, Vroege G J and Lekkerkerker H N W 2001 Isotropic-nematic density inversion in a binary mixture of thin and thick hard platelets *J. Phys. Chem. B* **105** 10610
- [220] Varga S, Galindo A and Jackson G 2003 New types of phase behaviour in binary mixtures of hard rod-like particles *Mol. Phys.* **101** 817
- [221] Galindo A, Haslam A J, Varga S, Jackson G, Vanakaras A G, Photinos D J and Dunmur D A 2003 The phase behavior of a binary mixture of rodlike and dislike mesogens: Monte Carlo simulation, theory and experiment *J. Chem. Phys.* **119** 5216
- [222] Purdy K R, Varga S, Galindo A, Jackson G and Fraden S 2005 Nematic phase transitions in mixtures of thin and thick colloidal rods *Phys. Rev. Lett.* **94** 057801
- [223] Varga S, Purdy K, Galindo A, Fraden S and Jackson G 2005 Nematic-nematic phase separation in binary mixtures of thick and thin hard rods: results from onsager-like theories *Phys. Rev. E* **72** 051704
- [224] van Roij R, Mulder B and Dijkstra M 1998 Phase behavior of binary mixtures of thick and thin hard rods *Physica A* **261** 374
- [225] Lekkerkerker H N W, Poon W C-K, Pusey P N, Stroobants A and Warren P B 1992 Phase behaviour of colloid + polymer mixtures *Europhys. Lett.* **20** 559
- [226] Schmidt M and von Ferber C 2001 Amphiphilic hard body mixtures *Phys. Rev. E* **64** 051115
- [227] Schmidt M and Denton A R 2002 Colloids, polymers and needles: demixing phase behavior *Phys. Rev. E* **65** 021508
- [228] Philips J and Schmidt M 2010 Bulk phase behavior of binary hard platelet mixtures from density functional theory *Phys. Rev. E* **81** 041401
- [229] de las Heras D and Schmidt M 2013 Bulk fluid phase behaviour of colloidal platelet-sphere and platelet-polymer mixtures *Phil. Trans. R. Soc. A* **371** 20120259
- [230] Sear R P and Mulder B M 1996 Phase behaviour of a symmetric binary mixture of hard rods *J. Chem. Phys.* **105** 7727
- [231] Koda T, Nishioka A and Ikeda S 2005 Computer simulation of binary mixtures of anisotropic hard particles *J. Phys.: Condens. Matter* **17** S2875
- [232] Cui S-M and Yu Chen Z 1994 Columnar and smectic order in binary mixtures of aligned hard cylinders *Phys. Rev. E* **50** 3747
- [233] Koda T and Kimura H 1994 Phase diagram of the nematic-smectic a transition of the binary mixture of parallel hard cylinders of different lengths *J. Phys. Soc. Japan* **63** 984

- [233] Sear R P and Jackson G 1995 Stability of the nematic phase of a mixture of aligned cylinders with respect to the smectic and columnar phases *J. Chem. Phys.* **102** 2622
- [234] Koda T, Numajiri M, Ikeda S 1996 Smectic-A phase of a bidisperse system of parallel hard rods and hard spheres *J. Phys. Soc. Japan* **65** 3551
- [235] Dogic Z, Frenkel D and Fraden S 2000 Enhanced stability of layered phases in parallel hard spherocylinders due to addition of hard spheres *Phys. Rev. E* **62** 3925
- [236] Martínez-Ratón Y, Cinacchi G, Velasco E and Mederos L 2006 Depletion effects in smectic phases of hard-rod-hard-sphere mixtures *Eur. Phys. J. E* **21** 175
- [237] Vesely F J 2005 Smectic phases in hard particles mixtures: Koda's theory *Mol. Phys.* **103** 679
- [238] Peroukidis S D, Vanakaras A G and Photinos D J 2010 Liquid crystalline phases and demixing in binary mixtures of shape-anisometric colloids *J. Mater. Chem.* **20** 10495
- [239] Varga S, Gábor A, Velasco E, Mederos L and Vesely F J 2008 Demixed and ordered phases in hard-rod mixtures *Mol. Phys.* **106** 1939
- [240] Varga S, Velasco E, Mederos L and Vesely F J 2009 Stability of the columnar and smectic phases of length-bidisperse parallel hard cylinders *Mol. Phys.* **107** 2481
- [241] Cinacchi G, Mederos L and Velasco E 2004 Liquid-crystal phase diagrams of binary mixtures of hard spherocylinders *J. Chem. Phys.* **121** 3854
- [242] Cinacchi G, Velasco E and Mederos L 2004 Entropic segregation in smectic phases of hard-body mixtures *J. Phys. Condens. Matter* **16** S2003
- [243] Martínez-Ratón Y, Velasco E and Mederos L 2005 Stability of smectic phases in hard-rod mixtures *J. Chem. Phys.* **123** 104906
- [244] Cinacchi G, Martínez-Ratón Y, Mederos L and Velasco E 2006 Smectic, nematic and isotropic phases in binary mixtures of thin and thick hard spherocylinders *J. Chem. Phys.* **124** 234904
- [245] de las Heras D and Schmidt M 2013 Phase stacking diagram of colloidal mixtures under gravity *Soft Matter* **9** 8636
- [246] McMullen W E, Gelbart W M and Benshaul A 1985 Isotropic-nematic transition in micellized solutions *J. Chem. Phys.* **82** 5616
- [247] Odijk T 1986 Theory of lyotropic polymer liquid crystals *Macromolecules* **19** 2313
- [248] Sluckin T J 1989 Polydispersity in liquid crystal systems *Liq. Cryst.* **6** 111
- [249] Chen Z Y 1994 Effect of polydispersity on the isotropic-nematic phase transition of rigid rods *Phys. Rev. E* **50** 2849
- [250] Clarke N, Cuesta J A, Sear R, Sollich P and Speranza A 2000 Phase equilibria in the polydisperse Zwanzig model of hard rods *J. Chem. Phys.* **113** 5817
- [251] Speranza A and Sollich P 2002 Simplified Onsager theory for isotropic-nematic phase equilibria of length polydisperse hard rods *J. Chem. Phys.* **117** 5421
- [252] Warren P B 1998 Combinatorial entropy and the statistical mechanics of polydispersity *Phys. Rev. Lett.* **80** 1369
Warren P B 1998 Combinatorial entropy and the statistical mechanics of polydispersity *Phys. Rev. Lett.* **80** 3671 (erratum)
- [253] Sollich P and Cates M E 1998 Projected free energies for polydisperse phase equilibria *Phys. Rev. Lett.* **80** 1365
- [254] Cates M E, Sollich P and Warren P B 2001 Moment free energies for polydisperse systems *Adv. Chem. Phys.* **116** 265
- [255] Sollich P 2002 Predicting phase equilibria in polydisperse systems *J. Phys.: Condens. Matter* **14** R79
- [256] Fasolo M, Sollich P and Speranza A 2004 Phase equilibria in polydisperse colloidal systems *Reactive Funct. Polym.* **58** 187
- [257] Speranza A and Sollich P 2003 Isotropic-nematic phase equilibria of polydisperse hard rods: the effect of fat tails in the length distribution *J. Chem. Phys.* **118** 5213
- [258] Speranza A and Sollich P 2003 Isotropic-nematic phase equilibria in the Onsager theory of hard rods with length polydispersity *Phys. Rev. E* **67** 061702
- [259] Wensink H H and Vroege G J 2003 Isotropic-nematic phase behavior of length-polydisperse hard rods *J. Chem. Phys.* **119** 6868
- [260] Martínez-Ratón Y and Velasco E 2012 Effect of polydispersity, bimodality and aspect ratio on the phase behavior of colloidal platelet suspensions *J. Chem. Phys.* **137** 134906
- [261] Velasco E and Martínez-Ratón Y 2014 Interplay between columnar and smectic stability in suspensions of polydisperse colloidal platelets *Phys. Chem. Chem. Phys.* **16** 765
- [262] Martínez-Ratón Y and Cuesta J A 2002 Enhancement by polydispersity of the biaxial nematic phase in a mixture of hard rods and plates *Phys. Rev. Lett.* **89** 185701
- [263] Martínez-Ratón Y and Cuesta J A 2003 Phase diagrams of Zwanzig models: the effect of polydispersity *J. Chem. Phys.* **118** 10164
- [264] Belli S, Patti A, Dijkstra M and van Roij R 2011 Polydispersity stabilizes biaxial nematic liquid crystals *Phys. Rev. Lett.* **107** 148303
- [265] Bohle A M, Holyst R and Vilgils T 1996 Polydispersity and ordered phases in solutions of rodlike macromolecules *Phys. Rev. Lett.* **76** 1396
- [266] Martínez-Ratón Y and Cuesta J A 2009 Smectic and columnar ordering in length-polydisperse fluids of parallel hard cylinders *Mol. Phys.* **107** 415
- [267] van der Kooij F M, Kassapidou K and Lekkerkerker H N W 2000 Liquid crystal phase transitions in suspensions of polydisperse plate-like particles *Nature* **406** 868
- [268] Bates M A and Frenkel D 1998 Influence of polydispersity on the phase behavior of colloidal liquid crystals: a Monte Carlo simulation study *J. Chem. Phys.* **109** 6193
- [269] Bates M A and Frenkel D 1999 Nematic-isotropic transition in polydisperse systems of infinitely thin hard platelets *J. Chem. Phys.* **110** 6553
- [270] Chaikin P M and Lubensky T C 2000 Principles of Condensed Matter Physics (Cambridge: Cambridge University Press)
- [271] Straley J P 1971 Liquid crystals in two dimensions *Phys. Rev. A* **4** 675
- [272] Frenkel D and Eppenga R 1985 Evidence for algebraic orientational order in a 2D hard-core nematic *Phys. Rev. A* **31** 1776
- [273] Winkle D H and Clark N A 1988 Direct measurement of orientation correlations in a 2D liquid-crystal system *Phys. Rev. A* **38** 1573
- [274] Nelson D R and Pelcovits R A 1977 Momentum-shell recursion relations, anisotropic spins and liquid crystals in $2 + \epsilon$ dimensions *Phys. Rev. B* **16** 2191
- [275] Cuesta J A and Frenkel D 1990 Monte Carlo simulation of 2D hard ellipses *Phys. Rev. A* **42** 2126
- [276] Cuesta J A, Tejero C F and Baus M 1989 Isotropic-nematic transition of hard ellipses *Phys. Rev. A* **39** 6498
- [277] Bates M A and Frenkel D 2000 Phase behavior of 2D hard rod fluids *J. Chem. Phys.* **112** 10034
- [278] Morishige K, Kawai N and Shimizu M 1993 Occurrence of 2D smectic liquid crystal in n-propanol adsorbed on graphite *Phys. Rev. Lett.* **70** 3904
- [279] Khandkar M and Barma M 2005 Orientational correlations and the effect of spatial gradients in the equilibrium steady state of hard rods in two dimensions: a study using deposition-evaporation kinetics *Phys. Rev. E* **72** 051717

- [280] Chrzanowska A 2005 On the application of the Onsager DFT theory to two-dimensional system of hard needles *Acta Phys. Pol. B* **36** 3163
- [281] Chrzanowska A and Ehrentraut H 2002 Velocity correlations of 2D hard needles from molecular dynamics *Phys. Rev. E* **66** 012201
- [282] Varga S and Szalai I 1998 Phase transitions of hard ellipses and hard ellipses with circular square-wells based upon density functional theory *Mol. Phys.* **95** 515
- [283] de las Heras D, Mederos L and Velasco E 2009 Density-functional study of defects in 2D circular nematic nanocavities *Liq. Cryst.* **37** 45
- [284] Triplett D A and Fichthorn K A 2008 Monte Carlo simulation of 2D hard rectangles: confinement effects *Phys. Rev. E* **77** 011707
- [285] Schlacken H, Mögel H-J and Schiller P 1998 Orientational transitions of 2D hard rod fluids *Mol. Phys.* **93** 777
- [286] Wojciechowski K W and Frenkel D 2004 Tetratic phase in the planar hard square system? *Comput. Methods Sci. Technol.* **10** 235
- [287] Martínez-Ratón Y, Velasco E and Mederos L 2005 Effect of particle geometry on phase transitions in 2D liquid crystals *J. Chem. Phys.* **122** 064903
- [288] Martínez-Ratón Y 2007 Capillary ordering and layering transitions in 2D hard-rod fluids *Phys. Rev. E* **75** 051708
- [289] Narayan V, Menon N and Ranaswamy S 2006 Nonequilibrium steady states in a vibrated-rod monolayer: tetratic, nematic and smectic correlations *J. Stat. Mech.* P01005
- [290] Wojciechowski K W, Frenkel D and Brańka A C 1991 Nonperiodic solid phase in a 2D hard-dimer system *Phys. Rev. Lett.* **66** 3168
- [291] Donev A, Burton J, Stillinger F H and Torquato S 2006 Tetratic order in the phase behavior of a hard-rectangle system *Phys. Rev. B* **73** 054109
- [292] Martínez-Ratón Y, Velasco E and Mederos L 2006 Orientational ordering in hard rectangles: the role of three-body correlations *J. Chem. Phys.* **125** 014501
- [293] Martínez-Ratón Y and Velasco E 2009 Enhanced stability of the tetratic phase due to clustering *Phys. Rev. E* **79** 011711
- [294] Zhao K, Harrison C, Huse D, Russel W B and Chaikin P M 2007 Nematic and almost-tetratic phases of colloidal rectangles *Phys. Rev. E* **76** R040401
- [295] Geng J, Selinger J V 2009 Theory and simulation of 2D nematic and tetratic phases *Phys. Rev. E* **80** 011707
- [296] Avendaño C and Escobedo F A 2012 Phase behavior of rounded hard-squares *Soft Matter* **8** 4675
- [297] Bernard E P and Krauth W 2011 Two-step melting in two dimensions: first-order liquid-hexatic transition *Phys. Rev. Lett.* **107** 155704
- [298] Zhao K and Mason T G 2009 Frustrated rotator crystals and glasses of brownian pentagons *Phys. Rev. Lett.* **103** 208302
- [299] Zhao K, Bruinsma R and Mason T G 2011 Entropic crystal-crystal transitions of Brownian squares *Proc. Natl Acad. Sci.* **108** 2684
- [300] Schilling T, Pronk S, Mulder B and Frenkel D 2005 Monte Carlo study of hard pentagons *Phys. Rev. E* **71** 036138
- [301] Perusquía R A, Peón J and Quintana J 2005 2D model for mixtures of enantiomers, bent hard needles: a Monte Carlo simulation *Physica A* **345** 130
- [302] Peón J, Saucedo-Zugazagoitia J, Pucheta-M F, Perusquía R A, Sutmann G and Quintana-H J 2006 2D chiral model for liquid crystals, bent hard needles: a Monte Carlo simulation *J. Chem. Phys.* **125** 104908
- [303] Martínez-Ratón Y, Velasco E and Mederos L 2005 Demixing behavior in 2D mixtures of anisotropic hard bodies *Phys. Rev. E* **72** 031703
- [304] Martínez-Ratón Y 2011 Phase behaviour of mixtures of hard ellipses: a scaled particle density functional study *Liq. Cryst.* **38** 697
- [305] de las Heras D, Martínez-Ratón Y and Velasco E 2007 Demixing and orientational ordering in mixtures of rectangular particles *Phys. Rev. E* **76** 031704
- [306] Kaganer V M, Möhwald H and Dutta P 1999 Structure and phase transitions in Langmuir monolayers *Rev. Mod. Phys.* **71** 779
- [307] Halperin A, Alexander S and Schechter I 1987 Mean field theory of nematic order for grafted rods *J. Chem. Phys.* **86** 6550
- [308] Moore B G 1989 Comment on: 'Mean field theory of nematic order for grafted rods' *J. Chem. Phys.* **91** 1381
- [309] Halperin A, Alexander S and Schechter I 1989 Reply to the Comment on: Mean field theory of nematic order for grafted rods *J. Chem. Phys.* **91** 1383
- [310] Chen Z-Y, Talbot J, Gelbart W M and Ben Shaul A 1988 Phase transitions in systems of grafted rods *Phys. Rev. Lett.* **61** 1376
- [311] Somoza A M and Desai R C 1992 Tilt order in Langmuir monolayers *J. Phys. Chem.* **96** 1401
- [312] Martínez-Ratón Y, Varga S and Velasco E 2014 Phase behavior of liquid-crystal monolayers of rod-like and plate-like particles *J. Chem. Phys.* **140** 204906
- [313] Kolli H B, Frezza E, Cinacchi G, Ferrarini A, Giacometti A and Hudson T S 2014 Communication: From rods to helices: Evidence of a screw-like nematic phase *J. Chem. Phys.* **140** 081101
- [314] Kolli H B, Frezza E, Cinacchi G, Ferrarini A, Giacometti A, Hudson T S, de Michele C and Sciortino F 2014 Self-assembly of hard helices: a rich and unconventional polymorphism *Soft Matter* accepted
- [315] Wittmann R, Marechal M and Mecke K 2014 Fundamental measure theory for smectic phases: scaling behavior and higher order terms *J. Chem. Phys.* **141** 064103